AD-A163 818 A DYNAMIC FIBER COMPOSITE CONTINUUM MODEL OF THE TYMPANIC MEMBRANE PART 1.. (U) RENSSELAER POLYTECHNIC INST TROY N Y DEPT OF MECHANICAL ENGIN.. R D RABBITT

1/1

UNCLASSIFIED JUL 85 RRI-151-PT-1 ARO-20474.3-MA F/G 6/16 NL

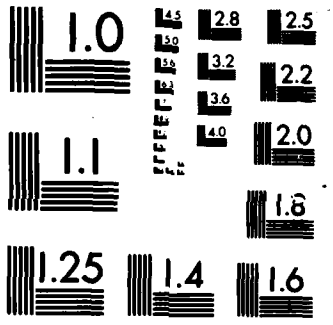

MICROCOPY RESOLUTION TEST CHART
NATIONAL BUREAU OF STANDARDS-1963-A

(2)

A Dynamic Fiber Composite Continuum Model of the Tympanic Membrane

Part I: Model Formulation

by

Richard D. Rabbitt

Rensselaer Polytechnic Institute
Troy, New York 12181

ARO 20474.3-MA

(2)

R.P.I. Math. Report No. 151
July, 1985

A Dynamic Fiber Composite Continuum Model of the Tympanic Membrane

Part I: Model Formulation

by

Richard D. Rabbitt

Department of Mechanical Engineering

Rensselaer Polytechnic Institute

Troy, New York 12180-3590

This work was supported by the U.S. Army Research Office,
Contract Number DAAG29-83-K-0092

ACKNOWLEDGEMENT

This work was conducted under the guidance of Dr. Mark H. Holmes, Department of Mathematical Sciences, Rensselaer Polytechnic Institute. His comments and suggestions were invaluable throughout the preparation of this report.

Partial support was contributed by the U.S. Army Research Office Grant DAAG29-83-K-0092.

ABSTRACT

Fibrous layers of the lamina propria influence dynamic behavior of the tympanic membrane by producing strong anisotropic extensional stiffness, while the mucous and epidermal layers are primarily responsible for curvature dependent structural damping and relatively weak isotropic bending stiffness. These mechanical properties are combined with curvilinear shell equilibrium equations to formulate a comprehensive dynamic continuum model of the tympanic membrane. The resulting model contains several small parameters that are exploited to construct closed form asymptotic solutions for the general problem. Using the geometry and ultrastructure of the cat eardrum coupled with the outer ear, ossicular chain and tympanic cavities, the asymptotic solution reproduces the manifold of experimentally observed frequency and excitation dependent vibrational shapes. Demonstration of the model's ability to duplicate experimental results concludes part I. However, since the model is based on the actual geometry and ultrastructure, future investigations may use the model to address questions related to tympanoplasty, tympanosclerosis, tensor tympani cogency, as well as energy transmission and tympanic cavity coupling.

CONTENTS

Chapter | Page

CHAPTER 1

INTRODUCTION

1.1 The Spirit of Mathematical Physics

"Since the seventeenth century, physical intuition has served as a vital source for mathematical problems and methods. Recent trends and fashions have, however, weakened the connection between mathematics and physics; mathemathcians, turning away from the roots of mathematics in intuition, have concentrated on refinement and emphasized the postulational side of mathematics, and at times have overlooked the unity of their science with physics and other fields. In many cases, physicists have ceased to appreciate the attitudes of mathematicians. This rift is unquestionably a serious threat to science as a whole; the broad stream of scientific development may split into smaller and smaller rivulets and dry out. It seems, therefore, important to direct our efforts toward reuniting divergent trends ..."

R. Courant, 1953

1.2 Mathematical Modeling of the Eardrum

In the spirit of mathematical physics described by R. Courant, a mathematical model must have an intimate connection to the physical reality it is intended to describe. Dynamic behavior of the eardrum is governed by the conservation laws (mass, momentum, energy), and the thermodynamic entropy inequality. When applied to the tympanic membrane (TM), these physical laws can be used to derive mathematical expressions describing its behavior. Unfortunately, including all of the detailed anatomy, geometry, and ultra-structure of the eardrum when deriving the model is an immense, and perhaps imprudent, task. To create a moderately tractable mathematical model of the tympanic membrane it appears necessary to consider a simplified, idealized,

system. The degree to which the mathematics associated with the simplified system describes behavior of the eardrum, depends upon how well the idealization represents the actual physics. The simplification process and its associated reduction in physical content, raises the question: What physical axioms should be included in a tympanic membrane model? Part of the answer lies in how the model is to be used.

Many potential applications of the TM model can be found in clinical areas. Most current clinical methods used in assesment of hearing function rely on external acoustic stimuli such that the test results contain tympanic membrane factors. A mathematical model can help clinicians evaluate the eardrum, and can also be used to remove tympanic membrane factors from the data permitting a more direct examination of the inner ear. In addition to the audiological applications, it is desireable to have a model that can assess tympanosclerosis conditions and impairments caused by tympanoplasty. From a function and failure point of view, the model should also be capable of estimating dynamic stress and deflection fields under a wide variety of stimuli. To address energy transmission and noise related damage, coupling of the TM to the outer ear, ossicular chain, and tympanic cavity must be included. Deriving a model with these features requires detailed study of the geometry and ultrastructure of the eardrum. The ability to describe a range of geometries and fine structures will give the model the flexibility to describe individual diversity and differences between species.

Prior to actual formulation of the model, Chapter 2 reviews historically popular tympanic membrane models. This review is followed by two chapters discussing importance of various physical aspects of the drum. Chapter 5 contains the model derivation, while Chapter 6 discusses perturbations on the model caused by the Eustachian tube and middle ear air chambers.

To provide completeness and qualitatively describe the function of the TM, the following section briefly reviews the macroscopic anatomical construction of the hearing system.

1.3 Macro-Anatomy of the Hearing System

The hearing system in man and most mammals is generally discussed in terms of five broad subregions; the external ear, the middle ear, the internal ear, the ascending neuronal chain, and the auditory cortex. These subregions interact with each other in a nearly sequential way. External acoustic waves are first encountered by the pinna and external auditory meatus of the outer ear as indicated in Figure 1.1. The acoustic signal felt by the tympanic membrane differs both spatially and in amplitude spectrum from the external stimuli due to action of the outer ear (Rodgers, 1981; Stinson and Shaw, 1982;

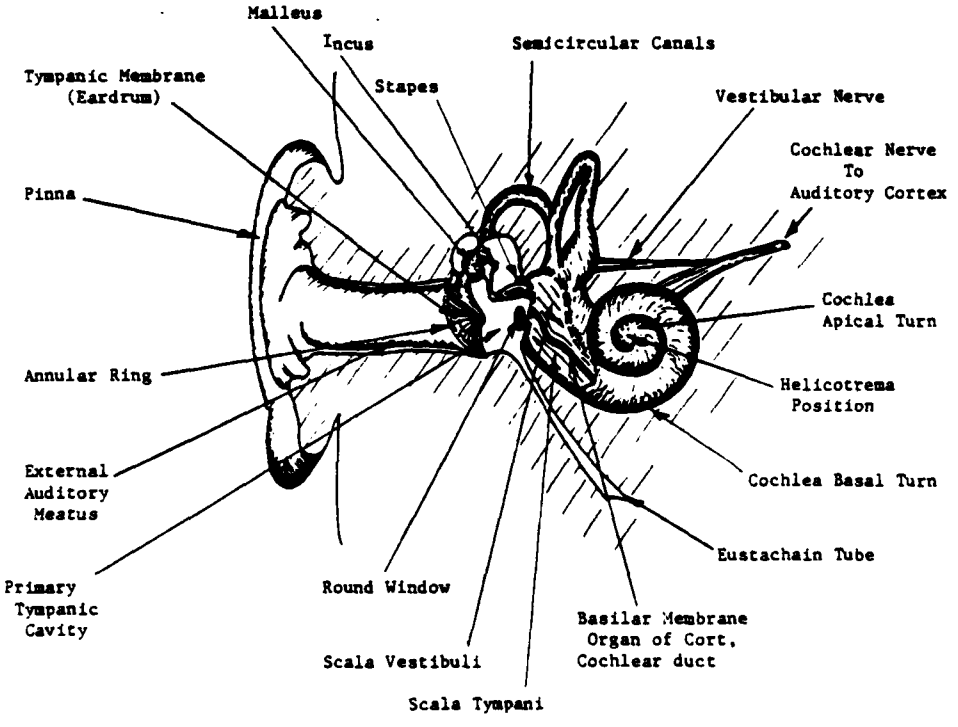

Fig. 1.1 Schematic of the Human Ear

Hudde, 1982). The eardrum is generally considered part of the middle ear with its external surface bounding on the external ear canal. The modified acoustic signal acting on the tympanic membrane causes stress and deflection of the membrane, coupling the acoustic signal to mechanical motion. The stresses in the membrane interact directly with the malleus bone of the middle ear. Stresses in the eardrum at its connection to the malleus provide the force imparted on the ossicles by the eardrum.

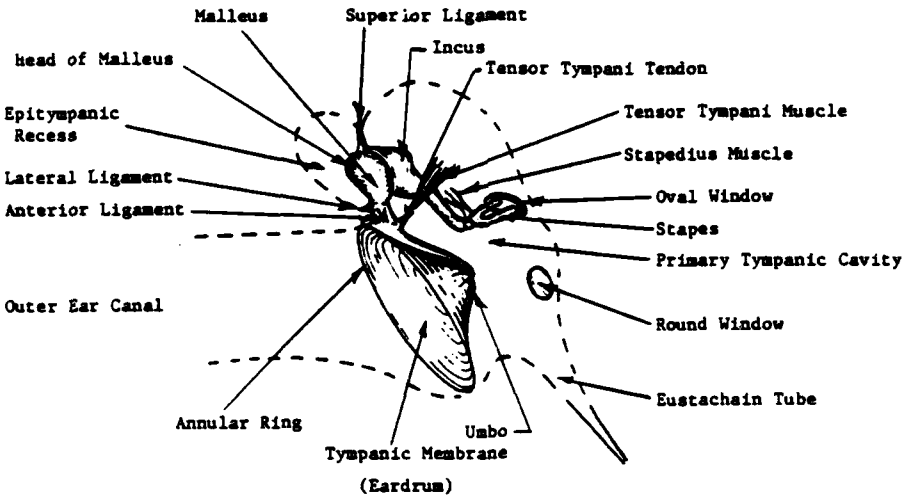

Fig. 1.2 Schematic of the Human Middle Ear

In addition to its coupling to the ear canal and malleus, the tympanic membrane interacts with the air (and fluid) within the primary middle ear air cavity. The spatial distribution of pressure within the primary cavity of the middle ear is dependent upon the spectrum of the stimuli, function of the

Eustachian tube, tensor tympani muscle action, and fluid in the cavity. For normal ears subject to acoustic stimuli well below 5 KHZ, the primary air chamber acts essentially as a closed cavity with homogeneous pressure and density. As shown in Chapter 6, for high frequencies the pressure distribution within the middle ear air chambers is not uniform.

In humans the eardrum is shaped like a shallow convex cone. The "cone" is inclined to the ear canal cross section and attached to the wall of the canal along the annular ring. Near the umbo (apex of the cone) the malleus is integrally attached to the tympanic membrane by woven fibers and tissue. Attachment of the malleus to the tympanic membrane becomes looser towards the annular ring (Graham, 1978).

These features of the tympanic membrane allow it to perform its primary function of converting acoustic stimuli into mechanical force and motion of the ossicles. The first ossicle, the malleus, is supported by three ligaments, a muscle, and the eardrum as depicted in Figure 1.2. The superior, anterior and lateral ligaments are passive supports having relatively low bending stiffnesses and high axial stiffnesses. In contrast, the tensor tympani when stimulated is capable of forcing the malleus inducing deformation and prestress in the tympanic membrane. Deflection of the malleus relative to its size is very small such that the malleus instant center of velocity is essentially stationary at a given frequency.

Attached almost rigidly to the malleus is the incus, the second ossicle. The incus is supported by the passive posterior ligament in addition to its strong connection to the malleus. Despite their apparent rigid attachment, the malleus-incus joint can partially decouple under specific strong overstimulation providing an apparent internal safety mechanism.

The tip of the incus forces the final ossicle, the stapes. The stapes is supported by a synovial joint at the incus tip and is bonded to the oval window membrane of the cochlea. A second primary muscle of the middle ear, the stapedius muscle forces the stapes transverse to the line of incus action providing active control of input from the stapes to the cochlea. When the stapedius muscle, is relaxed motion of the stapes is nearly rectilinear, imparting a piston like motion to the round window. Excitation of the stapedius kinetically constrains the stapes to a rocking motion, reducing the spatially averaged displacement of the oval window.

The cochlea is the final mechanical element in the auditory system and performs the conversion from mechanical motion to a discrete set of frequency and amplitude coded neural signals. The interpretation of neural signals generated in the cochlea is performed by the auditory cortex. To close the loop, feedback is sent from the neural system to active devices including the tensor tympani and stapedius muscles of the middle ear.

This brief description of the macro-anatomy of the hearing system is presented as an orientation for studying details of the mechanics of the tympanic membrane. Comments and descriptions of the system have been kept brief. In addition to the references mentioned, F. Netter (1900) has produced several very clear illustrations of the human hearing system.

CHAPTER 2

A CRITICAL HISTORICAL REVIEW OF TYMPANIC MEMBRANE MODELS

2.1 Introduction

Significant efforts to quantitatively describe the behavior of the middle ear in animals and humans dates back to the early eighteen hundreds. Prior to that time the gross anatomy and structure was known, however the description of the mechanics of the middle ear function in mathematical terms had not yet begun. Early theoretical modeling of the entire middle ear system, including the tympanic membrane, was started essentially without the aid of quantitative experimental data and with very little qualitative data. Despite this lack of experimental results and detailed anatomical descriptions, pioneer researchers quickly came to the (perhaps obvious) conclusion that the tympanic membrane plays a major role in the function of the middle ear. In fact, the tympanic membrane is responsible for a large percentage of the static force ratio apparent in the entire middle ear system.

The geometrical shape and structure of the eardrum is complex and has forced researchers to limit the degree of the actual physics contained in mathematical models of the system. Models of TM are created by considering a finite number of restoring, dissipation, and inertia mechanisms coupled with kinematics of the deformation. Various models currently in existence address different degrees, or levels, of physical content. The content of the model dictates its ability to reproduce experimental results, and more importantly, to predict untested behavior of the real physical system. Models appearing in the literature over the last century can be grouped into five basic catagories depending on the type of physical mechanisms contained in the model.

The groups are:

1. Lumped Parameter Models
2. Curved Lever Models
3. Stiff Plate Models
4. Membrane Models
5. Shell Bending Models

Even the simplest lumped parameter models are able to describe some of the behavior of the tympanic membrane, however distributed parameter models are necessary to describe actual stresses, vibrational shapes, and effects of structural changes on the system. To gain a global understanding of the catagories, each type of model will briefly be discussed pointing out some of their fundamental strengths and weaknesses.

2.2 Lumped Parameter Models

Lumped parameter models of the middle ear and the tympanic membrane are the earliest and simplest mathematical representations of the hearing mechanism. Perhaps due to their simplicity, the lumped (or discrete system) models have aged with the least controversy and have been the outstanding choice when incorporating eardrum models in comprehensive hearing models to date. The recent emergence of continuous (distributed parameter) systems of equations as the clear leader in the understanding of cochlear mechanics has initiated a move away from the discrete models toward a more realistic description of the physics (Steele 1976; Holmes and Cole 1983). It seems clear that detailed descriptions of the tympanic membrane will also require continuum modeling in order to overcome some of the shortcomings of discrete models.

Historically, the first lumped parameter models considered the tympanic membrane to act like a piston in a cylinder forcing a pushrod connected to the manubrium. The result of such a simple model is an algebraic equation relating the average sound pressure level at the tympanic membrane to the force developed at the manubrium tip (Esser, 1947). More recent models have

incorporated average transverse inertia terms as well as dissipation terms in order to more accurately reproduce the experimental data. In many of the common lumped parameter models the tympanic membrane is represented as a second order ordinary differential equation (or a system of n first order differential equations). One of the more widely used models is an electrical anology presented by Zwislocki (1962) as outlined in Figure 2.1.

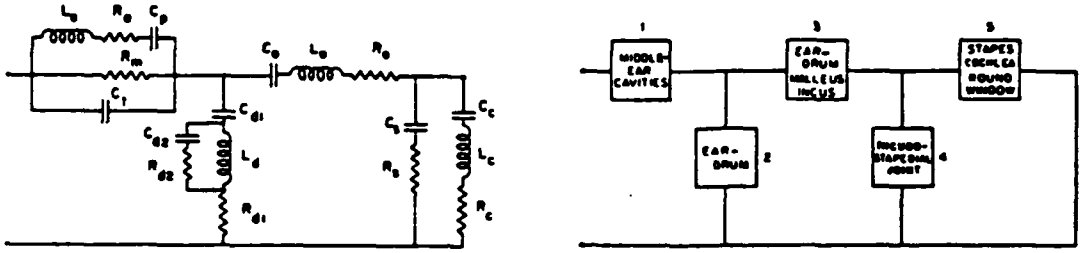

Electric analog of the normal ear.

Block diagram of the middle-ear mechanism.

Figure 2.1 Zwislocki's (1962) circuit model of the middle ear.

The model has the ability to reproduce some experimental data including components of reactive and resistive acoustic impedance over a range of forcing frequencies. Improvements in the discrete models have been presented by many researchers including Zwislocki, Moller, Nuttall, Fischler, Rubenstein, and

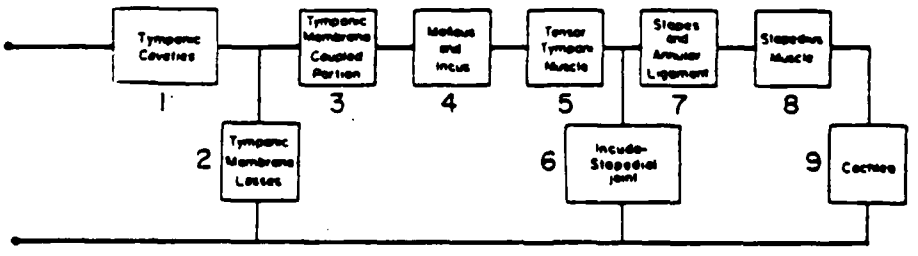

Figure 2.2 Nuttall's (1974) modification of the lumped parameter circuit model.

Stuhlman. These improvements essentially amount to increasing the degrees of freedom of the ordinary differential system. As an example, Figure 2.2 indicates the lumped parameter system suggested by A. Nuttall (1974) modeling tympanic muscle effects on middle-ear transfer characteristics. To improve the ability of the lumped parameter models to reproduce experimental data above 4 KHz, Shaw (1977, 1982) modeled the TM as two coupled pistons doubling the degrees of freedom over original models. The lumped parameter models are able to reproduce some of the global features of the so-called middle ear transfer function, however they have no hope of predicting transmission alterations caused by tympanoplasty applied directly to the membrane structure and are not suited to describe vibrational modes or shapes of the eardrum. The numerical values of parameters (resistance, inductance, capacitance) used in the lumped parameter models are usually selected on the basis of fitting experimental test data curves. This method of selecting the parameter values can optimize the ability of the model to reproduce experimental data, but may remove any real physical meaning attached to the numerical values. Without a physically based derivation of the parameter values, it is very difficult (or impossible) to predict alteration of the values related to changes in the system. When using the discrete models it is usually necessary to conduct a series of tests on systems that have been altered and attempt to correlate changes in the parameters necessary to reproduce the results.

In an effort to describe the vibrational shape(s) of the tympanic membrane in terms of its physical features and sound pressure(s) applied, the discrete models must be expanded to higher dimensions. The obvious step is to consider a series of continuum models, each model in the series containing varying degrees of the actual physics of eardrum. The earliest of the continuum models was presented by Helmholtz, published in the middle eighteen hundreds.

2.3 Curved Lever Models

The pioneer continuum type model of the tympanic membrane was presented by Helmholtz in a paper entitled "The Mechanism of the Ossicles of the Ear and Membrana Tympani" in which he presented the 'curved membrane' theory of the mechanism of the tympanic membrane. No explicit model was presented, in fact a complete mathematical representation and solution of the mechanism remains open; however, a physical mechanism describing action of the ear drum was given. The theory rests on the convex cone shape of the tympanic membrane. If we imagine that the membrane consists of a number of curved radial fibers connecting the malleus to the annular ring, then it is possible to describe a 'lever type' action of each of the radial fibers acting on the malleus. To illustrate this, Figure 2.3 shows a single radial curved fiber attached rigidly to the annular ring exposed to a pressure differential P. If the fiber is essentially inextensible then inward displacements of the manubrium will be accompanied with an increased radius of curvature of the fiber, and outward displacements of the manubrium will be accompanied with a diminished radius of curvature. These changes in curvature alter the distance between the endpoints of particular radial fibers causing the manubrium to move accordingly (Fig. 2.3). The kinematics described converts large displacement (low force) motions of the membrane into small displacement (high force) motions of the manubrium and hence inherits the name curved lever model.

The original curved membrane theory presented by Helmholtz assumed that the radial fibers were inextensible and that changes in curvature of the radial fibers was opposed by elastic behavior of the circumferential fibers. This premise of Helmholtz's curved membrane theory is reasonable only if the radial stiffness is much greater than the circumferential stiffness.

Experimental data indicates that the bending modulus of the drum material in the radial direction is the same order of magnitude as the bending modulus in the circumferential direction (von Bekesy, 1948; Kirikae, 1960). Due to the fiber composite structure, this bending stiffness observation does not imply the same conclusion for membrane type stiffnesses (see Chapter 3). The membrane stiffnesses may be more orthotropic than the bending stiffnesses. Several authors have argued that the relatively isotropic bending stiffness discounts the curved membrane theory (Funnell and Laszlo, 1978; Khanna and Tonndorf, 1972). It should be pointed out that axial stiffnesses are appropriate to use in such an arguement, not bending stiffnesses. Secondly, the restoring mechanism in the curved lever theory need not be restricted to extension of the circular fibers, but is more likely connected to the total

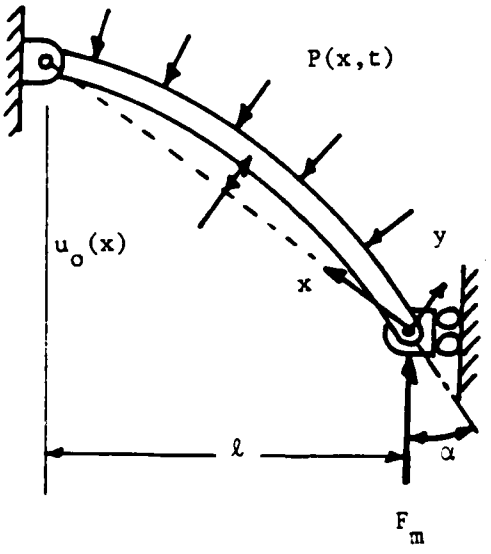

Figure 2.3. Using a static force balance, and assuming small deformations, the force per unit length on the mallus due to one radial fiber has the form $F_m \sim P[\cos(\alpha)(\frac{\partial^2 u_o}{\partial x^2})^{-1} + \ell/2]$.

deformation through a general anisotropic constitutive law. Hence, historical arguments used to justify neglecting radial curvature and anisotropic construction are not valid these items may indeed play a first order role.

In the middle 1940's, prior to Lim's work, Esser (1947) formalized Helmholtz's curved membrane theory into an axisymmetric set of equilibrium equations relating the stress to the curvature, thickness, and applied pressure. The static equations used by Esser are axisymmetric pressure vessel equations and are given by:

$$\frac{d}{dr}(rh\sigma_m) - h\sigma_t = 0$$
$$h\sigma_m \frac{d}{dr}(\cos\alpha) + h\sigma_t \frac{1}{r}\cos\alpha = P \qquad (2.3.1)$$

where P is the applied pressure, σ_t is the tangential stress, σ_m is the meridian stress, h is the thickness α is the local angle of a normal from the membrane surface, and r is the radial position coordinate.

Since the stresses depend on the deformation, and since α also depends on the deformation, the equations are nonlinear. Esser considered several simplified forms as assumed stress states in order to estimate the effective static "lever ratio" of the membrane as predicted by Helmholtz. Essers' approximate solutions indicate that curvature may indeed play a role in the function of the tympanic membrane. Although the results of Esser may be written in terms of a "lever ratio", it should be noted that dynamic effects, quasilinearities in stress, nonsymmetric shape, and kinematic coupling were not considered. (For an indication of the mathematics involved in expanding the equations to the case of "Thin Elastic Membranes" see Pujara and Ladner, 1978, or Yang and Feng, 1970.) Omission of these factors makes the "model" inadequate for comprehensive study, and should simply be viewed as evidence

of the importance of curvature and membrane type stress.

The curved membrane theory was rekindled by Tonndorf and Khanna (1972) with their suggestion that the restoring force may be due to shearing of the radial fibers over the circumferential and parabolic fibers rather than the original extensional restoring force. The modified theory maintains the "lever type" action of the membrane and allows both sets of primary fibers to have similar elastic moduli imbedded in a base material having a much lower stiffness. One difficulty with the modified theory is that the circular fibers must slide a distance of approximately two diameters over the radial fibers during a typical deformation if both sets of fibers are indeed inextensible (Tonndorf and Khanna, 1972). This distance seems large when one considers that almost no material exists between the two sets of fibers (Lim, 1968 a,b, 1970). Calculations done in Chapter 3 indicate that the membrane indeed contains an internal lever system, however, the restoring mechanism may be dominated by tension and bending terms rather than the shear or extensional mechanisms mentioned above. The experimentally based results of Chapter 3 also show that the membrane stress induced in the radial fibers by a positive pressure is extensional rather than compressive, discounting the original curved lever mechanism postulated by Helmholtz.

2.4 Membrane Models

The "curved membrane" model initialized by Helmholtz includes kinematics associated with curvature and normal membrane type stresses. Elementary stresses in the plane of a thin material surface are considered of the membrane type if their resultant bending moment is zero on every normal cut

through the surface; mathematically this means:

$$\int_S \int_{-h/2}^{h/2} \sigma z \, dz \, ds = 0 \qquad (2.4.1)$$

where σ is the stress tangent to the middle surface, z is the distance from the neutral surface, h is the thickness, and s is an arbitrary curve in the middle surface. With this definition, a mathematical model is considered a membrane model if membrane type stresses are the only stresses considered when formulating the model. Simple membrane models assume that the membrane stress is uniform through the thickness, and that variations in the stress resulting from deformation are small relative to some initial stress. More detailed membrane theories, such as presented by Yang and Feng (1970), are able to describe changes in membrane stress due to applied pressures and resulting deformation. Membrane equations or theories used to model the tympanic membrane have addressed simple linear membrane theory for "small" deformations and "large" initial prestress.

Early attempts to model the tympanic membrane as a vibrating membrane, having only membrane type stress as the restoring mechanism, are represented by Franks' (1923) flat membrane model. The differential equation considered by Frank was the simple linear membrane equation subject to a fixed circular boundary condition and radial manubrium constraint

$$\sigma h \nabla^2 u + P = h\rho \frac{\partial^2 u}{\partial t^2} \quad , \qquad (2.42)$$

where u is deformation normal to the membrane surface, ρ is the mass density, σ is the in-plane tension, P is the applied normal pressure, h is the thickness, t is time and ∇^2 is the Laplace operator.

A numerical solution of the curved membrane problem, subject to the relatively complex boundary conditions imposed at the manubrium and annular ring, was not practical at the time, forcing Frank to simplify the problem

such that an analytical solution could be found. For simplicity Frank elected to consider a round, flat, isotropic membrane having the manubrium attached along one radial segment pivoting at the annular ring. His results can be used to suggest areas of maximum deflection and estimate possible vibrational shapes at low forcing frequencies; the restrictive assumptions however, prevent the model from being of much practical use.

Proceeding along the same lines as Frank, Funnell (1975) relaxed assumptions on the circular shape and manubrium attachment in order to model the cat eardrum (as well as several other mammals). Funnell also assumed a flat isotropic membrane operator, however he imposed more realistic boundary conditions at the malleus and annular ring. A solution of the membrane equations subject to boundary conditions was estimated using a finite element

Figure 2.4 Experimentally recorded time averaged vibration shapes of the the cat eardrum (retouched from Khanna and Tonndorf, 1972).

approximation. The tension used in the model was adjusted such that the calculated vibrational shapes corresponded to the shapes observed in experiment

at selected frequencies. Using this method, Funnell was able to reproduce a transition from the fundamental vibratory shape into a rather complex shape similar to that observed experimentally (Fig. 2.4). The amplitude and transmitted force predicted by the plane membrane model corresponded in a gross qualitative way to experimental results, however, the connection "was not of the quality desired in a tympanic membrane model" (Funnell, 1975). The vibrational shapes corresponded quite well to the observed shapes; it should be noted however, that the shapes are generally insensitive to the particular model and restoring forces selected. The qualitative shape of vibration at low frequency is influenced strongly by the boundary shape and constraints, and is less sensitive to the type of restoring forces.

The qualitative picture obtained using plane membrane models is quite informative, but we must remember that the model neglects initial curvature of the drum, ignores bending stiffness, and disregards bending dissipation. In addition to these primary factors, the membrane type models discussed neglect quasilinear stress terms, anisotropic construction, rotary inertia, and similar terms that could be included in the membrane type equation(s).

2.5 Shell Bending Models

In addition to membrane type restoring forces, it is clear from experimental observation that bending terms also play a role in deformation of the tympanic membrane. The fact that the eardrum maintains its shape after it has been removed from its supporting structure can not be explained using membrane stresses alone, and requires inclusion of bending type restoring forces (Gram, 1968). The bending mechanism, however, may be secondary in the vibrating drum due to pressure induced membrane stress and tensor tympani prestress.

If a surface with thickness undergoes a change in curvature, then in general nonuniform strain is induced across the thickness. For materials having some elasticity, the strain will be resisted by stress such that strain energy will be stored or released due to the changes in curvature. If a particular model contains terms describing this energy, then the model is said to contain "bending type" restoring forces. For example, the Kirchhoff plate equation given below is the simpliest of the plate bending theories

$$- D \nabla^2\nabla^2 u + P = \rho h \frac{\partial^2 u}{\partial t^2} \quad , \tag{2.5.1}$$

where D is the bending stiffness, u is the deflection normal to the plate, P is the applied pressure, h is the thickness, ρ is the mass density, t is time and ∇^2 is the Laplace operator. In the form given, the Kirchhoff plate equation assumes the plate is flat, isotropic, uniform, undergoes small amplitude deformations, has no membrane type stresses or deformations, and moves at low frequencies. Some of these assumptions can be relaxed by considering the Von Karman plate or shell equations containing bending and membrane type restoring forces. Early models of the tympanic membrane have neglected one or the other of the two primary restoring mechanisms. Some membrane type models have already been discussed. In addition to the models containing purely membrane type stresses, models have been formulated containing purely bending type terms. In reality both effects exist in the tympanic membrane, but for the sake of mathematical simplicity, researchers have historically considered the most degenerate forms that seemed reasonable. Following experimental observations by Bekesy that indicated larger bending effects than had previously been considered, Gram (1968) modeled the eardrum as a simple flat, isotropic Kirchhoff plate. He computed an approximate solution subject to simply supported edge conditions and simple support at the manubrium using the

Rayleigh-Ritz method. From the results of his model, he calculated the stiffness of the plate that would be required in order for the model results to match the experimental impedance data. In order to match the data, the model plate required a stiffness two orders of magnitude larger than the actual stiffness measured in experiment (Bekesy, 1948; Kirikae, 1960). This discrepency strongly suggests that the model is not appropriate for the eardrum.

The first attempt to include both the "curved cone" shape of the drum along with bending type restoring forces was presented by Funnell and Laszlo (1977) in the form of a finite element approximate solution of a thin shell model of the cat eardrum. The finite element method is clearly an effective way for estimating solutions to some particular differential system of equations and constraints, however the ability of the approximate solution to describe the behavior of the physical system under study depends on the original set of differential or integral equations used. Funnell and Laszlo elected to use a static (or low frequency) thin shell functional in which shell bending stresses were the primary restoring forces considered in the original equations. The functional used contained membrane type terms, however, Funnell and Laszlo did not impose any prestress and did not consider the fibrous ultrastructure such that the membrane restoring forces were of second order. The use of bending stress as the physical mechanism storing strain energy during the deformation had often been considered secondary to other mechanisms in earlier models. Helmholtz's original curved membrane theory postulated tension in the circumferential fibers as the dominant restoring force, and Tonndorf and Khanna's version of the curved membrane theory considers internal axial shear as the dominant storage mechanism. This change in the model content is somewhat masked by the fact that Funnell and

Laszlo were the first to apply a computationally intensive method (finite element) to the eardrum problem.

The restoring force(s) considered in a particular model alter the mechanism by which the tympanic membrane interacts with the manubrium and the annular ring, and thus may alter predicted transmission characteristics of the drum. The curved membrane models predict the tympanic membrane will force the manubrium through a membrane stress in the radial fibers while the shell bending model forces the manubrium through transverse shear and moment terms. This difference in the mechanism of force transmission may be the primary

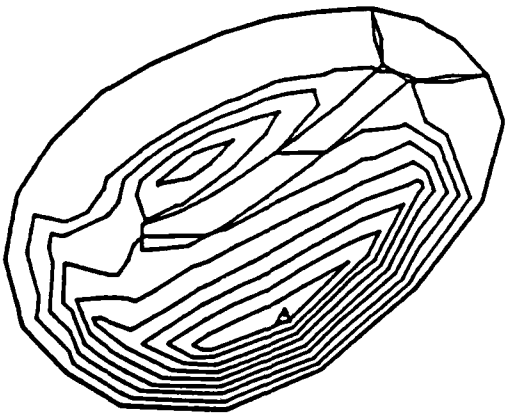

Figure 2.5 Vibration pattern calcuated by Funnell and Laszlo, 1977. The contour lines are lines of constant vibration amplitude, equally spaced on an amplitude scale. Only displacements shown correspond to the component of displacement measured in the holographic experiments of Khanna and Tonndorf. The small triangle represents the point of maximal vibration amplitude, corresponding to 0.32 μm for a low-frequency pure-tone input of 100 dB SPL. (From Funnell and Laszlo, 1977.)

difference between the model types. In a purely small deformation bending model it is not possible to have the internal 'lever action' of the membrane that is inherently contained in membrane type models. Although the force transmission values are expected to differ considerably when the restoring mechanism is changed, the fundamental vibrational mode shape will qualitatively remain unchanged. Figure. 2.5 shows a numerical plot of deformation of the tympanic membrane of a cat when forced at low frequencies (Funnell and Laszlo, 1977).

An apparent shortcoming of the isotropic thin shell model is that natural asymmetric modes of vibration (realized as peaks on the "Malleus tip vs. TM amplitude graph") appear with spacing of $(2n)^2$ (n = 1,2,3). The $(2n)^2$ spacing is wider than that seen experimentally (Manley and Johnstone, 1974). The thin shell model with no damping is also unable to reproduce decreases in malleus motion with frequency and average phase shift observed experimentally (Manley and Johnstone, 1974; Moller, 1972).

Despite some inconsistencies with experimental work, the vibrational shape calculated by Funnell and Laszlo is very similar to the shape that has been observed experimentally for low forcing frequencies. At higher frequencies, when inertia is added the bending shell model does not reproduce the complicated vibrational shapes observed in vibrating eardrums. It is expected that this behavior is directly tied to the anisotropic membrane stress and construction of the drum, and cannot be reproduced using a simple isotropic shell bending model.

2.6 Stiff Plate Models

In the early 1940's George von Bekesy recorded the first measurements of the vibrating human eardrum using a capacitive probe on fresh cadaver specimens.

His measurements, at frequencies below 2000 Hz, indicated that the tympanic membrane has a vibrational shape similar to a flat plate rotating around a pivot near the head of the malleus. Displacement of the eardrum in the stiff plate mode is sketched in Figure 2.6. The shape von Bekesy inferred from his data is now known to be incorrect, however it is worth mentioning due to its historical significance and influence on middle ear research.

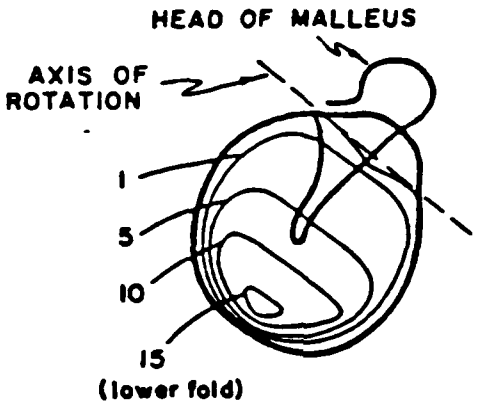

Figure 2.6 Stiff plate vibration pattern of the human tympanic membrane as reported by von Bekesy (1941).

From a modeling point of view, the stiff plate concept, if correct, would mean the tympanic membrane would admit nicely to a discrete or lumped parameter model. In fact, belief that the drum vibrates as a stiff plate gave rise to simple discrete modeling concepts like the drum effective area, as a fraction of the actual frontal area, to be used as a hydraulic lever area. Existence of the shape suggested by von Bekesy requires the eardrum to bend and deform drastically in the lower part and has directed past researchers to look for a 'lower fold' that is now known not to exist. If such a fold did exist it would place significant structural constraints on the tympanic membrane. Inspection of the membrane structure itself would suggest that a 'lower fold' is not expected. It is assumed that von Bekesy arrived

at the stiff plate theory on the basis of experimental data that was not as point sensitive as he expected.

2.7 Concluding Remarks

Of the four model types discussed, the lumped parameter models have commanded the vast majority of attention in the literature and have provided tools for interpreting some clinical data. The lumped models, however, are by nature unable to describe detailed vibrational behavior of the drum and are often linked to the actual physics only through parameter curve fitting. In the interest of gaining a more complete understanding of the middle ear function, higher order discrete systems or continuous system models must be addressed. Mathematically, the only complete continuum formulation to date is the bending shell model presented by Funnell and Laszlo that uses standard small deformation isotropic shell theory. The highly anisotropic fiber construction of the drum has motivated others to formulate partial models based on restoring mechanisms other than the shell bending device. Complete mathematical representations of the tension of shear (other than bending) models has not been presented and, hence, results from such models are not available for evaluation.

One important point that appears to be lacking in the literature is a systematic evaluation of possible restoring mechanisms along with inertial and damping devices within the actual tympanic membrane. Analysis and discussion contained in the following four chapters will center around determining the primary mechanisms governing action of the tympanic membrane and deriving mathematical descriptions of the physics. As a starting point, the ultra-structure of the eardrum is studied in order to estimate its mechanical properties. Once the properties are known, restoring and dissipation is

addressed followed by formulation of dynamic equilibrium equations to complete the model. A special closed form asymptotic solution of the model is determined in Chapter 5 by using natural small parameters appearing in the system equations.

CHAPTER 3

TYMPANIC MEMBRANE ULTRASTRUCTURE AND STIFFNESS DECOMPOSITION

3.1 Introduction

The human tympanic membrane can be divided into two regions having distinct tissue ultrastructures. Pars tensa represents a majority of the drum with the exception of a small triangular region superior to the short process of the malleus that consists of pars flaccida (Fig. 3.1). The annular ligament provides a distinct border between the external auditory meatus and the pars tensa. Bordering the pars flaccida however, the annular ligament terminates making the pars flaccida integral with the external auditory meatal skin (Lim, 1970). For adults the major diameter of the annular ring ranges from 9.0 to 10.2 mm and the minor diameter ranges from 8.5 to 9.0 mm.

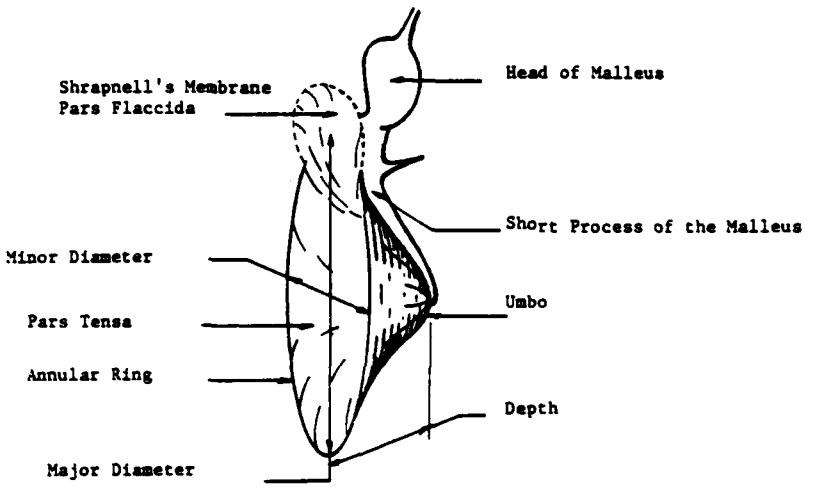

Figure 3.1 Sketch showing gross anatomical regions of the human tympanic membrane.

Tympanic membranes of other mammals including cats, guinea pigs, rabbits, and squirrel monkeys have gross anatomical properties similar to that of human, although the size and shape of the membranes vary as well as the fraction of total area accounted for by pars flaccida (Funnell, 1975). The shape of the pars flaccida region is generally triangular or half elliptical, depending on the particular mammal, with the base of the triangle or half ellipse contacting the skin of the outer ear canal. The pars tensa of the rabbit has approximately four times the surface area as the pars flaccida, approximately eight times for the cat, and fifteen times for the squirrel monkey. An exception reported by Lim (1968b) is the sheep having a pars tensa of approximately twice the area of the pars flaccida.

Correcting some historical misconceptions, Lim (1968a, 1968b, 1970) has shown by light and electron microscope investigations that the pars flaccida is generally thicker than the pars tensa. The pars flaccida of the rabbit is 20 to 30 times thicker than the pars tensa and the sheep pars flaccida is 10 to 20 times thicker than the pars tensa (Lim, 1968b). Historically, the thickness of the pars flaccida was believed thinner based on experimentally observed large static deflections of the pars flaccida (Shrapnell, 1832). This misinterpretation of experimental observation resulted from not knowing or understanding mechanical stiffness properties of the membrane tissues. It was later discovered that the ultrastructure of pars flaccida and pars tensa regions are quite different resulting in different mechanical properties (Nishiyama, 1937; Lim, 1968a,b).

From a modeling point of view, if we wish to accurately predict deformation and behavior of the tympanic membrane the mechanical properties must be known. Viewing the eardrum as a general Von Karman composite shell, there may exist as many as 36 independent mechanical stiffness constants at each point

in the drum. Due to the membrane's small size, fragile cellular structure, and post-mortem changes, current testing technology is not able to measure all of the mechanical stiffnesses. Even if such an ability did exist, individual diversity of ultrastructure including scar tissue, tympanoplasty, and normal differences would also need to be measured and understood. Rather than attempting to develop an advanced mechanical testing ability, analytical estimation of the mechanical properties based on the local membrane ultrastructure seems to be a much more tractable and reasonable task. Study of the fine ultrastructure of the pars tensa and pars flaccida allows estimation of their mechanical stiffnesses based on properties and geometry of the tissue components.

To derive estimates of mechanical properties of the tympanic membrane at various locations, we must study its ultrastructure. Figure 3.2 shows a cross sectional view of the pars tensa of a squirrel monkey (Lim 1968a).

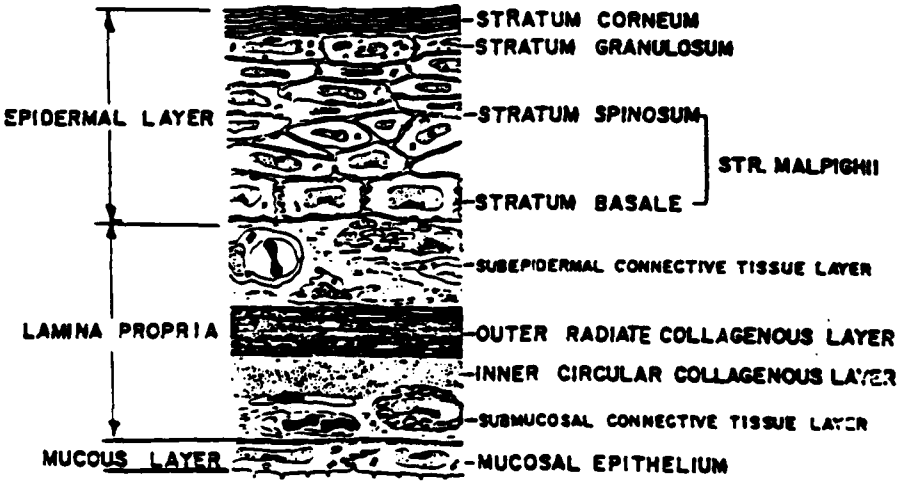

Figure 3.2 A schematic of a radial cross sectional view of the pars tensa of the squirrel monkey (from Lim, 1968a).

The pars tensa region of the tympanic membrane is constructed of several layers of tissue bonded together in a laminate structure. The three primary layers are the outer epidermal layer, the middle lamina propria, and the inner mucous layer. (The following descriptions are condensed from Lim, 1968a.)

Epidermal layer

The epidermis is divided into the stratum corneum, the stratum granulosum, and the stratum Malpighii. The stratum corneum is a thin layer consisting of degenerate compressed cellular structures. Directly inside of the stratum corneum, two layers of keratohyalin granules form the stratum granulasum. The outer part of the stratum Malphigii is stratum spinosum consisting of several layers of squamous cells. Cells in the stratum spinosum are not as compressed as in the stratum granulosum having more intercellular space. The squamous cells are bordered by abundant desmosomes which Lim (1968a) suggests act as "tightening apparatus which bound each cell together". The stratum basale is the innermost layer of the epidermis and consists of a single layer of cells separated from the connective tissue by a membrane.

Lamina propria

The lamina propria contains the strong fibers of the tympanic membrane separated from the epidermus and mucous by connective tissues. The subepidermal connective layer consists of loose typical collagen fibrils, loose protocollagen fibrils, fibroblasts, and nerve fibers. Neurosecretory granules, neurofilaments, and neurovesicles exist in the nerve fibers. Tissue of the connective layer blends between radial fibers of the outer radiate collageneous layer. Between the radial and circular fiber layers, a thin parabolic fiber layer exists in humans (Lim, 1970). The subepidermal connective layer and the radial fiber layer are generally more developed than

the parabolic and circular fiber layers. The radial and circumferential fibers consist of fine fibrils having rectangular or square cross sections. The fine fibrils are mixed with typical collagen fibrils. In general, the fine rectangular fibrils dominate in both the radial and circular layers, however, in humans more collagen fibrils are found in the circular layer. The rectangular fibrils do not show tropocollagen banding and are finer in size (approx. 50A vs. 200 - 400A for typical collagen). Some indirect evidence suggests the fine fibrils are reticulin based (Ciges, 1965) or keratin based (Hamiton, 1967). The circular fiber layer borders on the innermost lamina submucosal connective tissue layer. Content and structure of the submucosal layer is similar to the subepidermal layer, except that the submucosal layer is thinner.

Mucous Layer

The innermost layer bordering on the tympanic cavity is the mucous layer composed mostly of simple squamous epithelial cells. Near the annular ring some cuboidal cells and cilia are found. No tonofilaments, kerato hyalin granules or secretory granules are found in this thin layer.

These comments on the ultrastructure of the pars tensa are very condensed. Quantitative content and size of the various layers changes with position on the tympanic membrane and with species. In addition to local structure, blood vessel (Politzer, 1892) and nerve fiber (Wilson, 1907) networks have been documented macroscopically. More detailed descriptions of the cellular structure including brief historical accounts and photomicrographs can be found in Lim (1968a,b, 1970).

The ultrastructure of the pars flaccida differs from that of the pars tensa primarily in the lamina propria. Lim (1968b) has shown that a lamina propria does exist in the pars flaccida, however, contains no organized fiber

structures similar to the radial or circular fibers found in the pars tensa. The fine "rectangular" fibrils of the radial and circular fibers are not found in the pars flaccida. Larger collagenous fibers are organized into a thin cloth within the lamina propria of the pars flaccida imbedded in a substantial amount of extracellular amorphous ground substance. This ground substance and lack of a middle fibrous layer make the thicker pars flaccida more translucent than the pars tensa. The lamina propria of the pars flaccida also contains abundant elastic fibers not found in the pars tensa.

Both the pars tensa and pars flaccida consist of relatively stiff fibers imbedded in relatively flexible base materials. The geometry, orientation, and fiber fractions dictate mechanical behavior of the material(s). In general, for a fiber composite material of this type, the first order linear constitutive law has the form

$$\begin{aligned} \underset{\sim}{N} &= \underline{Q}\ \underset{\sim}{\varepsilon} + \underline{B}\ \underset{\sim}{k} \\ \underset{\sim}{M} &= \underline{B}\ \underset{\sim}{\varepsilon} + \underline{D}\ \underset{\sim}{k} \quad , \end{aligned} \tag{3.1.1}$$

where $\underset{\sim}{N}$ is the normal force vector, $\underset{\sim}{M}$ is the moment vector, $\underline{Q}$ is the membrane stiffness matrix, $\underline{B}$ is the membrane-bending coupling matrix, $\underline{D}$ is the bending stiffness matrix, $\underset{\sim}{\varepsilon}$ is the strain vector, and $\underset{\sim}{k}$ is the curvature vector.

We would like to determine constants appearing in the matricies in terms of the ultrastructure of the tympanic membrane. To simplify the equations, define a local cartesian coordinate system (x,y) coincident with the direction of the radial and circular fibers. Since the inner circular fibers are approximately orthogonal to the outer radial fibers, selecting the local x axis to coincide with a radial fiber will result in y running approximately along a circular fiber (Fig. 3.3).

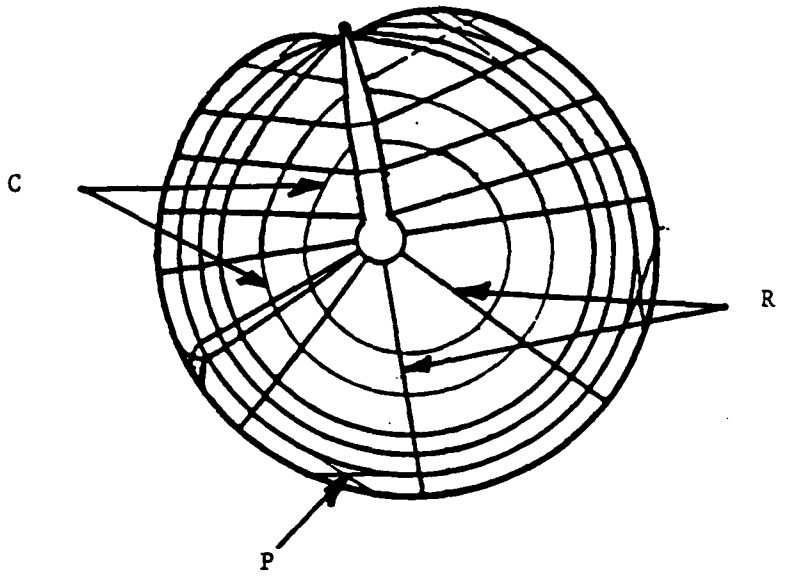

Figure 3.3. Sketch of the fiber arrangement of the human tympanic membrane. R: radial fibers; P: parabolic fibers; C: circular fibers (based on Shimada and Lim, 1971).

As a first approximation it is assumed that the radial and circular fibers represent a majority of the stiff fibers. The material is idealized mechanically as consisting of a set of locally orthogonal radial and circular fibers imbedded in a base tissue. Mechanical properties of the fibers and base material are independent and combine to give global stiffnesses in eq. (3.1.1). Based on this idealization, the bending stiffnesses, membrane stiffnesses, and torsional stiffnesses will be estimated in the local circumferential and radial directions using the geometry and properties of constituent components.

3.2 Membrane Stiffness

The membrane stiffness represents the resistance to tensile deformation in the plane of the membrane. This stiffness is analogous to Young's modulus

for isotropic materials multiplied by the thickness. For the idealized material, Appendix A approximates the membrane stiffness in the direction of the i fiber as (i may represent only the radial direction or the circular direction)

$$Q_i \sim \frac{1}{\lambda_i}\left\{\frac{E_b}{1-\nu_b^2}\left(h\lambda_i - \frac{\pi d_i^2}{4}\right) + \frac{E_i}{1-\nu_i^2}\,\frac{\pi d_i^2}{4}\right\} \quad , \tag{3.2.1}$$

where the subscript b represents the base material, d is the equivalent fiber diameter, h is the total thickness, λ is the center to center fiber spacing, E is the elastic moduli for the constituent, and ν is Poission's ratio for the constituent.

Using estimates for the cat (Funnell, 1975) $h = 40 \times 10^{-4}$cm, $d_i = 8 \times 10^{-4}$ cm, $E_b = 10^8$ dyn/cm^2, $E_i = 10^{10}$ dyn/cm^3, $\nu_b = \nu_i = 0.3$, we find for sparse fiber spacing that $Q_{i\text{-sparse}} \sim 4.4 \times 10^4$ dyn/cm. For tight spacing with the fibers touching each other $Q_{i\text{-tight}} \sim 6.9 \times 10^6$ dyn/cm. In the radial direction, most of the membrane is packed very tightly with radial

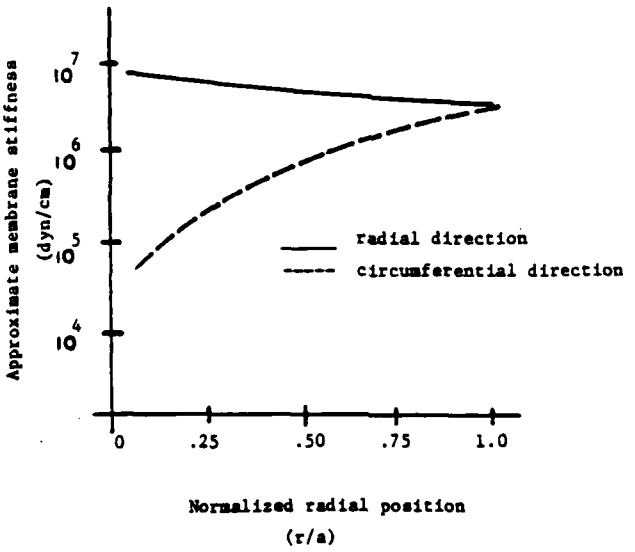

Figure 3.4 Estimated membrane stiffness vs. radial position.

fibers (Shimada and Lim, 1971). In the circular direction, however, spacing is relatively tight near the annular ring but becomes very sparse near the umbo. Hence, membrane stiffness is highly anisotropic particularly near the umbo. Figure 3.4 graphically shows estimates of the axial stiffnesses in the radial and circumferential directions for various positions on the tympanic membrane. If we were to calculate the effective elastic moduli in the radial direction near the umbo based on the total thickness the result would be $E_m^* = 8.6 \times 10^9$ dyn/cm^2. No experimental data of the membrane in pure axial tension has been reported, and hence, we have no data to compare to this stiffness. The numerical values used to calculate the axial stiffness are physically consistent with the types of materials in the actual drum. In fact, it will be shown in the following section that the above values reproduce elastic moduli derived from bending stiffness tests.

3.3 Bending Stiffness

By applying the Kirchhoff hypothesis for bending of shells, it is possible to derive the bending stiffness of the idealized drum material in terms of its construction and constituent materials. By integrating the curvature induced stress over the cross section (see Appendix A) the bending stiffness for the i direction is estimated to be

$$D_i \sim \frac{E_b}{1-\nu_b^2}\left\{\frac{h_2^3 + h_1^3}{3} - \frac{\pi d_i^4}{64\lambda_i} - a_i^2\, d_i^2\, \frac{\pi}{4\lambda_i}\right\} + \frac{E_i}{1-\nu_i^2}\left\{\frac{\pi d_i^4}{64\lambda_i} + a_i^2\, d_i^2\, \frac{\pi}{4\lambda_i}\right\} \tag{3.3.1}$$

In addition to the parameters defined in (3.2.1), a_i is the distance from the i layer to the neutral surface in the i direction, h_1 is the thickness above the neutral surface, and h_2 is the thickness below the neutral surface.

Fibers of the eardrum are much stiffer than the supporting cellular structure forcing the neutral surface to be centered in the middle fiberous layer. Hence, for the eardrum eq. (3.3.1) approximately reduces to

$$D_i \sim \frac{E_b}{1-\nu_b^2}\left\{\frac{h_2^3 + h_1^3}{3} - \frac{d_i^4}{4\lambda_i}\right\} + \frac{E_i}{1-\nu_i^2}\,\frac{d_i^4}{4\lambda_i} \quad . \tag{3.3.2}$$

Using parameter estimates from the previous section we find for a tightly packed fiber spacing, representative of the radial direction near the umbo, that the bending stiffness is approximately 1.37 dyn-cm. This stiffness remains essentially constant as the fiber density is changed because it depends primarily upon the base material parameters. Insensitivity of the bending stiffness to fiber densities explains why von Bekesey (1949), and Kirikae (1960) experimentally measured a homogeneous bending stiffness value across the pars tensa. The fact that the bending stiffness is approximately homogeneous has been misinterpreted by some researchers as indicating that the drum acts isotropically.

Despite the nearly homogeneous bending stiffness, comparison to analytically estimated membrane stiffnesses indicates that the pars tensa is highly anisotropic. To illustrate this, if the material is treated as a single phase material then Young's modulus can be extracted from the bending stiffness using $D_i = E_d^* h^2/12(1-\nu^2)$. For $D_i = 1.37$ dyn-cm and $\nu = 0.3$ we find Young's modulus from the bending stiffness to be $E_d^* \simeq 2.35 \times 10^8$ dyn/cm^2. This elastic modulus value is essentially identical to the moduli experimentally obtained by several researchers (von Bekesey, 1949; Kirikae, 1970). All of the experimental values were obtained by measuring the bending stiffness D_i and calculating E_d^* from D_i just as was done here making the bending stiffness estimate of eq. (3.3.1) directly comparable to experimental values. The

elastic modulus E_m^* obtained from the membrane stiffness, however, is not directly comparable to experimentally derived moduli values. If the eardrum were isotropic then E_d^* would be identical to E_m^*. For the model eardrum ultrastructure the membrane based moduli E_m^* greatly exceeds the bending based moduli E_d^* (Fig. 3.5).

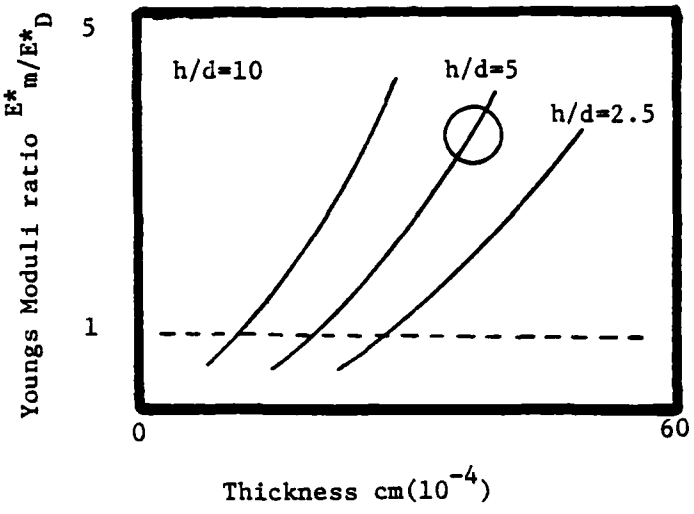

Figure 3.5. Approximate membrane stiffness/bending stiffness vs. total thickness. Circle indicates TM range, dashed line represents isotropic limit.

If the tympanic membrane were treated as isotropic or even single phase anisotropic then matching the bending stiffness to experimental values would underpredict the membrane stiffness. This fact strongly indicates that a single phase constitutive law, isotropic or orthotropic, may not be reasonable for the tympanic membrane.

3.4 Torsional Stiffness

The torsional stiffness may be estimated using results of Appendix A in a way similar to the bending stiffness. From Appendix A

$$S_{12} \sim \frac{1}{\lambda_1}\left\{\frac{E_b}{1-\nu_b}\left(\frac{2\lambda_1}{3}\left(h_1^3 + h_2^3\right) - \frac{\pi d_1^4}{64} - a_1^2\, d_1^2\, \frac{\pi}{4}\right)\right.$$

$$\left. + \frac{E_1}{2(1+\nu_1)}\left(\frac{\pi d_1^4}{32} + a_1^2\, d_1^2\, \frac{\pi}{4}\right)\right\} . \qquad (3.3.3)$$

Using parameters from Section 3.2 the torsional stiffness is approximately $S_{12} \sim 0.19$ dyn - cm. If the material were single phase then Young's moduli determined by $E_s^* h^3/12(1-\nu^2) \sim (D_1\nu_{12} + S_{12})$ would be $E_s^* \sim 1.3 \times 10^8$ dyn/cm^2. This modulus differs from the bending derived modulus by a factor of 2, and differs from the membrane derived modulus by an order of magnitude. This, again, discredits use of the single phase constitutive laws for the eardrum.

3.5 Conclusions

In addition to membrane, bending, and torsional terms some coupling between these terms may exist in the tympanic membrane. Selecting a locally orthogonal coordinate system approximately coincident with the fiber directions eliminates most of the coupling. Since the fibers are not exactly orthogonal and since the radial and circular fibers are on different levels, some coupling will exist. The ultrastructure, however, suggests that the coupling is small and that it may not be necessary to include such terms to model primary action of the drum. For this reason, the coupling moduli will not be estimated here.

Example stiffness calculations are done in Sections 3.2, 3.3 and 3.4 for the pars tensa of a cat. By using different parameters, the equations may also be applied to the pars flaccida. The stiffnesses are local and change depending on the local ultrastructure of the tympanic membrane. By changing parameters the model ultrastructure is changed geometrically and materially. Parameter selection allows the stiffness formuli to estimate mechanical properties for other mammals including guinea pigs, sheep, and humans.

In conclusion it is stressed that the fiberous tympanic membrane ultrastructure has anisotropic mechanical properties. Evidence of isotropic bending stiffness should not be misconstrued as evidence of isotropy. In fact, estimation of membrane and torsional stiffnesses indicates very anisotropic properties. The anisotropy is primarily seen in membrane stiffness terms. Modeling the tympanic membrane as isotropic, or single phase anisotropic may induce order of magnitude errors in the membrane terms even if the bending stiffness is matched exactly. The stiffnesses derived herein, may aid in development of a consistent tympanic membrane model by allowing direct nondimensionalization of anisotropic curvilinear shell equations accompanied with direct deduction of primary terms.

3.6 Appendix A: Approximate Stiffness Decomposition

Bending, membrane, and torsional stiffnesses of the tympanic membrane can be estimated based on mechanical properties of the lamina propri, mucous, and epidermal layers. To derive approximate expressions for stiffnesses in terms of constituent components, consider an idealized ultrastructure consisting of locally orthogonal fibers imbedded in a base material as shown in Figure 3.6. The composite shell is constructed of a set of fibers running parallel to the x axis having diameters d_1 and spacing λ_1, and a set of fibers running parallel to the y axis having diameters d_2 and spacing λ_2. The

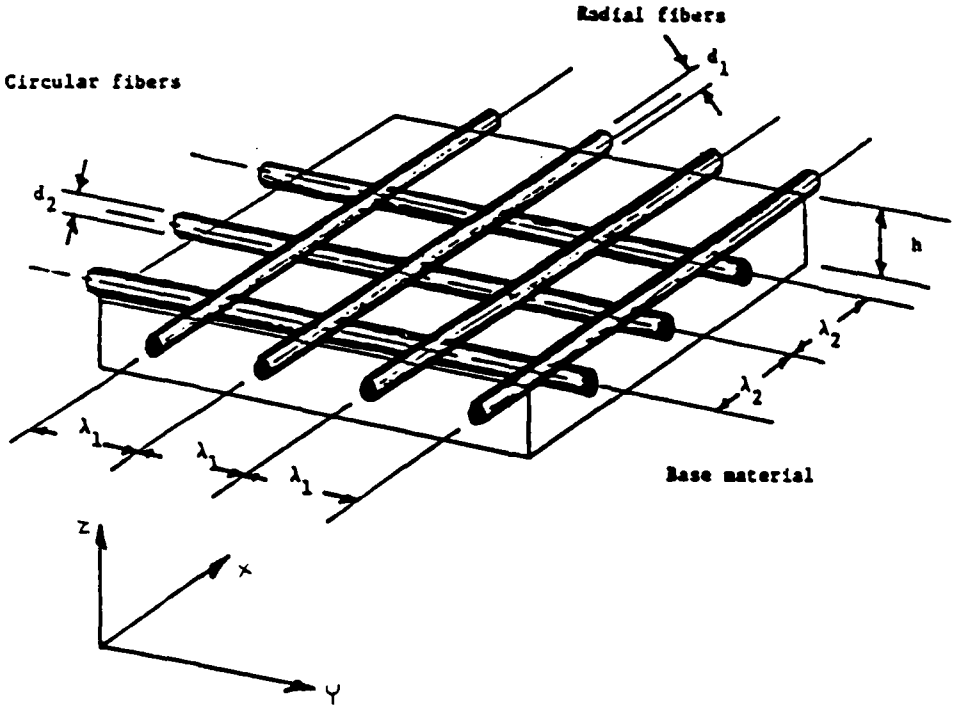

Figure 3.6 Local orthogonal fiber composite model of the tympanic membrane material (Fiber spacing and size not to scale.)

relatively stiff orthogonal set of fibers is imbedded in a base material having thickness h. The force and moment equilibrium equations must hold regardless of the presence of the fiber reinforcement in the drum. Hence, in order to formulate continuous shell equations that approximate behavior of the discrete composite structure, we need to determine material constants or stiffnesses that will represent the discrete system. One way to estimate the stiffnesses would be to determine the behavior of one unit element of the grid and substitute the resulting parameters into equilibrium equations. (Fig. 3.7). Renton (1970), Lightfoot (1964) and Yettram (1964) have applied this

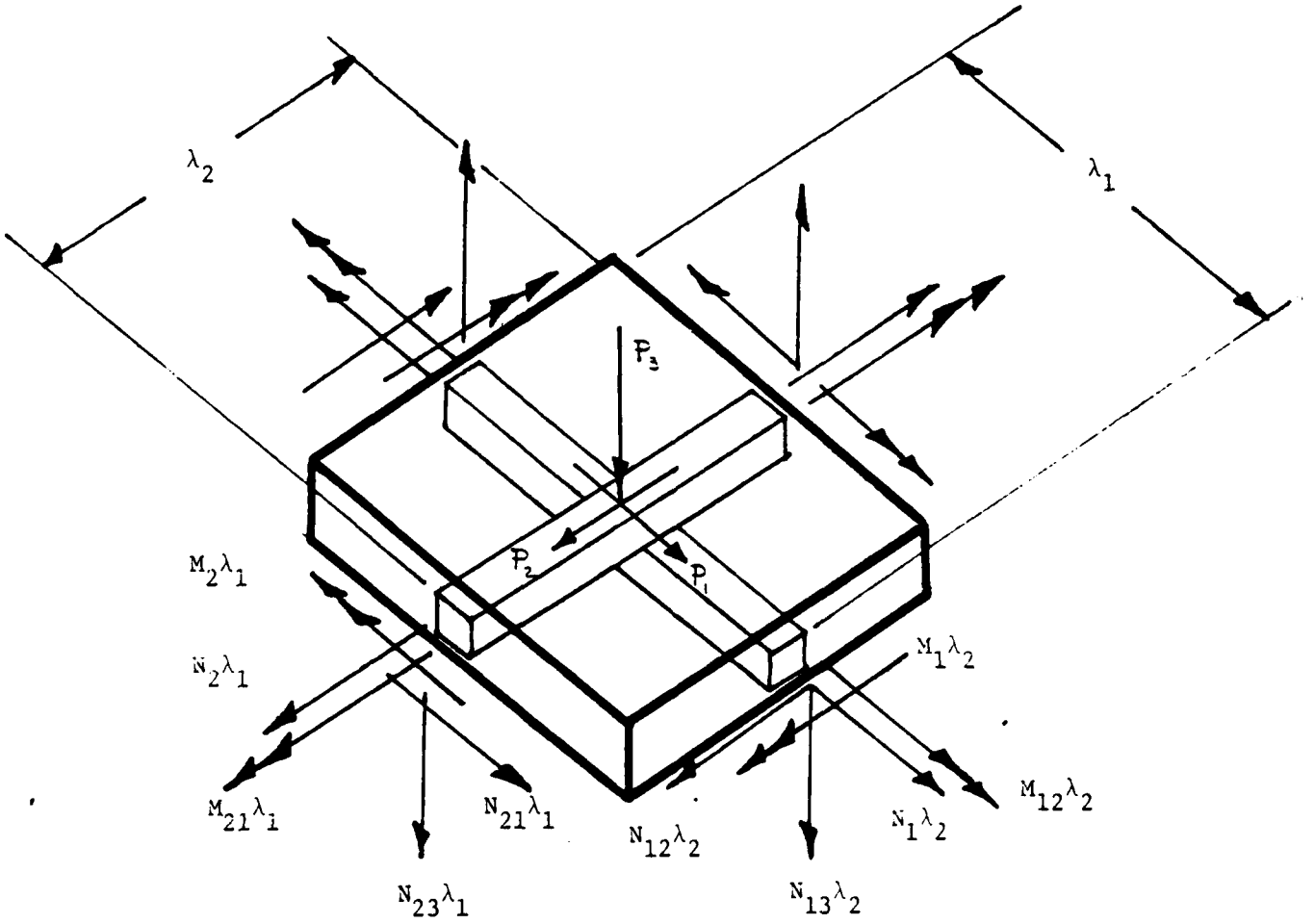

Figure 3.7 Equilibrium of a grid element. N_{ij} denotes forces and M_{ij} denotes moments on each cross sectional face.

approach to estimate parameters of plates for finite difference gridworks. When discretizing a continuous plate into a finite gridwork particular attention should be paid to the effect of Poisson's ratio. Obviously, if material coupling between the x and y directions is removed then increased stiffness due to Poisson's ratio will be lost. This fact can beseen by inspecting cross product terms in the orthotropic plate equations. For a homogeneous orthotropic plate, the coefficient of the product moment term (representing torsional resistence) is

$$D_x \nu_{xy} + D_y \nu_{yx} + S_{xy} + S_{yx} ,$$

where D_x is the bending stiffness in the x direction, D_y is the bending stiffness in the y direction, ν_{xy} is the first Poisson ratio, ν_{yx} is the second Poisson ratio, and S_{xy} are torsional stiffnesses.

For a discrete gridwork the coefficient multiplied by Poisson's ratio will approach zero as d_n/λ_n approaches zero. Hence, if we have a plate with uniform bending stiffness D, and we have a gridwork with the same bending stiffness D then the overall torsional stiffness of the plate will exceed that of the gridwork. The same comments apply to the effect of Poisson's ratio on axial stiffnesses, such that the deflection of a gridwork having axial stiffness and bending stiffness identical to that of the plate, may deflect quite differently from the plate under identical loads. With these comments in mind we would like to find the appropriate stiffnesses for use in an equivalent continua representation of the discrete composite plate.

In order to estimate the bending stiffness in the x direction, suppose we assume that the Kirchhoff hypothesis is reasonable, such that the bending moment may be obtained as an integral of the stress over the section.

$$M_x = \lim_{m\to\infty} \frac{1}{m\lambda_2} \int_0^{m\lambda_2} \int_{h_1}^{h_2} \sigma_x z\,dz\,dy \qquad (3.6.1)$$

Assuming linear Kirchhoff type strain, the integral may be estimated in the following way

$$M_x = \frac{1}{\lambda_2}\int_0^{\lambda_2}\{\int_B \frac{E_b}{1-\nu_b^2} z^2 w_{xx} dz + \int_B \frac{E_b \nu_b}{1-\nu_b^2} z^2 w_{yy} dz + \int_2 \frac{E_2}{1-\nu_2^2} z^2 (w_{xx} + \mu_{21} w_{yy}) dz\} dy \qquad (3.6.2)$$

$$= \frac{1}{\lambda_2}\{\frac{E_b}{1-\nu_b^2}[(h_2^3 + h_1^3)\frac{\lambda_2}{3} - (\frac{\pi d_2^4}{64} + a_2^2 d_2^2 \frac{\pi}{4})](w_{xx} + \nu_b w_{yy}) + \frac{E_2}{1-\nu_2^2}(\frac{\pi d_2^4}{64} + a_2^2 d_2^2 \frac{\pi}{4})(w_{xx} + \mu_{21} w_{yy})\}$$

where w is transverse deformation and x, y, z subscripts on w denote partial differentiation. It has been assumed that each of the constituent components behave in a linear elastic manner. The subscripts appearing on the material constants indicate: 1-fibers in the first direction, 2-fibers in the second direction, b-base material. Figure 3.8 indicates definitions of thickness and spacing parameters.

In addition to the above form the bending moment can be written as $M = D_2(w_{xx} + \nu_{21} w_{yy})$ defining the bending stiffness D_2 and Poisson's ratio as

$$D_2 = \frac{E_b}{1-\nu_b^2}\{\frac{h_2^3 + h_1^3}{3} - \frac{\pi d_2^4}{64\lambda_2} - a_2^2 d_2^2 \frac{\pi}{\lambda_2}\} + \frac{E_2}{1-\nu_2^2}\{\frac{\pi d_2^4}{64\lambda_2} + a_2^2 d_2^2 \frac{\pi}{4\lambda_2}\} \qquad (3.6.3)$$

$$\nu_{21} = \frac{1}{D_2}[\frac{E_b \nu_b}{1-\nu_b^2}\{\frac{h_2^3 + h_1^3}{3} - \frac{\pi d_2^4}{64\lambda_2} - a_2^2 d_2^2 \frac{\pi}{\lambda_2}\} + \frac{E_2 \mu_{21}}{1-\nu_b^2}\{\frac{\pi d_2^4}{64\lambda} + a_2^2 d_2^2 \frac{\pi}{4\lambda_2}\} \qquad (3.6.4)$$

Interchanging subscripts 2 and 1 in (3.6.3) and (3.6.4) defines D_1 and ν_{12}. Poisson's ratio for the fiberous layer μ_{21} may be estimated based on volume fractions and relative stiffnesses of the materials as

$$\mu_{21} \approx \frac{\pi d_2^2}{4\lambda_2 h}\left(\nu_2 - \frac{E_b \nu_b}{E_2}\right) + \frac{E_b \nu_b}{E_2} + \frac{\pi d_1^2 E_1}{4\lambda_1 h E_2}\left(\nu_1 - \frac{E_b \nu_b}{E_1}\right) . \qquad (3.6.5)$$

Interchanging subscripts 2 and 1 will give μ_{12}.

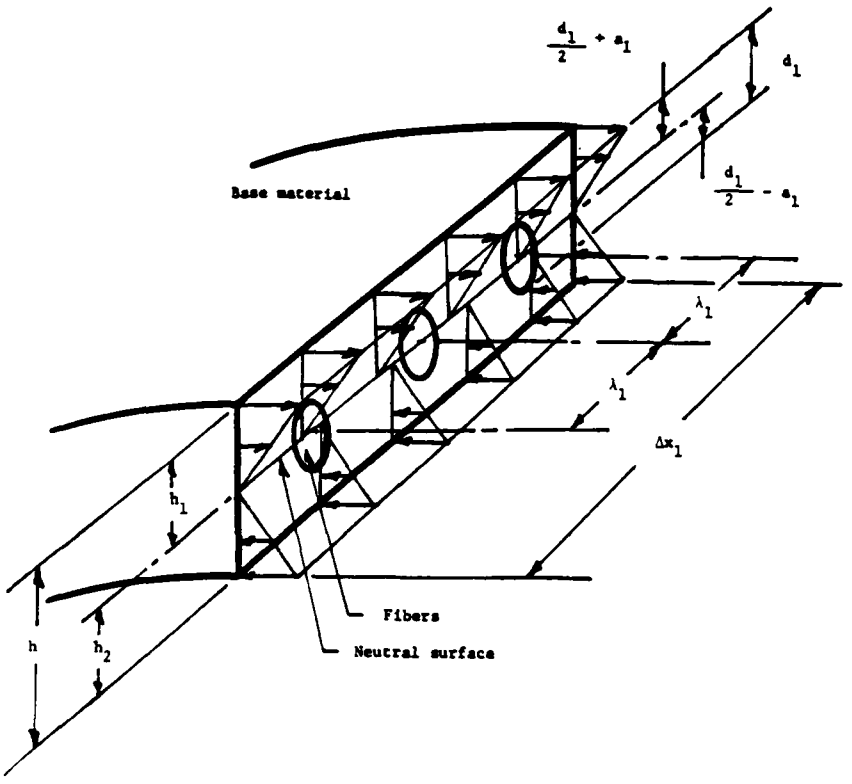

Figure 3.8 Schematic of a cross section indicating linear Kirchhoff type strain and middle surface location.

Torsional stiffnesses may be approximated in a similar way by integrating the shear stress over the cross section. The twisting moment is

$$M_{xy} = \lim_{m\to\infty} \frac{1}{m\lambda_2} \int_0^{m\lambda_2} \int_{-h_1}^{h_2} \tau_{xy}\, z\, dz\, dy$$

$$= -S_{21}\, w_{xy} \,. \tag{3.6.6}$$

Performing the integration for Kirchhoff type strain gives

$$S_{21} = \frac{1}{\lambda_2} \left[\frac{E_b}{1-\nu_b^2} \left\{ \frac{2\lambda_2}{3}(h_1^3 + h_2^3) - \frac{\pi d_2^4}{64} - a_2^2\, d_2^2\, \frac{\pi}{8} \right.\right.$$

$$\left.\left. + \frac{E_2}{2(1+\nu_2)} \left\{ \frac{\pi d_2^4}{32} + a_2^2\, d_2^2\, \frac{\pi}{4} \right\} \right] \right. \tag{3.6.7}$$

Once again an interchange of subscripts gives S_{12}.

The axial membrane stiffness may be derived by integrating the membrane stress over the thickness of the material. In the x direction the in-plane membrane force is

$$N_x = \lim_{m\to\infty} \frac{1}{m\lambda_2} \int_0^{m\lambda_2} \int_{-h_1}^{h_2} \sigma_x\, dz\, dy$$

$$= O_2\left(u_x + \frac{1}{2} w_x^2 + \nu_{21} \left(v_y + \frac{1}{2} w_y^2\right)\right) , \tag{3.6.8}$$

where u is deformation in the x direction, v is deformation in the y direction and O_2 is the membrane stiffness. Upon integration

$$N_x = \frac{1}{\lambda_2} \left\{ \frac{E_b}{1-\nu_b^2} \left(h\lambda_2 - \frac{\pi d_2^2}{4}\right)\left(u_x + \nu_b u_y + \frac{1}{2} w_x^2 + \frac{\nu_b}{2} w_y^2\right) \right.$$

$$\left. + \frac{E_2}{1-\nu_2^2} \frac{\pi d_2^2}{4}\left(u_x + \frac{1}{2} w_x^2 + \mu_{21}\left(v_y + \frac{1}{2} w_y^2\right)\right)\right\} . \tag{3.6.9}$$

Finally the in-plane shear is estimated by integrating the shear stress over the thickness

$$N_{xy} = \lim_{m\to\infty} \frac{1}{\lambda_2 m} \int_0^{\lambda_2 m} \int_{-h_1}^{h_2} \tau_{xy}\, dz\, dy \qquad (3.6.10)$$

$$= Q_{21}(u_y + v_x + w_x\, w_y) .$$

Performing the integration we find

$$Q_{21} = \frac{1}{\lambda_2} \left\{ \frac{E_b}{2(1+\nu_b)} \left(h\lambda_2 - \frac{\pi d_2^2}{4}\right) + \frac{E_2}{2(1+\nu_2)} \frac{\pi d_2^2}{4} \right\} . \qquad (3.6.11)$$

Interchanging subscripts 1 and 2 will provide Q_{12}.

With these stiffnesses the equivalent continua problem has been formulated. All of the expressions are approximate and are valid only for a limited range of parameters and conditions. When applied to dynamic problems, the expressions are reasonable only for low frequency vibrations where material wave propagation is negligible. An alternative to the "strength of materials" approach presented herein is presented by Tiersten and Jahanmir (1977) modeling composites as interpenetrating continua.

CHAPTER 4

SIMPLE EVIDENCE OF MEMBRANE STRESS AND DAMPING IN THE TYMPANIC MEMBRANE

4.1 Introduction

In order to formulate a simple yet physically realistic model of the tympanic membrane we must study its structure and behavior in order to identify the important features. The problem is to properly identify all of the dominant mechanisms. There are two basic schemes of searching for important or primary features when formulating a model. The first method is to write a complete, and relatively large, set of equations describing behavior of the eardrum and subsequently use known behavior to nondimensionalize and simplify the model. For the eardrum, this would involve writing von Karman type shell equations for the fiber composite structure in general curvilinear coordinates coupled with acoustic models of connecting fluids and ossicular chain constraints. The curvilinear geometry, fiber composite structure, and internal damping of the tympanic membrane would make even a numerical solution impractical at this time. Although it is possible to formulate a relatively complete model, many features may be of secondary importance. If such terms could be located apriori, then the modeling task could be greatly simplified. While the first method of searching for primary terms requires a relatively complete formulation, the second method attempts to exclude selected physical features by estimating their contribution prior to formulation of the model. In the interest of simplicity, importance of several physical features of the tympanic membrane will be estimated for consideration in an eardrum model. Actual experimental results will be used to make the analytical estimates.

Since the tympanic membrane is a thin fiber composite shell it is natural to think of it in terms of dynamical shell theory. When formulating a shell model, the physics may be divided into three catagories. 1) Inertia: transverse,

rotary, shear, axial ... 2) Restoring forces: shear, bending, axial, external ... 3) Damping: transverse, bending, shear ... . This chapter addresses existence of dominant mechanisms in each of these catagories beginning with a discussion of inertia.

Using holographic interferometry the vibrational shape of the tympanic membrane has been recorded under various experimental conditions (Khanna and Tornndorf, 1972; Tonndorf and Khanna, 1972; Dancer, 1975; Ogura, 1974). The displaced shapes can be used to estimate magnitudes of shear, transverse, and rotary inerta mechanisms. Most of the membrane motion is transverse to its resting position indicating that transverse inertia dominates other inertia types (for frequencies in the audible range). The only possible exception is in the area of taught radial fibers separating the anterior from posterior regions where connection of the malleus induces larger than average tangential accelerations. However, since the audio excitation frequencies represent speeds much slower than the sound speeds of shear and dilatational waves, local material accelerations represent much less kinetic energy change than global accelerations (Graff, 1970). Therefore, rectilinear momentum, primarily tranverse, represents the primary inertia in the vibrating tympanic membrane.

Determination of the dominant restoring mechanisms is not as simple as the inertia mechanism. Based on some kinematic considerations, however, it is possible to estimate the strain energy density stored by bending, the potential energy density stored by membrane stress, and the potential energy stored by shear mechanisms. In order to estimate the energy density stored in membrane type action it is necessary to first determine the magnitude of an in-plane stress existing in the eardrum. There are several ways to infer the magnitude

of the membrane stress based on experimental results - three methods will be presented here and compared.

4.2 Approximate Global Static Equilibrium

Consider an idealized boundary that supports the tympanic membrane through membrane type forces as indicated in Fig. 4.1. In reality, there will exist some transverse shear and bending moment at the boundary accompaning the membrane stress, however the intent here is to estimate the membrane stress if it dominates over the bending stresses. To obtain an order of magnitude approximation, consider a cone of diameter 2a, and apex angle 2α forced by a pressure P, tympani force F_T, ossicular moment M_m and membrane stress σ_m^*. Summing moments about the manubrium instant center of velocity we find

$$\sigma_m^* \sim \frac{F_T b + P\pi a^3 - M_m}{0.17\, a^2 h \sin\alpha} , \qquad (4.2.1)$$

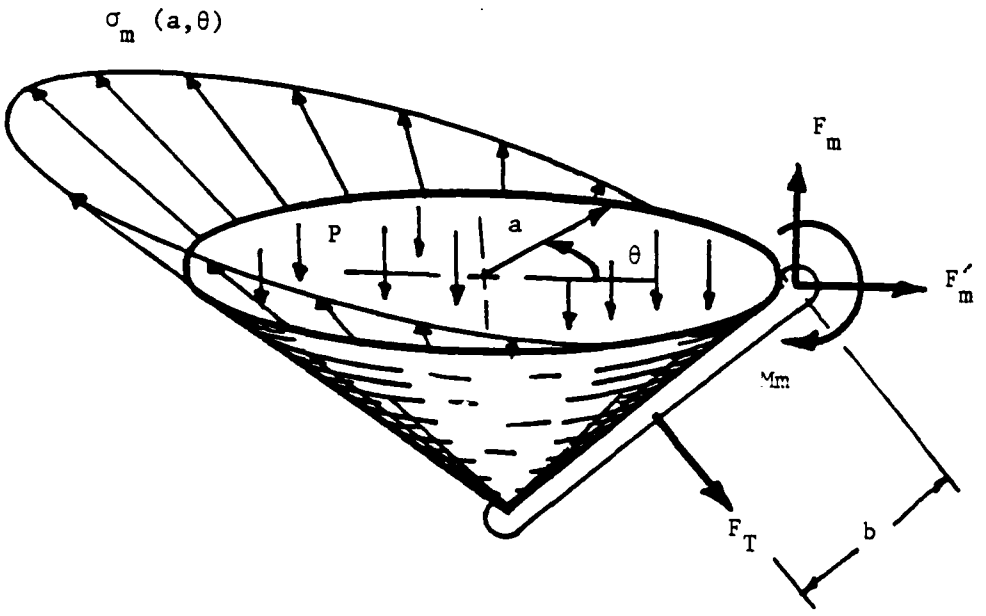

Figure 4.1 Approximate global equilibrium of the tympanic membrane.

where the moment M_m may include reverse inertial terms representing an integrated mass of the hearing system as well as damping and compliance terms. Also, writing the moment as an operator on malleus displacement then $M_m = \phi K_m[\phi,\phi,\phi,...]$, where ϕ is the instantaneous rotation of the malleus.

The tensor tympani force and perhaps some of the moment M_m can be viewed as inducing a prestress σ_p such that σ_m^* is the sum of a prestress and a deformation induced stress. To estimate the magnitude of the membrane stress σ_m^*, dimensions representative of a cat are combined with observed deformation to obtain the following

$$\sigma_m^* \sim \sigma_p + 1.23 \times 10^5 \frac{dyn}{cm^2} . \qquad (4.2.2)$$

The estimate in (4.2.2) was done at 100 db SPL using deformation rotation $\phi \sim 1.5 \times 10^{-5}$ rad. measured by Khanna and Tonndorf (1972) and $h = 40 \times 10^{-4}$ cm, $a = 0.45$ cm, $b = 0.25$ cm, $\alpha = 0.64$ rad, and from Funnell (1977) $K_m \sim 28 \times 10^3$ dyn - cm. The membrane stress estimate of (4.2.2) is insensitive to any errors in the malleus spring constant. Also, the prestress σ_p induced by the tensor tympani or tendons has been left arbitrary for now.

4.3 Radial Fiber Strain

To verify the estimate of radial stress based on global static equilibrium (4.2.2), strain in the fibers can be estimated from experimental results and combined with the membrane elastic moduli to obtain a comparative value. The strain of a radial fiber for small deformations can be written as a sum of strain due to endpoint motion and strain induced by transverse deformation $\varepsilon_r \approx \varepsilon_r^{(e)} + \varepsilon_r^{(q)}$, where the superscript e represents endpoint motion and the superscript q represents quasilinear stress induced by the transverse deformation.

To estimate strain due to endpoint motion consider boundaries defined by a cone shape such that any planar cut through the umbo perpendicular to the plane of the annular ring will yield a triangular cross section. The cross section is allowed to change with θ so the cone may be distorted. This shape is used to estimate endpoint motion only, so curvature of the drum does not come into the calculation. Fig. 4.2 illustrates the approximate boundaries under consideration.

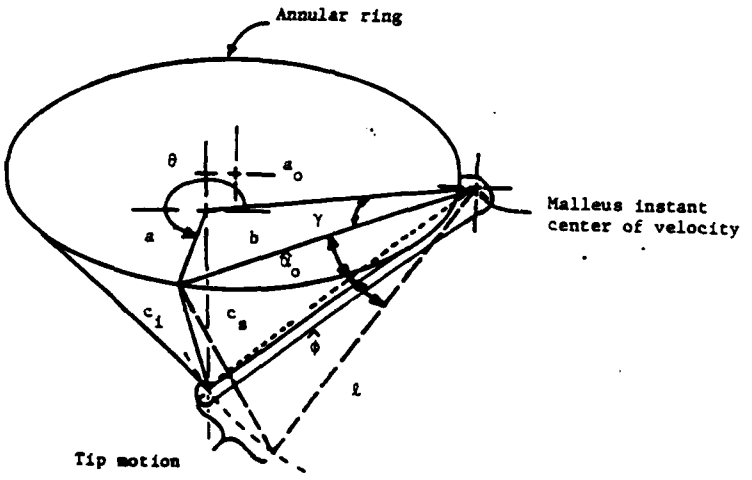

Figure 4.2 Membrane boundaries used to estimate radial fiber strain.

Strain on a radial fiber due to endpoint motion is given by

$$\varepsilon_r^{(e)} = \frac{1}{2} \frac{C_s^2 - C_i^2}{C_i^2} , \tag{4.3.1}$$

where C_i and C_s are initial and final fiber lengths, respectively. Noting that b and ℓ are constant during the deformation, and φ is small gives

$$\varepsilon_r^{(e)} \simeq \frac{b\ell\{\frac{1}{2}\phi^2 \cos \hat{\alpha}_o + \phi \sin \hat{\alpha}_o\}}{b^2 + \ell^2 - 2b\ell \cos \hat{\alpha}_o} , \tag{4.3.2}$$

where ϕ and $\hat{\alpha}_0$ are projections onto the plane of the triangle containing the radial fiber of interest, while ℓ, α_0 and b are shown in Fig. 4.1. Also

$$\phi = \frac{\hat{\phi}}{\cos \gamma} \quad , \quad \hat{\alpha}_0 = \frac{\alpha_0}{\cos \gamma} \quad , \tag{4.3.4}$$

and

$$\gamma \simeq \text{ARCCOS} \left(\frac{a_0^2 + b^2 - a^2}{2\, a_0 b}\right) .$$

We must add to (4.3.2) the strain due to transverse deformation. Since the drum is initially convex, strain caused by positive endpoint motion will be positive, and strain due to inward transverse deformation will be negative. If we denote u(r) as the transverse deformation then

$$\varepsilon_r^{(q)} = \frac{1}{S_2 - S_1} \int_{S_1}^{S_2} \frac{1}{2} \left(\frac{\partial u}{\partial r}\right)^2 dr \ . \tag{4.3.5}$$

Approximating u(r) for low frequency vibration (less than 1000 Hz) as $u \sim u_o \sin\left(\pi(r - S_1)/(S_2 - S_1)\right)$ gives $\varepsilon_r^{(q)} \sim 6.9[u_o/(S_2 - S_1)]^2$, where u_o is the maximum transverse deflection of the drum relative to a cone deformed to meet the endpoint deformation.

In addition to the values representing the cat geometry given in Section 4.2, at 100 dB SPL the maximum transverse displacement after correcting for endpoint motion is approximately $u_o \sim 0.21 \times 10^{-4}$ cm. Using typical values we find that the strain associated with endpoint motion is approximately $\varepsilon^{(e)} \sim 1.17 \times 10^{-5}$ and the strain induced by transverse deformation is approximately $\varepsilon^{(q)} \sim -2.3 \times 10^{-8}$. Hence, the compressive strain induced by transverse deformation and change in curvature is two orders of magnitude less than the tensile strain induced by motion of the endpoints. This observation discredits simple Helmholtz curved lever theories of membrane action. The

curved lever theories require existence of a compressive stress in the radial fibers under the conditions estimated here. The fact that a tensile strain exists, not a compressive strain, suggests the curved lever mechanism is a secondary effect and does not dictate drum function.

To verify the fiber strain estimate, the membrane stiffness estimated by equation (3.2.1) can be used to estimate the stress σ_m^{**}. Doing so, we find $\sigma_m^{**} \sim 1.1 \times 10^5$ dyn/cm^2 + σ_p . This result is essentially identical to that obtained by global equilibrium (4.2.2) and hence seems very reasonable.

Since the membrane stress appears as an integral of the deformation, plus a prestress, it will be a quasilinear term in the tympanic membrane operator. If the prestress σ_p greatly exceeds the quasilinear term, then the system equations could be linearized (in terms of the membrane type stress) around the prestress. As discussed later, some dynamical and static experimental results indicate that the eardrum behaves as if a prestress dominates.

4.4 Restoring Potential Energy Densities

Knowing an approximate value of the membrane stress in typical radial fibers allows us to estimate the potential energy density stored in membrane type deformation. Again, using the cat as an example, the radial fiber along which the maximum deflection occurs at low vibration frequencies has a shape similar to a sine bay. As a rough estimate, transverse deformation from the resting position for a radial fiber is written $u(r,t) \sim u_o(t)\sin(\pi(r-S_1)/(S_2-S_1))$. Using this, the average potential energy per unit surface area ($\bar{U}_m$) stored along the radial fibers due to membrane type forces is approximately

$$\bar{U}_m \sim \frac{\pi \sigma_m h u_o^2}{(S_2 - S_1)^2} . \qquad (4.4.1)$$

At 100 dB SPL using estimates for the cat and stress σ_m^* of Section 4.2 we find

$$\bar{U}_m \sim 3.02 \times 10^{-6} \frac{\text{dyn-cm}}{\text{cm}^2} + \bar{U}_{mP} \quad , \tag{4.4.2}$$

where $\bar{U}_{mP}$ is due to prestress in the tympanic membrane and $\bar{U}_m - \bar{U}_{mP}$ is induced by deformation alone.

The strain energy stored in bending may be calculated for the same vibrational shape and amplitude as

$$\bar{U}_B \sim \frac{\pi^3 D_R u_o^2}{(S_2 - S_1)^4} \quad . \tag{4.4.3}$$

Thus, using identical values for a cat at 100 dB SPL

$$U_B \sim 4.51 \times 10^{-7} \frac{\text{dyn-cm}}{\text{cm}^2} \quad . \tag{4.4.4}$$

Based on these estimates at 100 dB SPL, the membrane type potential energy is at least an order of magnitude larger than the bending strain energy. If a substantial prestress exists in the eardrum, or is imposed externally, then the membrane type term may be several orders of magnitude larger than the bending term. The ratio ε_B of the two terms provides a measure of their relative importance and is defined by

$$\varepsilon_B = \frac{D_R \left\langle \frac{\partial^2 u}{\partial r^2} \right\rangle^2}{\sigma_m h \left\langle \frac{\partial u}{\partial r} \right\rangle^2} \quad , \tag{4.4.5}$$

where

$$\langle f \rangle = \frac{1}{S_2 - S_1} \int_{S_1}^{S_2} f(r)\, dr \quad . \tag{4.4.5}$$

The above comparison was applied to bending in the radial direction only; the same type of analysis may be applied in the circumferential direction. In order to estimate potential energy density due to membrane action in the

circumferential direction, it is necessary to estimate stress in the circumferential direction. This can be done by considering local dynamic force balance of the membrane. Local principle radii of curvature plays a primary role in relating radial stress to circumferential stress. Upon estimating bending and membrane energy densities stored due to deformation in the circumferential directions, it is found that both are small in comparison to membrane energy in the radial direction.

These simple energy density calculations are based on holographic interferometry measurements made by Khanna and Tonndorf (1972), and hence are based on accepted behavior of the drum. The only analytical approximation that may contain any appreciable error is the estimated quasilinear radial stress σ_m. The radial (or meridian) stress used was estimated using two distinct methods resulting in the same value of stress. Both methods determined the component of meridian stress superimposed on any resting tension or prestress. A numerical value of prestress could not be obtained by either method. If a prestress exists then the radial membrane type restoring mechanism may dominate by several orders of magnitude rather than just one order of magnitude.

4.5 Simple String Analogy

The question of prestress can be partially resolved by study of the vibrational shape of the membrane along with motion of the malleus. To address this question, suppose we look at behavior of a very simple string subject to a radial stress σ_m, supported by a spring on one end, and fixed at the other end. This string, in a very crude way, represents a bundle of radial fibers connected to a moving manubrium and fixed at the annular ring. (See Fig. 4.9, Appendix A). The string analogy is by no means complete but will suffice to illustrate several points.

The problem of interest is to allow the forcing fequency to vary and observe response of the string (analogous to TM) and associated motion of the spring (analogous to malleus motion). Solution to the linear string problem with a spring constraint can be solved exactly. For the case of no damping, response of the string is shown in Figs. 4.3 and 4.4. In terms of infering tympanic membrane radial prestress, peaks on the MAX TM AMPLITUDE/MALLEUS AMPLITUDE VS. FREQUENCY graph correspond to even numbered natural frequencies of vibration. Valleys on the graph correspond to odd natural modes of vibration. Since the natural frequencies are directly related to the stress σ_m, measurement of the peaks allows calculation of the radial tensile stress σ_m.

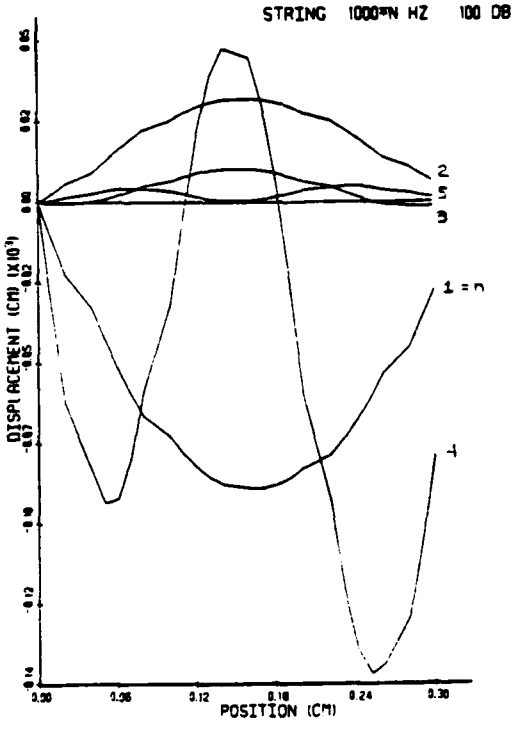

Figure 4.3 Undamped vibrations of a string with one end supported by a transverse spring for the case of no damping.

If damping and circumferential interactions are added to the simple string, then peaks on the TM/MALLEUS amplitude graph will be reduced to small spikes.

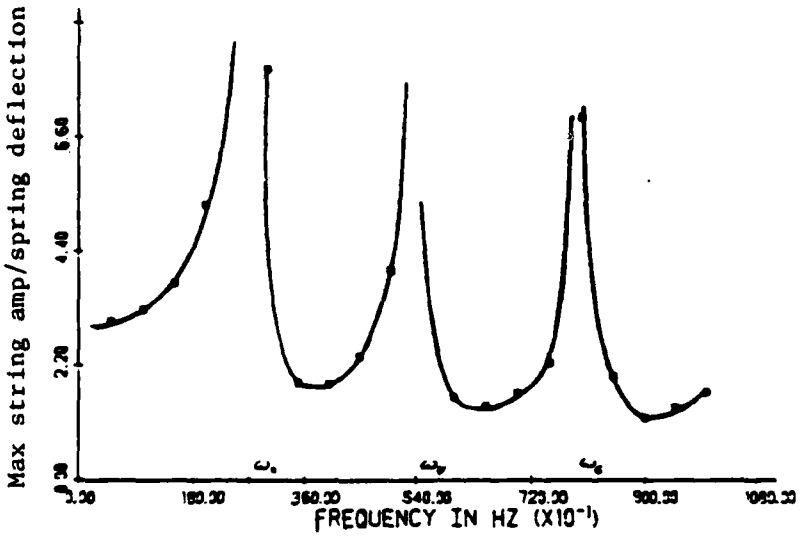

Figure 4.4 String analogy. Endpoint amplitude / maximum amplitude for no damping vs. frequency.

Depending on the frequency, the point of maximum displacement on the tympanic membrane moves. To illustrate this, at 1000 Hz the string has a maximum displacement approximately half way between the fixed end (annular ring) and moving spring (malleus). At 4000 Hz the maximum amplitude position moves toward the spring. Very similar behavior is seen when measuring vibratory behavior of real tympanic membranes. Manley and Johnstone (1974) have recorded displacement of the tympanic membrane of guinea pigs for several fixed points over a wide range of frequencies illustrating this behavior (see Fig. 4.5).

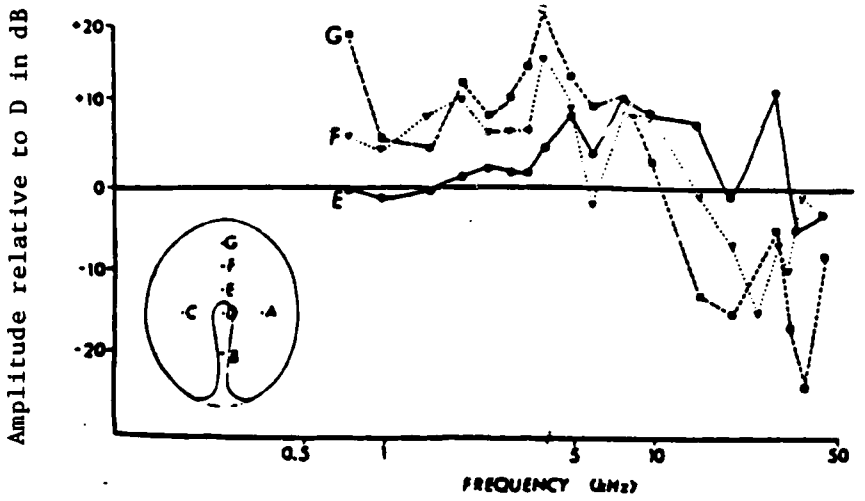

Figure 4.5 Displacement of sites E, F, and G (see inset diagram for eardrum measurement locations) relative to site D (in decibels) as a function of frequency. The zero line represents the displacement at D at all frequencies. Relative displacement of E shown as continuous line, filled circles; of F as dotted line, open triangles; and of G as dashed line, filled squares. Data for E from one individual, for F is a mean of three individuals, and for G is a mean of two individuals. The trends in all cases were the same. From Manley and Johnstone (1974).

By careful inspection of Manley and Johnstone's data, keeping in mind that the position of the maximum displacement moves with frequency, it is possible to locate the first four peaks on the TM/Malleus amplitude graph. They appear approximately at $\omega_2 \sim 1.86$ KHZ, $\omega_4 \sim 3.9$ KHZ, $\omega_6 \sim 5.1$ KHZ, and

ω_8 ~ 7.4 KHZ. These peaks correspond roughly to even modes of vibration of the radial fiber on which data was taken. If we match the value of ω_2 measured for the guinea pig to the result for the simple string problem we find ω_2^s ~ 1.86 KHZ, ω_4^s ~ 3.7 KHZ, ω_6^s ~ 5.6 KHZ, ω_8^s ~ 7.4 KHZ. The superscript s indicates the string analogy. This agreement is outstanding. Any differences are smaller than experimental accuracy of the measured frequencies. Similar results can be obtained for the cat eardrum. A graph for the cat by Khanna and Tonndorf (1972) is shown in Fig. 4.6.

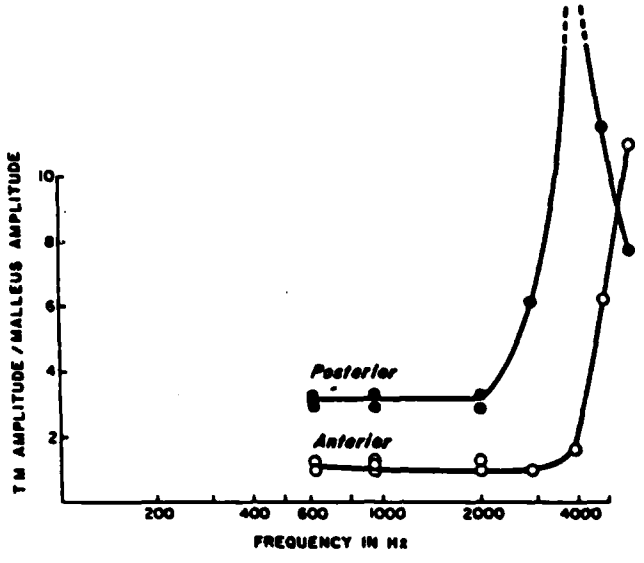

Figure 4.6 Maximum TM amplitude vs. malleus amplitude.
(From Khanna and Tonndorf, 1972)

By matching peaks on the TM/Malleus amplitude experimental graphs to the string problem it is found that the radial stress must be of order 10^6 dyn/cm^2

for the cat. As an indirect confirmation of this stress, Funnell (1975) used a prestress of 4×10^6 dyn/cm^2 in a single phase plane membrane model to produce complex vibratory shapes observed in cats. This value of stress is an order of magnitude larger than the quasilinear stress previously obtained in (4.2.2) indicating that there exists a prestress in the cat eardrum of order 10^6 dyn/cm^2. Since the tensor tympani plays a role in determining the prestress, the value may be sound pressure level dependent. The 10^6 dyn/cm^2 is based on results at 100 dB SPL.

In addition to the location of the peaks, a second item of importance is spacing of the natural frequencies. By experimental observation it is seen that peaks on the TM/MALLEUS amplitude graph have spacing of "2n" where n = 1,2,3,..., corresponding to a natural frequency have spacing of "n". This spacing can be reproduced by a mathematical model if the model contains a dominant membrane type restoring mechanism. If the mathematical model contains only bending restoring mechanisms, then the spacing of the peaks would be approximately $(2n)^2$. Spacing based on n^2 is not seen experimentally discrediting plate or shell 'bending models' of the tympanic membrane.

4.6 Perforation Tests

As additional evidence of existence of a tension field in the tympanic membrane, perforation tests are often mentioned (Kirikae, 1960; Funnell, 1975). A perforation test is done by cutting the membrane and measuring post cut deformation. Due to tissue damage caused by the cut along with post cut tissue distortion, it is questionable to attempt to derive a numerical value of stress from such observations. To address this question suppose we assume for the moment that no tissue distortion exists and apply a "no distortion" model to the slit test problem.

Modeling the slit as a Mode 1 crack, deformation (v) perpendicular to the

original cut is estimated using results from Theocaris and Pazis (1983)

$$v = \frac{k_1}{G}\left(\frac{r}{2\pi}\right)^{\frac{1}{2}} \sin\frac{\phi}{2}\left(\frac{1-\nu}{1+\nu}\sin^2\frac{\phi}{2}\right) + \frac{\nu k_1 r}{E(\pi a)^{\frac{1}{2}}}\sin\phi \quad , \tag{4.6.1}$$

$$k_1 = \sigma_0(\pi a)^{\frac{1}{2}} \quad ,$$

where σ_0 is the prestress, ϕ is the angular coordinate; r is the radial coordinate, G is the modulus of rigidity, E is Young's modulus, ν is Poisson's ratio, and a is the crack length. Using material parameters derived in Chapter 3 for a fiber composite cat eardrum drum, and slit test results by Kirikae (1960) we have $v \sim 0.05$ mm, $a \sim 0.25$ mm, $E \sim 8.6 \times 10^9$ dyn/cm^2. These values yield a prestress of $\sigma_0 \sim 4.9 \times 10^7$ dyn/cm^2. This value is much larger than the value inferred from vibrational behavior of the drum and is believed to be in error due to tissue distortion. Kirikae observed that the slits opened slowly over a time of approximately ten seconds. The initial deformation may have indeed been elastic and due to membrane type stress. The subsequent slow deformation due to tissue degredation causes calculations, such as the one above, to be in error. More detailed real time records of post cut tissue deformation may allow future researchers to obtain stress values from slit test data. The data presently available, however, can only be used to make qualitative comparisons and indicate higher stress in the radial fibers than in the circular fibers (as expected from calculations in Sections 4.2 and 4.3).

4.7 Dissipation and Damping

Evidence of damping within the structure of the tympanic membrane is indicated by several experimental results. Moller (1965) recorded a phase shift in average displacement of the eardrum relative to the stimuli for anesthetized cats having immobilized ossicular chains. If the ossicular chain

is fixed then the phase shift seen in acoustic impedance measurements is independent of the cochlea and ossicular chain. Hence, damping indicated by the phase shift must be in the tympanic membrane, fluid of the tympanic cavity, or air in the outer ear. The absence of appreciable flow within the outer ear and tympanic cavity suggests that structural damping within the tympanic membrane plays a primary role.

In addition to the phase shift data, the vibrational amplitude of the tympanic membrane can be used to infer internal damping within the eardrum. Accompanying the phase shift Moller (1965) observed a rapid decrease in acoustic impedance for cats with immobilized ossicular chains. This impedance decrease infers an average amplitude decrease that would not be as pronounced without damping.

Supporting the global impedance implications, Manley and Johnston (1974) directly measured displacements of various points on the tympanic membrane of guinea pigs using the Mossbauer technique. Their results show a very clear decrease in malleus amplitude over the entire audible frequency range. For frequencies up to 20 KHZ they also show that the ratio of peak tympanic membrane displacement to malleus displacement does not display the same decrease and in fact shows a discrete number of increasing peaks. The decrease in malleus displacement with increasing frequency that is accompanied by a substantial decrease in tympanic membrane vibration amplitude directly indicates existence of internal structural damping within the eardrum.

To include damping and dissipation in the model of the tympanic membrane it is necessary to determine the type of damping. Most continuum plate or shell models that include damping use a "transverse type" mechanism having a dissipative force proportional to the transverse velocity. This type of

damping however, has no direct physical connection to the structure of the eardrum. It may be possible to crudely equate the energy dissipation caused by the transverse velocity term to that observed in the eardrum, but such an endeavor violates the physics of the problem by introducing nonphysical terms in the model.

Rather than blind use of a transverse velocity type dissipation, the structure of the eardrum suggests a "bending type" dissipation. To show how the tympanic membrane structure gives rise to a bending type damping, suppose we look at behavior of a three layer lamina representing the membrane (Lim, 1968a, 1968b, 1970).

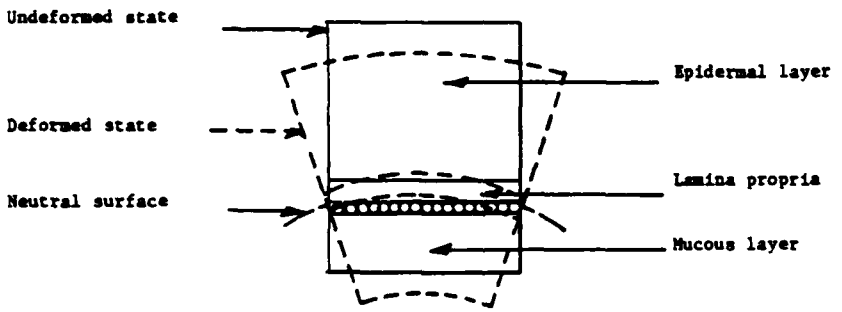

Figure 4.7 Bending dissipation in the epidermal and mucous layers.

Bending of the tympanic membrane causes the mucous and epidermal layers to change shape (maintaining similar volume as indicated in Fig. 4.7). Since the mucous and epidermal layers are water intensive cellular structures, the force required to change their shape will increase with the speed of displacement. By looking at changes in curvature induced by deformation it is found

that linear bending type dissipation for small deformations is proportional to two spatial and one time derivative of the deformation (denoted u_{xxt}). The "bending type" damping (u_{xxt}) differs from transverse type" (u_t) damping essentially by changing the slope on the amplitude vs. frequency graph.

To illustrate the difference consider two strings, one with transverse damping and one with bending type damping. Asymptotic behavior of the strings can be found using a multiscale method. In order to compare the results note that Fig. 4.8 has a log frequency scale, so equally spaced natural frequencies will become grouped together in the high frequency range indicating that forcing near a natural frequency is appropriate for comparison to the graph at high frequencies. At low frequencies the eigenvalues are separated by substantial distance on the graph (~ 1 KHZ) indicating that results of forcing at frequencies away from natural frequencies are appropriate for comparison to the graph. With this observation the results of Appendix A can be combined to indicate behavior in Fig. 4.8. The "bending type" dissipation has the correct

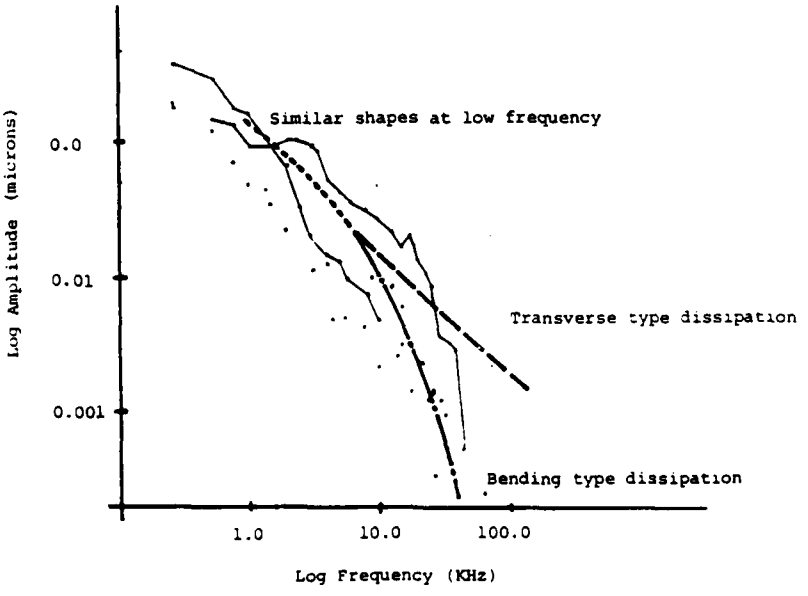

Figure 4.8 Qualitative malleus amplitude vs frequency for two dissipation mechanisms. Solid curves represent data from Manley and Johnstone (1974) for a guinea pig at 100 dB SPL.

shape to match the data, while the "transverse velocity type" dissipation indicates excessive malleus motion at high frequencies.

4.8 Concluding Remarks

Some simple analogies have been applied to address dominant mechanisms governing behavior of the tympanic membrane. At 100 dB SPL membrane type restoring forces dominate over bending and shear restoring forces. At lower sound pressure levels, evidence indicates existence of a prestress maintaining dominance of the membrane terms. Membrane stresses clearly dominate for SPL's near or above 100 dB. This observation indicates that a curvilinear membrane shell formulation may be sufficient to describe primary behavior of the restoring forces.

In addition to the restoring mechanism, it was determined that bending type damping is more reasonable than transverse type damping. The magnitude of damping may be determined by comparison to malleus amplitude vs. frequency curves or phase shift data.

Behavior of a string constrained by a linear spring at one end and fixed at the other end was used to illustrate concepts and ideas. The string is not to be misconstrued as a TM model - it is presented simply as an explanatory device. Readers interested in details of the string problem should see Appendix A.

4.9 APPENDIX 4.1: LINEAR STRING PROBLEM

Consider vibration of a string supported by a spring on one end and clamped on the other. Including small bending and small transverse damping,

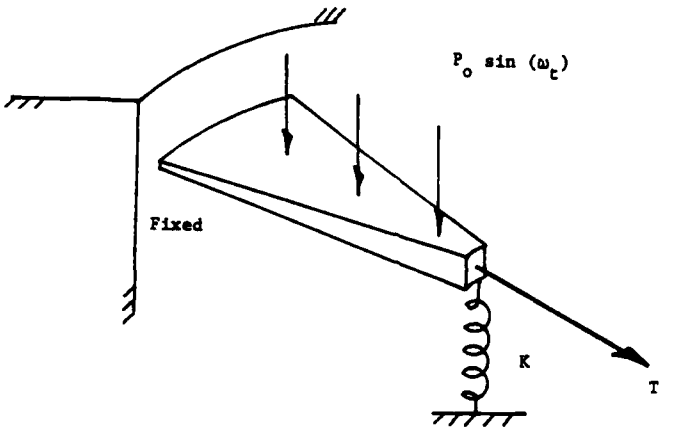

Figure 4.9 Simple string subject to a spring constraint and a fixed end.

the string motion is described by

$$u_{xx} + \varepsilon_B u_{xxt} + \varepsilon_T u_t - \frac{1}{c^2} u_{tt} = \frac{P_o}{T} \sin \omega t$$

where the boundary conditions are

$$u(0,t) = 0 \quad ,$$

and (4.9.1)

$$u_x(\ell,t) = \frac{K}{T} u(\ell,t) \quad ,$$

where T is the tension, c is the sound speed, P_o is the pressure amplitude, ω is the forcing frequency, and u is the transverse displacement. For the case of no damping $\varepsilon_B = \varepsilon_T = 0$, a direct expansion may be applied to find an asymptotic form for small endpoint motion ($|\frac{T}{T-k\ell}| \ll 1$). Ignoring transients, the result is

$$u(x,t,\varepsilon) \approx \sum_{n=1}^{\infty} \frac{2c^2 \sin\omega t}{T(\omega_n^2-\omega^2)} \{-\frac{P_o}{n\pi} \sin \frac{n\pi x}{\ell} \tag{4.9.2}$$

$$+ \varepsilon(-1)^n (\frac{P_1}{n\pi} \sin \frac{n\pi x}{\ell} - \frac{P_o x}{\ell}) + O(\varepsilon^2)\} \quad , (\omega \neq \omega_n)$$

where $$\varepsilon = \frac{T}{T+k\ell} \ ,$$

and $$P_1 = \sum_{n=1}^{\infty} \frac{P_o c^2 (-1)^n}{\ell(\omega_n^2 - \omega^2)} \ .$$

Also, k = spring const., Po = amplitude of applied pressure, $T = \sigma A$ = tension, $c = \sqrt{T/\rho}$ = sound speed, ℓ = length, ω = forcing frequency, $\omega_n = n\pi c/\ell$ = natural frequency, $1 >> \varepsilon$ = small endpoint motion parameter.

Since the endpoint motion is small it is advantageous to remove the endpoint motion from the boundary conditions and place it in the differential equation. To do so let

$$u = v - \varepsilon \, v_x(\ell,t) \, x \ , \tag{4.9.3}$$

so

$$v_{xx} + \varepsilon_B v_{xxt} + \varepsilon_T \, v_t - \frac{1}{c^2} \left(v_{tt} - \varepsilon \frac{x \, v_x(\ell,t)}{\ell} \right) = g(x) \sin \omega t \ ,$$

where

$$v(0,t) = 0 \ ,$$

and

$$v(\ell,t) = 0 \ . \tag{4.9.4}$$

For small ε we can use a direct expansion for the displacement as follows:

$$v(x,t;\varepsilon) \simeq v_o(x,t) + \varepsilon \, v_1(x,t) + \ldots \ . \tag{4.9.5}$$

Using a multiscale analysis for $\omega = \omega_n$ we find for bending damping ($\varepsilon_T = 0$)

$$v_o^{(B)} \simeq \frac{g^* c^2}{\varepsilon_B \, \omega_n^3} \left(1 - \exp\left(-\frac{\varepsilon_B \omega_n^3 t}{2}\right)\right) \cos \omega_n t \, \sin \frac{n\pi x}{\ell} \tag{4.9.6}$$

where

$$g^* = \left\langle -g(x), \sin \frac{n\pi x}{\ell} \right\rangle$$

By a similar method for $\omega = \omega_n$ and $\varepsilon_B = 0$, the result for transverse damping

is

$$v_o^{(T)} \simeq \frac{g^*}{\varepsilon_T \omega_n} \left(1-\exp\left(\frac{-\varepsilon_T c^2 t}{2}\right)\right) \cos \omega_n t \sin \frac{n\pi x}{\ell} \tag{4.9.7}$$

where

$$g^* = \langle -g(x), \sin \frac{n\pi x}{\ell} \rangle .$$

If $\omega \neq \omega_n$ then both $v_o^{(T)}$ and $v_o^{(B)}$ have ω^{-2} dependence very similar to the undamped case. Motion at the spring is given by

$$u(\ell,t) = v(\ell,t) - \varepsilon\, v_x(\ell,t)\ell , \tag{4.9.8}$$

and so

$$u(\ell,t) = \varepsilon\, v_x(\ell,t)\ell .$$

Thus, the spring motion to order ε is given directly as the spatial derivative of v_o as

$$u(\ell,t) \simeq -\varepsilon \frac{\partial v_o}{\partial x}\bigg|_{x=\ell} \ell + O(\varepsilon^2) . \tag{4.9.9}$$

CHAPTER 5

FORMULATION OF A DYNAMIC FIBER COMPOSITE MEMBRANE SHELL MODEL OF THE TYMPANIC MEMBRANE

5.1 Equilbrium Equations

The previous chapter uses the tympanic membrane ultrastructure and experimental test data to argue that membrane type stresses represent the primary restoring force in the eardrum. If we neglect bending terms and include only membrane stresses, then conservation of linear momentum written in component form gives the following curvilinear membrane force equilibrium equations (Novozhilov, 1959).

$$\frac{1}{H_1H_2}\left\{\frac{\partial}{\partial q_1}(H_2N_1) + \frac{\partial H_1}{\partial q_2}N_{12} + \frac{\partial}{\partial q_2}(H_1N_{21}) - \frac{\partial H_2}{\partial q_1}N_2\right\} + P_1 = 0 \qquad (5.1.1)$$

$$\frac{1}{H_1H_2}\left\{\frac{\partial}{\partial q_2}(H_1N_2) + \frac{\partial H_2}{\partial q_1}N_{21} + \frac{\partial}{\partial q_1}(H_2N_{12}) - \frac{\partial H_1}{\partial q_2}N_1\right\} + P_2 = 0 \qquad (5.1.2)$$

$$\frac{1}{H_1H_2}\left\{\frac{\partial}{\partial q_1}(H_2(\theta_1N_1 + \theta_2N_{12})) + \frac{\partial}{\partial q_2}(\theta_2N_2 + \theta_1N_{21}))\right\} \qquad (5.1.3)$$

$$- \frac{N_1}{R_1} - \frac{N_2}{R_2} + P_3 = 0 \ ,$$

where N_{ij} are the products of membrane stresses with local thickness, R_i are radii of curvature, q_i are the curvilinear coordinates, P_i are generalized D'Alembert pressures, H_i are coordinate metrics, and θ_i are transverse deformation gradients. As written, damping and inertia terms are contained in P_i.

The force equilibrium equations when combined with an appropriate constitutive law describe dynamic behavior of general curvilinear membranes. For the eardrum, coupling to the ossicular chain appears as a boundary condition along the malleus-tympanic membrane attachment. This boundary condition is not simple and in its full form contains terms describing dynamics of the ossicular chain and cochlea. The boundary condition at the malleus couples

the membrane equations to the middle and inner ear. In addition to the malleus boundary condition, the tympanic membrane is supported around its outside periphery at the annular ring providing a second boundary condition. Since we are interested in describing both steady and transient dynamic behavior, initial displacement and velocity fields must also be prescribed. Any initial tympanic cavity pressure or dynamic changes in the middle ear pressure are contained in P_3.

Rather than application of a numerical method, it is desirable to find an approximate closed form solution describing dynamic displacement of the tympanic membrane. To do so, we begin by determining geometrically dependent terms in the equilibrium equations for a general eardrum shape. The shape of the eardrum can be described as a "perturbed cone" where departure from the perfect cone shape is given by $\varepsilon g(r,\theta)$. The resting position is defined by $f(r,\theta) = \alpha r + \varepsilon g(r,\theta)$ as shown in Figure 5.2. Definition of the eardrum shell surface in this manner introduces the natural small parameter ε.

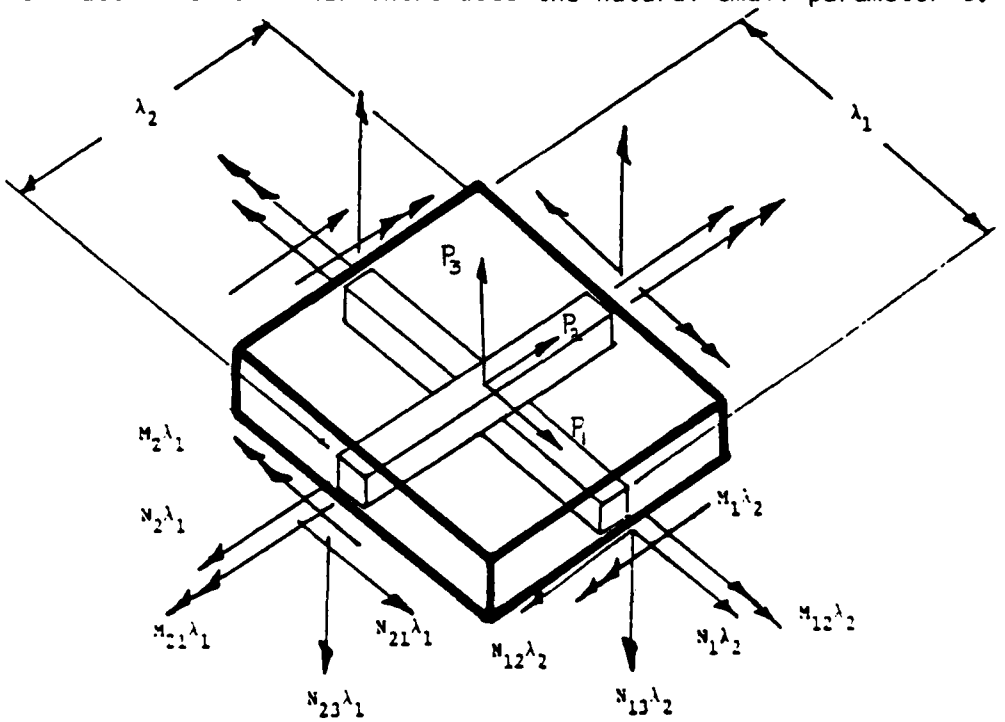

Figure 5.1 Equilibrium of an element of composite material.

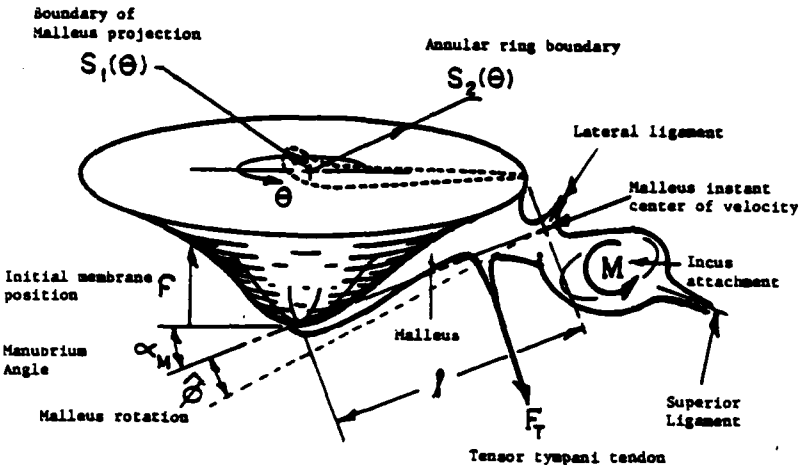

Figure 5.2 Geometrical sketch of the tympanic membrane.

Selecting polar coordinates $q_1 = r$ and $q_2 = \theta$ defines the position vector $\underset{\sim}{r}$.

$$\underset{\sim}{r} = r\cos\theta\,\underset{\sim}{i} + r\sin\theta\,\underset{\sim}{j} + (\alpha r + \varepsilon g)\underset{\sim}{k} \quad , \tag{5.1.4}$$

where $\underset{\sim}{i}$, $\underset{\sim}{j}$, are in the plane of the annular ring and $\underset{\sim}{k}$ denotes the axial direction. On the surface, tangent vectors to coordinate lines are

$$\underset{\sim}{r}_1 = \frac{\partial r}{\partial r}\cos\theta\,\underset{\sim}{i} + \sin\theta\,\underset{\sim}{j} + (\alpha + \varepsilon g_r)\underset{\sim}{k} \quad , \tag{5.1.5}$$

$$\underset{\sim}{r}_2 = \frac{\partial r}{\partial \theta} = -\,r\sin\theta\,\underset{\sim}{i} + r\cos\theta\,\underset{\sim}{j} + \varepsilon g_\theta\,\underset{\sim}{k} \quad .$$

Using these the coordinate metric normalizers are

$$H_2 = r + O(\varepsilon^2) \quad ,$$

$$H_1 = (1+\alpha^2)^{1/2} + \frac{\varepsilon\alpha g_r}{2(1+\alpha^2)^{1/2}} + O(\varepsilon^2) \quad , \tag{5.1.6}$$

and

$$H_{12} = \varepsilon\alpha g_\theta + O(\varepsilon^2) \quad .$$

After finding unit normals to the surface, principal radii of curvature are determined to be

$$\varepsilon R_1 = \frac{-1}{n_0 g_{rr}} + \varepsilon \frac{r(1+\alpha^2)}{n_0\,\alpha} + O(\varepsilon^2) ,$$

$$R_2 = \frac{r(1+\alpha^2)}{n_0\,\alpha} + O(\varepsilon) , \qquad (5.1.7)$$

and

$$n_0 = (1+\alpha^2)^{-1/2} - \varepsilon \frac{\alpha g_r}{2(1+\alpha^2)^{3/2}} + O(\varepsilon^2) .$$

Also, letting $w(r,\theta,t)$ denote the deformation normal to the inital position (transverse deformation), then

$$\theta_1 = \frac{\partial w}{\partial r}\left\{(1+\alpha^2)^{1/2} - \varepsilon\, g_r \frac{\alpha}{2(1+\alpha^2)^{3/2}} + O(\varepsilon^2)\right\} , \qquad (5.1.8)$$

and

$$\theta_2 = \frac{\partial w}{\partial \theta}\left\{\frac{1}{r} + O(\varepsilon^2)\right\} .$$

The membrane stresses in the tympanic membrane are related to strains and curvatures through a constitutive law. The most general linear constitutive law for membrane stresses in a composite has the form (Jones, 1979)

$$\underset{\sim}{N} = \underline{Q}\ \underset{\sim}{\varepsilon} + \underline{B}\ \underset{\sim}{k} , \qquad (5.1.9)$$

where N_i is the membrane force, Q_{ij} is the membrane stiffness, ε_i is the strain, B_{ij} represents coupling to changes in curvature, and k_i is the change in curvature. Since the TM ultrastructure is not symmetric through its cross section, $\underline{B}$ will be nonzero - a complication not encountered with isotropic materials. The curvatures are

$$k_1 = \frac{-1}{H_1}\frac{\partial \theta_1}{\partial q_1} - \frac{\theta_2}{H_1 H_2}\frac{\partial H_1}{\partial q_2} ,$$

$$k_2 = \frac{1}{H_2}\frac{\partial \theta_2}{\partial q_2} - \frac{\theta_1}{H_1 H_2}\frac{\partial H_2}{\partial q_1} , \qquad (5.1.10)$$

and

$$k_{12} = -\frac{1}{2}\left(\frac{1}{H_1}\frac{\partial \theta_2}{\partial q_1} + \frac{1}{H_2}\frac{\partial \theta_1}{\partial q_2}\right) .$$

Defining $u_1(r,\theta)$ and $u_2(r,\theta)$ as deformations tangent to the surface then

$$\varepsilon_1 = \frac{1}{2}\theta_1^2 + \frac{1}{H_1}\frac{\partial u_1}{\partial q_1} + \frac{1}{H_1 H_2}\frac{\partial H_1}{\partial q_2}u_2$$

$$\varepsilon_2 = \frac{1}{2}\theta_2^2 + \frac{1}{H_2}\frac{\partial u_2}{\partial q_2} + \frac{1}{H_1 H_2}\frac{\partial H_2}{\partial q_1}u_1 \qquad (5.1.11)$$

and

$$\gamma_{12} = \theta_1\theta_2 + \frac{1}{H_1}\frac{\partial u_2}{\partial q_1} + \frac{1}{H_2}\frac{\partial u_1}{\partial q_2} - \frac{1}{H_1 H_2}\frac{\partial H_2}{\partial q_1}u_2 + \frac{1}{H_1 H_2}\frac{\partial H_1}{\partial q_2}u_1$$

To insure existence of a single valued deformation field associated with the stress forms we need to satisfy the following compatibility condition (Novozhilov, 1959).

$$\frac{\partial}{\partial q_1}\left[\frac{1}{H_1}\frac{\partial}{\partial q_1}(H_2\varepsilon_2) - \frac{1}{H_1}\frac{\partial H_2}{\partial q_1}\varepsilon_1 - \frac{1}{2}\frac{1}{H_1^2}\frac{\partial}{\partial q_2}(H_1^2\gamma)\right]$$

$$+ \frac{\partial}{\partial q_2}\left[\frac{1}{H_2}\frac{\partial}{\partial q_2}(H_1\varepsilon_1) - \frac{1}{H_2}\frac{\partial H_1}{\partial q_2}\varepsilon_2 - \frac{1}{2}\frac{1}{H_2^2}\frac{\partial}{\partial q_2}(H_2^2\gamma)\right]$$

$$= \frac{1}{2}\frac{\partial}{\partial q_1}\left[\frac{1}{H_1}\frac{\partial}{\partial q_1}(H_2\theta_2^2) - \frac{1}{H_1}\frac{\partial H_2}{\partial q_1}\theta_1^2 - \frac{1}{H_1^2}\frac{\partial}{\partial q_2}(H_1^2\theta_1\theta_2)\right]$$

$$+ \frac{1}{2}\frac{\partial}{\partial q_2}\left[\frac{1}{H_2}\frac{\partial}{\partial q_2}(H_1\theta_1^2) - \frac{1}{H_2}\frac{\partial H_1}{\partial q_2}\theta_2^2 - \frac{1}{H_2^2}\frac{\partial}{\partial q_1}(H_2^2\theta_1\theta_2)\right]$$

With this result, the general formulation is complete.

5.2 Ultrastructure Simplifications

The middle plane spacing of the fibers within the tympanic membrane indicates that the bending - membrane coupling coefficients B_{ij} are relatively small. For a symmetric laminate composite $\underline{B}$ is identically zero. In addition to small bending - membrane coupling, the membrane shear stiffness Q_{33} and shear couplings Q_{23}, Q_{13}, are small for the eardrum material. Neglecting

these terms in (5.1.9) gives

$$\begin{bmatrix} N_1 \\ N_2 \end{bmatrix} = \begin{bmatrix} Q_{11} & Q_{12} \\ Q_{21} & Q_{22} \end{bmatrix} \begin{bmatrix} \varepsilon_1 \\ \varepsilon_2 \end{bmatrix} \tag{5.2.1}$$

Moreover, $N_{12} = 0$, $M_{ij} \simeq 0$, and $\underline{B} \simeq 0$. If we also neglect in-plane inertia then $P_1 = 0$ and $P_2 = 0$. With these simplifications the equilibrium equations (5.1.1) - 5.1.3) reduce to

$$\frac{\partial}{\partial r}(H_2 N_1) - \frac{\partial H_2}{\partial r} N_2 = 0 , \tag{5.2.2}$$

$$\frac{\partial}{\partial \theta}(H_1 N_2) - \frac{\partial H_1}{\partial \theta} N_1 = 0 , \tag{5.2.3}$$

and

$$\frac{1}{H_1 H_2}\left\{\frac{\partial}{\partial r}(H_2 \theta_1 N_1) + \frac{\partial}{\partial \theta}(H_1 \theta_2 N_2)\right\} - \frac{N_1}{R_1} - \frac{N_2}{R_2} + P_3 = 0 . \tag{5.2.4}$$

Using (5.1.6) the first two equilibrium equations can be combined to show that the membrane forces have the form

$$\begin{aligned} N_2 &= N_2(r) + O(\varepsilon) \\ N_1 &= \frac{1}{r}\int_0^r N_2(\eta)\partial\eta + \frac{C_1(\theta)}{r} + O(\varepsilon) \end{aligned} \tag{5.2.5}$$

where $C_1(\theta)$ is a constant of integration. Using this in the third equilibrium equation (5.2.4) gives

$$\frac{1}{rH_1}\left\{\frac{N_2}{N_1}\left(\theta_1 + \frac{\partial}{\partial \theta}(\theta_2 H_1)\right) + r\frac{\partial \theta_1}{\partial r}\right\} - \frac{1}{R_1} - \frac{N_2}{N_1 R_2} + \frac{P_3}{N_1} \tag{5.2.6}$$

$$+ O(\varepsilon) = 0 .$$

Nondimensionalizing r by the average radius a, and $w(r,\theta)$ by the experimentally observed maximum transverse deformation shows that the ratio of the average circumferential force $\overline{N}_2$ to the average radial force $\overline{N}_1$ provides a second natural small parameter $\kappa = \overline{N}_2/\overline{N}_1$. Representing $w(r,\theta,t)$ by an expansion in

κ we have

$$w(r,\theta,t;\kappa) = w_0(r,\theta,t) + \kappa\, w_1(r,\theta,t) + \ldots$$

Substitution into the reduced equilibrium equations (5.2.2, 5.2.3, 5.2.6) yields the following sequence of problems when making use of relations (5.1.8).

$O(1)$

$$\frac{\partial^2 w_0}{\partial r^2} + \zeta \frac{\partial^3 w_0}{\partial r^2 \partial t} = \frac{1}{C^2} \frac{\partial^2 w_0}{\partial t^2} + q \ , \quad S_1(\theta) < r < S_2(\theta) \ , \quad 0 < \theta < 2\pi \tag{5.2.8}$$

where

$$w_0(S_2,\theta,t) = \gamma\phi[w_0]$$

$$w_0(S_2,\theta,t) = 0 \ .$$

$\gamma\phi$ is an operator describing the malleus boundary condition including ossicular and cochlear dynamic terms. Assuming $\varepsilon/\kappa = O(1)$, then the order κ problem on the same domain is

$O(\kappa)$

$$\begin{aligned} \frac{\partial^2 w_1}{\partial r^2} + \zeta \frac{\partial^3 w_1}{\partial r^2 \partial t} &= \frac{1}{C^2} \frac{\partial^2 w_1}{\partial t^2} - \zeta \frac{1}{r} \frac{\partial^2 w_0}{\partial r \partial t} - \frac{\zeta}{r^2} \frac{\partial^3 w_0}{\partial \theta^2 \partial t} \\ &\quad - \left\{ \frac{1}{rN_1} \frac{\partial w_0}{\partial r} + \frac{(1+\alpha^2)}{r^2 N_1} \frac{\partial^2 w_0}{\partial \theta^2} - \frac{(1+\alpha^2) r}{R_2} \right\} \\ &\quad + \frac{\varepsilon}{\kappa} \frac{\alpha g r}{2} \left\{ \frac{1}{R_1} + \frac{P}{N_1} + \frac{\beta}{N_1} \frac{\partial^2 w_0}{\partial t^2} \right\} \end{aligned} \tag{5.2.9}$$

where

$$w_1(S_1,\theta,t) = 0 \ ,$$

and

$$w_1(S_2,\theta,t) = 0 \ ,$$

and

$$\beta = \rho h \ ,$$

where a D'Alembert reverse inertial pressure has been included transverse to the resting position. The boundary $r = S_1(\theta)$ represents projection of the malleus boundary onto the (r,θ) plane, and $r = S_2(\theta)$ represents projection of the annular ring boundary onto the (r,θ) plane. The ζ terms represent first order linear bending type damping (see section 4.1).

If the radial membrane force N_1 were known then the O(1) problem could be solved directly.

As $\varepsilon \to 0$ and the shell becomes a cone we find $N_1 \to a\tilde{N}_1(\theta)/r$. It can also be shown by looking at equilibrium equation (5.2.2) that $N_1 \to a\tilde{N}_1(\theta)/r$ as $\kappa \to 0$. Hence it seems very reasonable to let

$$N_1 = \frac{a\tilde{N}_1(\theta)}{r} \tag{5.2.10}$$

for small κ and small ε. Using this form it is straightforward to estimate N_1 using the orthotropic constitutive law approximations of Chapter 3.

The form of equation (5.2.8) suggests that it may be appropriate to model the tympanic membrane as a set of coupled radial fibers. This alternative approach is outlined in Appendix A.

5.3 Asymptotic Solution For w_0

Consider the case when the damping and sound speed are constant to first order such that ζ and c appear as constant coefficients. To homogenize the boundary conditions in (5.2.8) introduce a transformation on the dependent variable

$$w_0(r,\theta,t) = u_0(r,\theta,t) + \frac{(r-S_2(\theta))}{(S_1(\theta)-S_2(\theta))}\,\gamma\,\phi[w_0] \tag{5.3.1}$$

The first order problem becomes

$$\frac{\partial^2 u_0}{\partial r^2} + \zeta\,\frac{\partial^3 u_0}{\partial r^2 \partial t} = \frac{1}{C^2}\left(\frac{\partial^2 u_0}{\partial t^2} + \frac{r-S_2}{S_1-S_2}\,\gamma\,\frac{\partial^2 \phi}{\partial t^2}\right) + q \tag{5.3.2}$$

with homogeneous boundary conditions

$$u_o\ (S_1,\theta,t) = 0\ ,$$

$$u_o\ (S_2,\theta,t) = 0$$

where γ is a third small parameter representing small motion of the malleus and ϕ is an operator describing middle ear and cochlear connections.

Looking for an asymptotic solution for small γ , consider a direct expansion of $u_o(r,\theta,t)$

$$u_o(r,\theta,t;\ ) = v_o(r,\theta,t) + \gamma\ v_1(r,\theta,t) + \ldots \qquad (5.3.3)$$

Substitution of this into (5.3.2) leads to the following sequence of problems

$O(1)$

$$\frac{\partial^2 v_o}{\partial r^2} + \zeta\ \frac{\partial^3 v_o}{\partial r^2 \partial t} = \frac{1}{C^2}\ \frac{\partial^2 v_o}{\partial t^2} + q\ , \quad S_1(\theta) < r < S_2(\theta)\ , \quad 0 < \theta < 2\pi \qquad (5.3.4)$$

where

$$v_o(S_1,\theta,t) = 0$$

$$v_o(S_2,\theta,t) = 0$$

$O(\gamma)$

$$\frac{\partial^2 v_1}{\partial r^2} + \zeta\ \frac{\partial^3 v_1}{\partial r^2 \partial t} = \frac{1}{C^2}\ \frac{\partial^2 v_1}{\partial t^2} + \frac{r-S_2}{C^2(S_1-S_2)}\ \frac{\partial^2 \phi[v_o]}{\partial t^2}\ , \qquad (5.3.5)$$

where

$$v_1(S_1,\theta,t) = 0$$

$$v_1(S_2,\theta,t) = 0\ .$$

For the case of harmonic forcing $q = q_0(r,\theta) \sin \omega t$, the solution to (5.3.4) is easily found by eigenfunction expansion to be

$$v_o = \sum_{n=1}^{\infty} \left\{ \frac{c^2 q_n \sin(\omega t + \psi_n)}{\omega_n^2 \sqrt{\left[1-\left(\frac{\omega}{\omega_n}\right)^2\right]^2 + (\zeta\omega)^2}} + c_n e^{-\zeta\omega_n^2 t/2} \sin\left[\sqrt{1 + \frac{1}{4}(\zeta\omega_n)^2}\ \omega_n t + \xi_n\right] \right\} \sin\left[n\pi\left(\frac{r-S_1}{S_2-S_1}\right)\right] , \tag{5.3.6}$$

where ζ is the damping coefficient, c is the sound speed, c_n, ξ_n are constants determined from the inital conditions,

$$\psi_n(\theta) = \text{Arctan}\left(\frac{\zeta\omega_n^2\,\omega}{\omega_n^2-\omega^2}\right) , \qquad \omega_n(\theta) = \frac{n\pi c}{S_2-S_1} \tag{5.3.7}$$

and

$$q_n(\theta) = \frac{-2}{S_1-S_2} \int_{S_2}^{S_1} q_0(r,\theta) \sin\left[n\pi\left(\frac{r-S_1}{S_1-S_2}\right)\right] dr.$$

To solve the $O(\gamma)$ problem in (5.3.5) it is necessary to find the malleus deformation. To determine the malleus motion, define the differential operator L relating angular deformation of the malleus $\hat{\phi}$ to the moment transmitted through the tympanic membrane (see Fig. 5.2).

$$L\left[\hat{\phi}\right] = M(t) \tag{5.3.8}$$

Expanding the moment $M = M_0 + \gamma M_1 + O(\gamma^2)$ allows direct calculation of the change in moment ΔM_0 as an integral of forces on the malleus imparted by tympanic membrane fibers.

$$\Delta M_0(t) = \Delta \int_{S_1} (\vec{N}_1 \times \vec{O})\cdot\hat{m}\ ds \tag{5.3.9}$$

Where $\vec{N}_1$ is the tension vector in the direction of a radial fiber at the malleus, $\vec{O}$ is the position vector from the malleus instant center of velocity

to S_1, and $\hat{m}$ is a unit vector along the instantaneous axis of rotation of the malleus (see Appendix B). This gives M_0 explicitly in terms of V_0 allowing direct calculation of the malleus motion by solving the differential system

$$\hat{\phi}(t) = L^{-1}[M_0(t)] \tag{5.3.10}$$

From the malleus angular deformation we can determine the deformation at a particular point on the malleus

$$\gamma\, \phi_0[V_0] = (\vec{0} \times \hat{m})\cdot\hat{s}\, \hat{\phi} \tag{5.3.11}$$

where $\hat{\phi}$ is the instantaneous rotation of the malleus and s is the unit normal in the direction of the component being calculated. With this result, the $O(\gamma)$ problem has the same form as in (5.3.6) where q is replaced by q*, given as

$$q^* = \frac{r-S_2}{c^2(S_1-S_2)}\, \frac{\partial^2\phi_0}{\partial t^2}\,. \tag{5.3.12}$$

Knowing ϕ_0, V_0 and V_1 determines w_0 to $O(\gamma^2)$.

$$w_0(r,\theta,t) \simeq V_0(r,\theta,t) + \gamma\, V\,(r,\theta,t) + \frac{r-S_2}{S_1-S_2}\,\gamma\,\phi_0 + O(\gamma^2)\,. \tag{5.3.13}$$

The above expression is a closed form asymptotic solution to the general tympanic membrane problem. It is coupled to the ossicles by membrane stresses and includes effects of middle ear and cochlear dynamics through the very general operator L. The outer ear and middle ear air chambers are indirectly included as perturbations on the excitation pressure field.

5.5 Qualitative Numerical Results

Representing the geometry of a cat we selected an annular ring superior

radius of 0.35 cm, and anterior radius of 0.30 cm, malleus angle defining depth of the drum of 0.64 radians, average density of 2.0 grams/cm^3, average thickness of 40×10^{-4} cm, and nondimensional damping coefficient of 3×10^{-5}. In addition to these parameters the local stiffnesses were estimated using equation (3.6.11) along with ultrastructural observations of the volume fractions of radial and circumferential fibers. A very small initial prestress was imposed by rotating the malleus 10^{-3} radians with respect to its no force position. This initial rotation could easily be imparted by the tensor tympani or ligament preloads.

Using these values, equation (5.3.13) reproduces vibrational shapes observed experimentally. Figure 5.3 indicates vibration of the drum when subjected to a pure 600 Hz tone at 105 dB SPL. The vibrational shape essentially matches that observed experimentally by Khanna and Tonndorf (1972). The shapes shown in Figure 5.3 are based on a simplified geometry and neglect the pars flaccida and hence the shapes deviate slightly from the results of Khanna and Tonndorf. The asymptotic solution given by (5.3.13) is capable of describing behavior for the more complex geometry and material, however the intent here is simply to look at qualitative behavior leaving detailed calculations for Part II of this report.

At 600 Hz the drum vibrates in its fundamental shape essentially in phase with the excitation pressure. As the frequency is increased the membrane vibrational amplitude decreases and begins to lag the excitation. Above 4000 Hz a transition from the simple fundamental vibrational shape to a complex shape is reproduced by the asymptotic solution. When forced at higher frequencies, the vibrational shape of the tympanic membrane is constantly changing in time. Figure 5.4 shows normalized displacement at 4000 Hz for two different times during the excitation cycle. Time averaged experimental

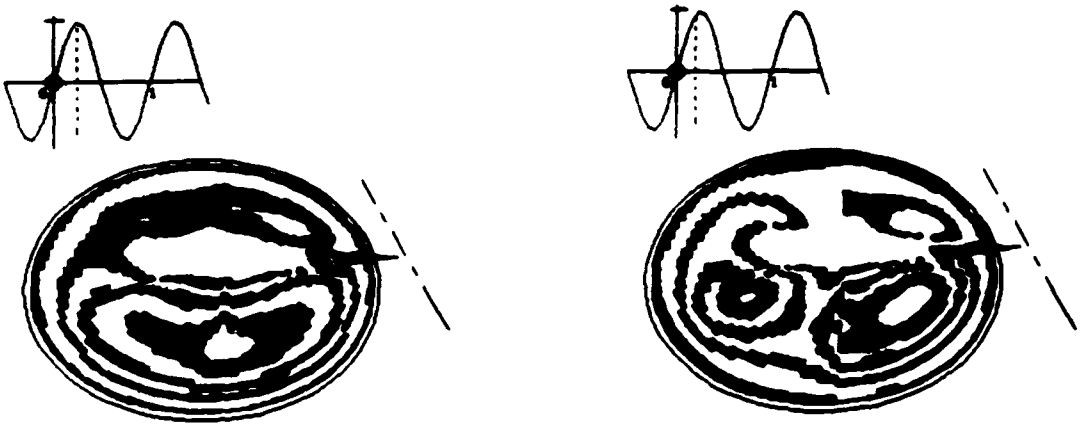

600 Hz 6000 Hz

Figure 5.3 Normalized vibrational shapes at 600 Hz and 6000 Hz, 105 dB SPL.

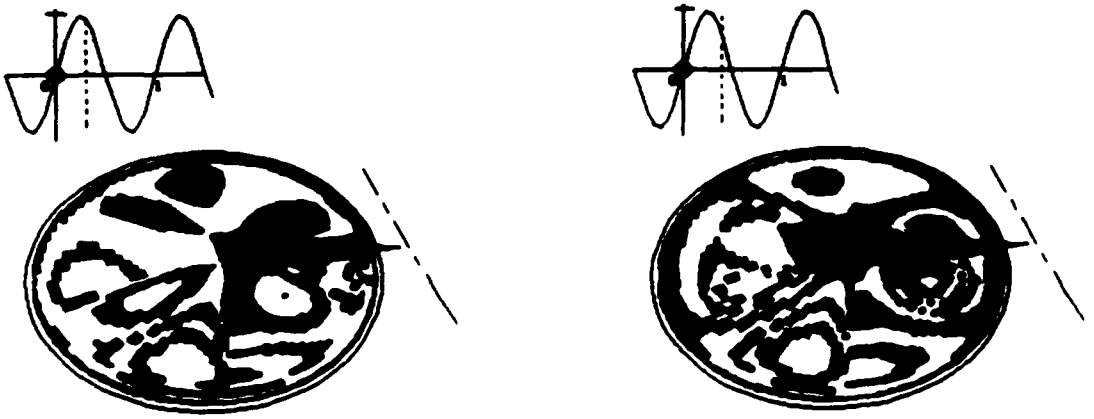

4000 Hz 4000 Hz

Figure 5.4 Normalized vibrational shapes at 4000 Hz for two distinct times during the cycle.

results represent a weighted average of many curves, as shown in Fig. 5.4, over numerous cycles (time averaged holography for example).

Results that can be obtained from the asymptotic solution are numerous. The effects of geometrical changes, material alterations, scar tissue, and middle ear changes represent only a few of the possible topics. In addition to these, many clinical applications may be found. Spatial integrations of the asymptotic solution can be compared directly to tympanograms and acoustic impedance data. The comparisons can be used to make the tympanic membrane transparent to clinicians or to assess function of the eardrum itself. Part II of this report will study the asymptotic solution and address some of the topics mentioned.

5.5 APPENDIX A

A FINITE RADIAL FIBER MODEL

By studying the behavior of the TM under various conditions, it appears that the radial (or meridian) fibers play the dominant role in the function of the drum. Any axial stresses in the meridian fibers act directly on the malleus, near the umbo in most cases, and thus transmit force directly to the ossicles. The complicated vibrational shape at high frequencies observed experimentally also suggests that the circumferential fibers play a secondary coupling role while the radial fibers dominate the shape and transmittance behavior. Assuming that this postulated radial dominance exists, it is possible to formulate a coupled set of m partial differential equations, that individually represent the physics of a sectional strip of the TM. Since most of the radial fibers run in the meridian direction originating at the umbo, most of the strips will be pie shaped sections of the membrane. Each radial structure, or pie shaped strip, is attached to the annular ring on the outside edge and attached to the malleus on the inside edge. It is assumed that the fiber elements interact with each other through a membrane type tension term, however the element itself contains both bending and tension energy storage mechanisms. Dissipation of energy is assumed to be of the bending type and hence will be proportional to time rate of changes in the two principle radii of curvature of the drum surface.

We begin the model by defining N coordinates X_N originating at the malleus attachment of each fiber directed outward toward the fiber attachment at the annular ring. The X_N coordinates are along straight lines, such that the middle plane of each radial element in its original static

equilibrium position is defined by $U_{ON}(X_N)$. For fibers attached at the umbo, the X_N coordinate will correspond to the polar coordinate r; for fibers attached on the shank of the malleus, the X_N coordinate will cut across polar coordinate lines.

In order to model one particular element, imagine that we have cut the fiber and its surrounding tissue from the membrane. The single radial fiber (or group of radial fibers) imbedded in the tissue slice is under a meridian stress σ_{mn}, has thickness $h_N(X_N)$, and width $w_N(X_N)$. The static equilibrium position of the Nth fiber element is described in global coordinates as $z^* = f(r,\theta)$, or in local element coordinates as $U_{ON}(X_N)$. Figure 5.5 indicates the coordinates for a typical radial element.

Viewing the radial element from the side, it appears as a curved

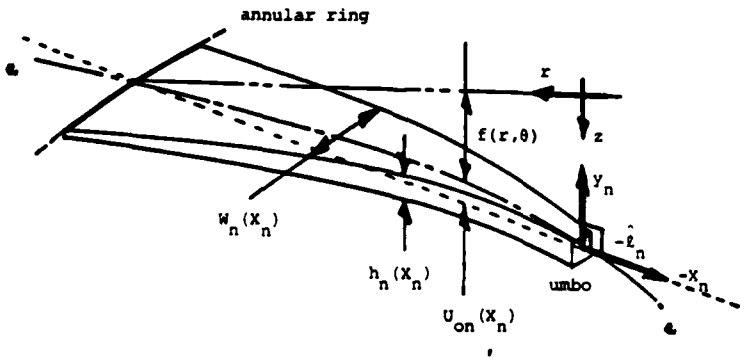

Figure 5.5 Sketch of a pie shaped slice of the tympanic membrane.

beam under axial tension forced by the applied pressure and adjacent elements. The fiber element, if originating from the umbo, will have a variable width nearly proportional to the lengthwise coordinate (or r). Denote the deflection of a point perpendicular to the static equilibrium position as $U_N(X_N,t)$, and the component of deflection normal to $U_N(X_N,t)$ as $V_N(X_N,t)$. Displacement at the malleus attachment is denoted ($U_{NE}(0,t)$, $V_{NE}(0,t)$).

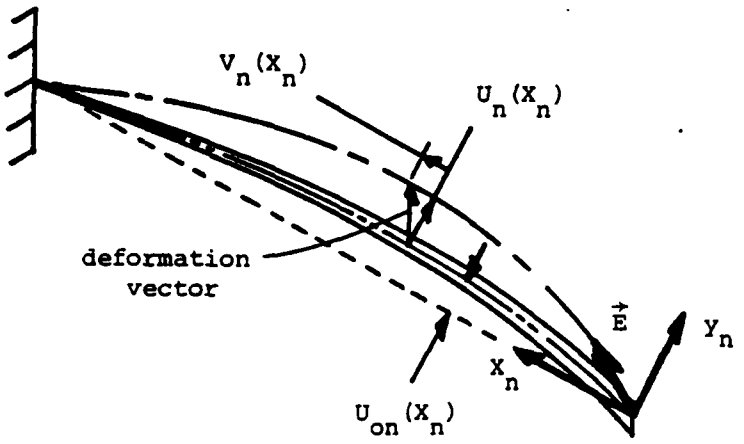

Figure 5.6 Side view of a single radial fiber in local coordinates.

Suppose the element thickness w << a (a=length) and that the initial curvature is much larger than the thickness (or in fact the length), such that a linear stress distribution due to internal bending moment(s) is a reasonable approximation. For the same reason it is assumed that the axial stress distribution can be approximated as uniform across each section.

Under such conditions the primary forces acting on a differential slice of the radial element in X are indicated in Fig. 5.7.

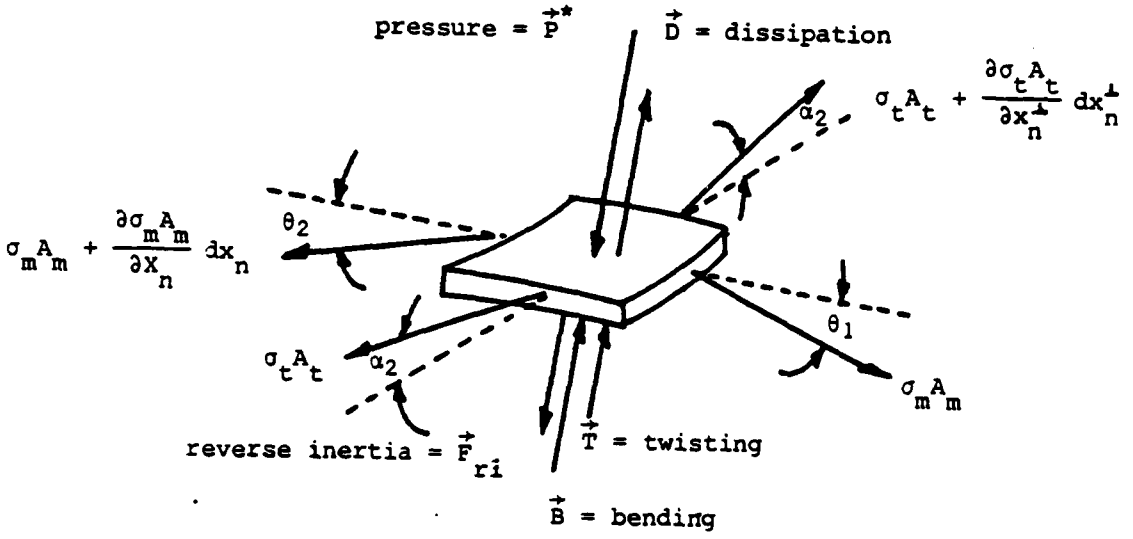

Figure 5.7 Equilibrium of an element of drum material.

Considering conservation of momentum normal to the membrane surface, we can derive a differential equation describing the element. Noting that:

$$\alpha_1 = \text{Arctan}\,\frac{u_n - u_{n-1}}{w_n} + \text{Arcsin}\,(\hat{i}_n \times \hat{i}_{n-1})\,\frac{1}{2}\,\frac{\partial f}{\partial r^*}$$

$$\alpha_2 = \text{Arctan}\,\frac{u_n - u_{n+1}}{w_n} + \text{Arcsin}\,(\hat{i}_n \times \hat{i}_{n+1})\,\frac{1}{2}\,\frac{\partial f}{\partial r^*}$$

$$B = \frac{\partial^2}{\partial x_n^2}\left(Q_m I_s \frac{\partial^2 u_n}{\partial x_n^2}\right) + B_t = \frac{\partial}{\partial x_n^2}\left(D_m \times_n \frac{\partial^2 u_n}{\partial x_n^2}\right) + B_t$$

$$F_{R1} = \frac{\partial}{\partial t}\left(\rho A \frac{\partial u_n}{\partial t}\right)$$

$$D \approx \frac{\partial}{\partial t}\left(C_m\, h\, W_n \frac{\partial^2 u_n}{\partial x_n^2} + c_T h \frac{u_{n+1} - 2u_n + u_{n-1}}{W_n}\right) \tag{5.5.1}$$

$$u_{Tn} = u_n + u_{on}$$

$$T \approx \frac{1}{X_n} \frac{\partial}{\partial x_n}\left(X_n \frac{\partial}{\partial x_n}\right) \frac{S_T}{W_n^2} \left(u_{n+1} - 2u_n + u_{n-1}\right)$$

$$B_T \approx \frac{D_c}{w_n^4} \left(u_{n+2} - 4u_{n+1} + 6u_n - 4u_{n-1} + u_{n-2}\right) w_n$$

Momentum gives

$$\begin{aligned} &\frac{\partial^2}{\partial x_n^2}\left(Q_m I_s \frac{\partial^2 u}{\partial x_n^2}\right) - \frac{\partial}{\partial x_n}\left(\sigma_m A \frac{\partial^2 u_{Tn}}{\partial x_n}\right) + \sigma_t h(\sin \alpha_1 + \sin \alpha_2) \\ &\quad + \frac{\partial}{\partial t}\left(c_m h\, w_n \frac{\partial^2 u_n}{\partial x_n^2} + c_t h \frac{1}{w_n}\left(u_{n+1} - 2u_n + u_{n-1}\right)\right) - B_T \\ &\quad + \frac{1}{X_n} \frac{\partial}{\partial x_n}\left(X_n \frac{\partial}{\partial x_n}\right) \frac{S_T}{W_n^2} \left(u_{n+1} - 2u_n + u_{n-1}\right) \\ &\quad = P w_n + \frac{\partial}{\partial t}\left(\rho A \frac{\partial u_n}{\partial t}\right) \end{aligned} \tag{5.5.2}$$

Expanding for small deformation, this can be written as

$$\begin{aligned} &\frac{\partial^2}{\partial x_n^2}\left(D_m w_n \frac{\partial^2 u_n}{\partial x_n^2}\right) + \frac{D_c}{w_n^3} \left(u_{n+2} - 4u_{n+1} + 6u_n - 4u_{n-1} + u_{n-2}\right) \\ &\quad - \frac{\partial}{\partial x_n}\left(T_m w_n \frac{\partial u_{Tn}}{\partial x_n}\right) + \frac{T_c}{w_n}\left(u_{T_{n+1}} - 2u_{T_n} + u_{T_{n-1}}\right) + \frac{T_c w_n}{x_n} \frac{\partial f}{\partial r^*} \\ &\quad + \frac{\partial}{\partial t}\left(c_m h\, w_n \frac{\partial^2 u_n}{\partial x_n^2} + \frac{c_t h}{w_n}\left(u_{n+1} + u_{n-1} - 2u_n\right)\right) \\ &\quad + \frac{1}{X_n} \frac{\partial}{\partial x_n}\left(X_n \frac{\partial}{\partial x_n}\right) \frac{S_T}{W_n^2} \left(u_{n+1} - 2u_n + u_{n-1}\right) \\ &\quad = P w_n + \frac{\partial}{\partial t}\left(\rho h w_n \frac{\partial u_n}{\partial t}\right) \end{aligned} \tag{5.5.3}$$

The previous equation reduces to the first order membrane shell model as the bending stiffness approaches zero. Equation (5.5.3) is not exact, but does contain bending terms and circumferential coupling not contained in the first order shell membrane equation.

APPENDIX B

MALLEUS MOMENT AND DISPLACEMENT RELATIONSHIPS

In order to determine the moment imposed by the tympanic membrane on the malleus about its instant center of velocity, the radial tension vector $\vec{T}$ and position $\vec{0}$ are defined as indicated in the diagram below

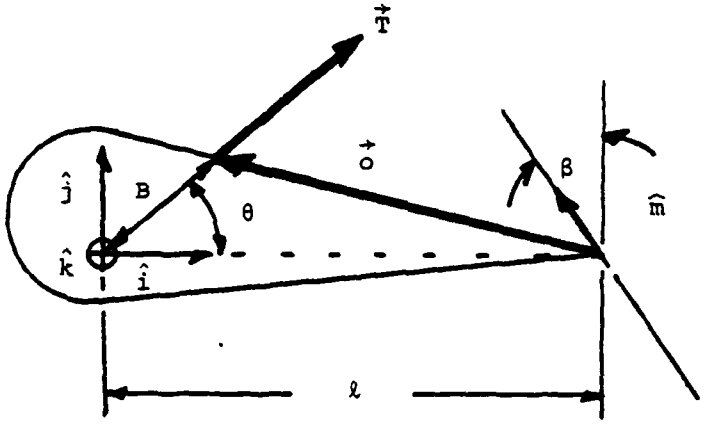

Figure 5.8 Sketch indicating tension vector due to a radial fiber on the malleus

The tension vector is

$$\vec{T} = T\cos\hat{\alpha}\,(\cos\theta\,\hat{i} + \sin\theta\,\hat{j}) + T\sin\hat{\alpha}\,\hat{k}$$

$$= \frac{T}{\sqrt{1+\alpha^2}}\,[\cos\theta\,\hat{i} + \sin\theta\,\hat{j} + \hat{\alpha}\,\hat{k}] \qquad (5.5.4)$$

$$= t_1\,\hat{i} + t_2\,\hat{j} + t_3\,\hat{k}$$

and the position vector is

$$\vec{0} = (\ell - B\cos\theta)(-\hat{i}) + B\sin\theta\,\hat{j} - (\ell - B\cos\theta)\sin\alpha_m\,\hat{k}$$

$$\vec{0} = 0_1\hat{i} + 0_2\hat{j} + 0_3\hat{k} \qquad (5.5.5)$$

The resulting moment is

$$\vec{M} = \vec{T} \times \vec{O} = \begin{vmatrix} i & j & k \\ t_1 & t_2 & t_3 \\ O_1 & O_2 & O_3 \end{vmatrix}$$

$$\vec{M} = M_1 \hat{r} + M_2 \hat{j} + M_3 \hat{k}$$

where

$$M_1 = \frac{T}{\sqrt{1+\alpha^2}} \sin\theta\,(B\cos\theta-\ell)\sin\alpha_m - \frac{T\alpha}{\sqrt{1+\alpha^2}} B\sin\theta$$

$$M_2 = \frac{T(B\cos\theta-\ell)}{\sqrt{1+\alpha^2}}(\alpha + \cos\theta \sin\alpha_m) \tag{5.5.6}$$

$$M_3 = t_1 O_2 - t_2 O_1$$

The component causing rotation about the instant center of velocity is

$$M = \vec{M} \cdot \hat{m}$$

$$= \vec{M} \cdot (-\sin\beta\,\hat{i} + \cos\beta\,\hat{j}) \tag{5.5.7}$$

$$M = \frac{T}{\sqrt{1+\alpha^2}}\left[\sin\theta \sin\beta\{(\ell-B\cos\theta)\sin\alpha_m + \alpha B\}\right.$$

$$\left. + (B\cos\theta-\ell)\cos\beta\,\{\alpha + \cos\theta \sin\alpha_m\}\right]$$

where we have taken the instant centerline to be in the plane of the annular ring. This assumption could easily be relaxed by including a third component in $\hat{m}$.

During a deformation α and T change. To obtain the change in the moment during the deformation let

$$\alpha(t) = \alpha + \Delta\alpha$$

$$T(t) = T + \Delta T \tag{5.5.8}$$

Substituting into the moment expression and using $\alpha >> \Delta\alpha$, $T >> \Delta T$ we obtain the change in moment

$$\Delta M \sim \frac{T\,\Delta\alpha}{\sqrt{1+\alpha^2}} \{(\ell - B\cos\theta)\cos\beta - B\sin\theta\sin\beta\} \tag{5.5.9}$$

$$\Delta\alpha = \frac{\partial v}{\partial r}\Big|_{s_1}$$

The displacement of the malleus at the attachment of a radial fiber is defined by vector $\vec{d}$ and is related to malleus rotation $\hat{\phi}$ by

$$\vec{d} = (\vec{0} \times \hat{M})\hat{\phi} \tag{5.5.10}$$

$$= \{0_3 \cos\beta\, \hat{i} + 0_3 \sin\beta\, \hat{j} - (0_1 \cos\beta + 0_2 \sin\beta)\, \hat{k}\}\hat{\phi}$$

The component in the $\hat{k}$ direction is

$$d_3 = \{(\ell - B\cos\theta)\cos\beta - B\sin\theta\sin\beta\}\hat{\phi} \tag{5.5.11}$$

APPENDIX C

IMPULSE RESPONSE

If the tympanic membrane is subjected to an impulse of magnitude I at time t = 0 then the V_o function is defined by

$$\frac{\partial^2 V_0}{\partial r^2} + \zeta \frac{\partial^3 V_0}{\partial r^2 \partial t} - \frac{1}{C^2} \frac{\partial^2 V_0}{\partial t^2} = I\ \delta(t) \qquad (5.5.12)$$

For an eardrum initially at rest $V_0(r,\theta,0) = 0$ and $V_{0_t}(r,\theta,0) = 0$. Integrating (5.5.12) across the impulse in time allows us to reformulate the problem as a homogeneous operator with nonzero initial conditions. The equivalent problem is

$$\frac{\partial^2 V_0}{\partial r^2} + \zeta \frac{\partial^3 V_0}{\partial r^2 \partial t} - \frac{1}{C^2} \frac{\partial^2 V_0}{\partial t^2} = 0 \qquad (5.5.13)$$

with initial conditions at time zero plus $V_0(r,\theta,0+) = 0$ and $V_0(r,\theta,0+) = -C_0^2 I$. The general solution to (5.5.13) can be written

$$V_0 = \sum_{n=1}^{\infty} C_n e^{-\zeta\, \omega_n^2 t/2} \sin\left\{\sqrt{1+\frac{1}{4}(\zeta\omega_n)^2}\ \omega_n t + \xi_n\right\} \sin\left(n\pi \frac{r-S_1}{S_2-S_1}\right) \qquad (5.5.14)$$

Imposing boundary conditions we find

$$V_0(r,\theta,0^+) = 0 = \sum_{n=1}^{\infty} C_n \sin\{\xi_n\} \sin\left(n\pi \frac{r-S_1}{S_2-S_1}\right)$$

so $\xi_n = 0 + \kappa\pi$, $(\kappa = 1,2,3\ldots)$ and

$$V_{0_t}(r,\theta,0^+) = -C_0^2 I = \sum_{n=1}^{\infty} C_n \sqrt{1+\frac{1}{4}(\zeta\omega_n^2)}\ \omega_n \sin\left(n\pi \frac{r-S_1}{S_2-S_1}\right) \qquad (5.5.15)$$

C_n may be found by taking the inner product of (5.5.15) with $\sin\left(n\pi \frac{r-S_1}{S_2-S_1}\right)$. For constant I we find

$$C_n = \frac{4\, C_0^2 I}{n\pi\omega_n \sqrt{1+\frac{1}{4}(\zeta\omega_n)^2}} \qquad (5.5.16)$$

AD-A163 818 A DYNAMIC FIBER COMPOSITE CONTINUUM MODEL OF THE TYMPANIC MEMBRANE PART 1.. (U) RENSSELAER POLYTECHNIC INST TROY N Y DEPT OF MECHANICAL ENGIN.. R D RABBITT

UNCLASSIFIED JUL 85 RRI-151-PT-1 ARO-20474.3-MA F/G 6/16 NL

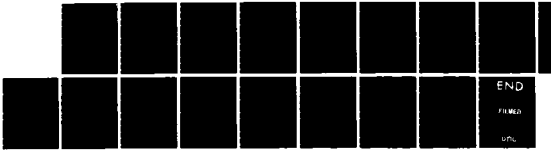

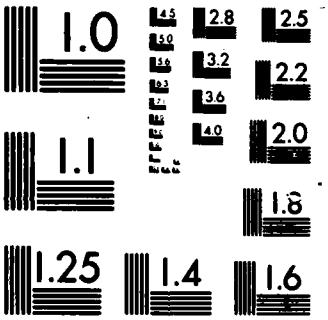

CHAPTER 6

A CONSISTENT MATHEMATICAL MODEL OF THE EUSTACHIAN TUBE AND MIDDLE-EAR AIR CHAMBERS

6.1 Importance of Wave Motion in the Middle Ear Air Chamber(s)

In order to formulate a simple model of the middle ear air chamber(s) that adequately describes action of the chambers, we must determine if it is reasonable to neglect wave motion within the chambers. As a rough estimate of the importance of wave motion, we may compare one quarter wavelength of the forcing pressure to a length characterizing the primary air chamber. Assuming that the sound speeds inside the chambers and outside the external ear have similar values, then the wavelength comparison amounts to comparing the period of the forcing signal to the time required for a signal to traverse the middle ear air chamber. If the traversing time is much less than the forcing period, then fluid properties within the primary air chamber will be essentially uniform and wave propagation can be ignored. On the other hand, if the traversing time is of the same order or greater than the forcing period, then wave propagation within the middle ear air chamber must be considered.

As a conservative estimate, the time required for a signal to traverse the primary chamber can be estimated as the distance divided by the sound speed. If the characteristic length of the primary chamber is taken to be 1.6 cm, and the sound speed is approximated as 350 m/s, the traverse time is 4.6×10^{-5} sec corresponding to a full wave frequency of 22 KHz and a quarter wave resonance of 5.5 KHz. Hence, if wave motion in the middle ear air chamber(s) is neglected, then the forcing frequencies must be limited to values well below 5.5 KHz for the example chamber size considered here.

6.2 Discrete Middle Ear Air Chamber and Eustachian Tube Model

Suppose we model the middle ear air cavities as consisting of one

primary cavity, connected to the Eustachian tube, and "n" secondary cavities as indicated below.

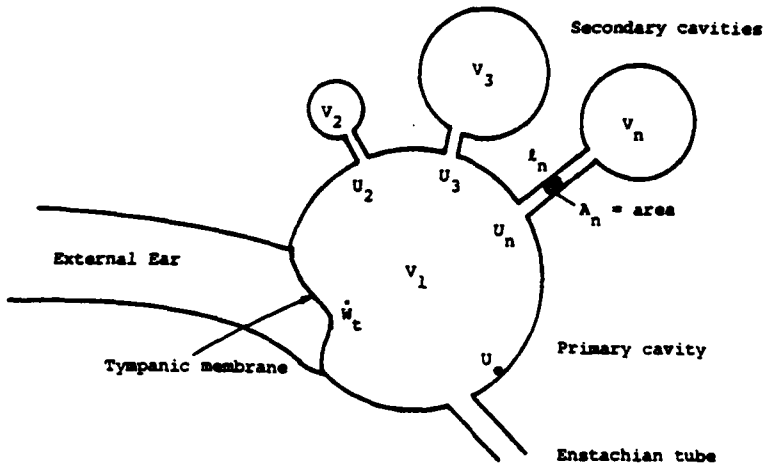

Figure 6.1. Schematic diagram of air chambers and Eustachian tube.

Displacement of the tympanic membrane is denoted by w_t. Fluid velocity down the Eustachian tube at the connection to the primary cavity is denoted by U_e, while fluid velocity into the secondary cavities is denoted $U_i (i=2,\ldots,n)$. The volume of each chamber is considered fixed for development of this discrete model. The fluid state is defined by pressure, P_n and density, ρ_n in each chamber volume V_n.

As a simple model, consider the case of "slow" TM vibrations such that wave motion within the middle ear chambers can be neglected and the state within each chamber is considered uniform.

a) Primary chamber

Conservation of mass may be written for a control volume enclosing the

primary chamber, traversing the connecting openings at the periphery of the primary cavity, as follows: (Potter and Foss, 1975)

$$\int_{V_1} \frac{\partial \rho}{\partial t} dV_1 + \int_{TM} \rho_1 \frac{\partial w_T}{\partial t} dA + \int_e \rho_1 u_e dA_i \qquad (6.2.1)$$

$$+ \sum_{i=2}^{n} \int_{A_i} \rho_1 u_i \, dA_i = 0 ,$$

where A_i is the cross section area of the connecting tubes (Fig. 6.1). For slow vibrations the properties within each cavity are considered uniform, and the velocities at the openings are approximated by their average values such that (6.2.1) may be written

$$\frac{d\rho_1}{dt} + \frac{\rho_1}{V_1} \left(\int_{TM} \frac{\partial w_T}{\partial t} dA + u_e A_e + \sum_{i=2}^{n} u_i A_i \right) = 0 . \qquad (6.2.2)$$

Suppose changes in density are small and denoted by $\delta(t)$, then conservation of mass for the primary chamber becomes

$$\rho_1 = \rho_0 + \delta_1(t) .$$

Combining this with (6.2.2) we find

$$\frac{d\delta_1}{dt} + \frac{\rho_0}{V_1} \left(\int_{TM} \frac{\partial w_T}{\partial t} dA + u_e A_e + \sum_{i=2}^{n} u_i A_i \right) = 0 . \qquad (6.2.3)$$

b) Secondary cavities

Conservation of mass for one of the secondary chambers may be written

$$\int_{V_n} \frac{d\rho}{dt} dV_n - \int_{A_n} \rho_n u_n dA = 0 . \qquad (6.2.4)$$

Again assuming uniform properties this reduces to

$$\frac{d\rho_n}{dt} - \frac{\rho_n}{V_n} u_n A_n = 0 . \qquad (6.2.6)$$

Applying conservation of linear momentum to a slug of fluid connecting the primary chamber to a secondary chamber we have

$$\frac{du_n}{dt} - \frac{C_n}{m_n} u_n = (P_1 - P_n) \frac{A_n}{m_n} \qquad n = 2,3 \ldots \tag{6.2.6}$$

where M_n = mass = $\rho_n A_n \ell$, C_n = viscous damping and A_n = cross sectional area. Combine this with (6.2.4) to obtain

$$\frac{d}{dt}\left(\frac{V_n}{\rho_n}\frac{d\rho_n}{dt}\right) + \frac{C_n V_n}{A_n \ell_n \rho_n^2}\frac{d\rho_n}{dt} = (P_l - P_h)\frac{1}{\rho_n \ell_n} \tag{6.2.7}$$

Assuming isentropic fluid behavior then

$$\frac{P}{\rho^\gamma} = \frac{P_0}{\rho_0^\gamma} = \text{constant} \tag{6.2.8}$$

Also assuming changes in density are small relative to initial density ρ_0 define

$$\rho_n(t) = \rho_0 + \delta_n(t) \ , \quad \text{for} \quad \delta_n << \rho_0 \tag{6.2.9}$$

Combining results, the first order problem for the perturbations in the density is

$$\frac{d}{dt}\left(\frac{V_n}{\rho_0}\frac{d\delta_n}{dt}\right) + \frac{C_n V_n}{A_n \ell_n \rho_0^2}\frac{d\delta_n}{dt}$$

$$= \frac{P_0}{\rho_0^\gamma}\left[(\rho_0 + \delta_1)^\gamma - (\rho_0 + \delta_n)^\gamma\right]\frac{1}{\rho_0 \ell_n} \tag{6.2.10}$$

$$\sim \frac{P\gamma}{\ell_n \rho_0^{\gamma+1}}(\delta_1 - \delta_n)$$

Hence the density in the Nth chamber may be described by

$$\frac{d^2\delta_n}{dt^2} + \frac{C_n}{A_n \ell_n \rho_0}\frac{d\delta_n}{dt} = \frac{P_0 \gamma}{\rho_0^\gamma \ell_n V_n}(\delta_1 - \delta_n) \tag{6.2.10}$$

Note that the density is coupled to the primary chamber through δ_1.

6.3 Eustachian Tube

Applying conservation of momentum to the Eustachian tube in the same way that it was done for the secondary air cavities we find

$$\frac{du_e}{dt} + \frac{C_e}{m_f} u_e = (P_1 - P_e) \frac{A_e}{m_f} \quad .$$

There are two cases of interest; when the tube is open and when the tube is closed.

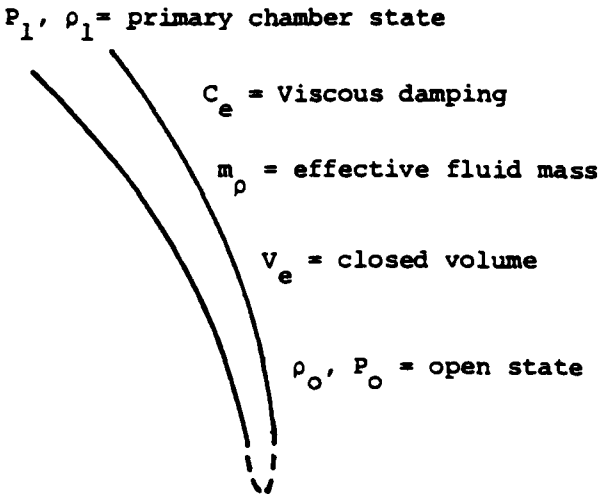

Figure 6.2 Schematic of the Eustachian tube.

i) Open tube.

If the tube is open then

$$P_1 - P_e \sim P_0\left(\left(\frac{\rho 1}{\rho_0}\right)^{\gamma} - 1\right) .$$

Combining this with (6.3.1) gives

$$\frac{du_e}{dt} + \frac{C_e}{m_f} u_e \simeq \frac{P_0 \gamma A_e \delta 1}{\rho_0 m_f} \text{ , OPEN} \qquad (6.3.2)$$

ii) Closed tube.

Apply conservation of mass to the closed tube to obtain another

secondary chamber equation in the following form

$$\frac{d^2\delta_e}{dt^2} + \frac{C_e}{m_f}\frac{d\delta_e}{dt} = \frac{P_0\,\gamma}{\rho_0^{\gamma-1} m_f}(\delta_1 - \delta_e)$$

$$u_e A_e = \frac{V_e}{\rho_e}\frac{d\delta_e}{dt} \quad , \quad \text{CLOSED} \tag{6.3.3}$$

6.4 Primary Middle Ear Air Chamber Acoustic Model

If the forcing frequency is of the order 5 KHz or greater, then wave propagation within the primary middle ear air chamber should be considered. Since the secondary chambers are usually much smaller than the primary chamber, the discrete model of their behavior will generally remain reasonable throughout the audible frequency range. Hence, in order to extend the middle ear air chamber model to be valid at frequencies above 5,000 Hz we must derive a new primary chamber equation that allows variable fluid properties within the chamber.

Equation (6.2.1) for the primary cavity remains valid and may be written as

$$\int_{V_1} \frac{\partial \rho}{\partial t}\, dV_1 + \rho_0\left(\int_{TM} \frac{\partial w_T}{\partial t}\, dA + u_e A_e + \sum_{i=2}^{n} A_i u_i\right) = 0 \ . \tag{6.4.1}$$

Introducing the velocity potential ϕ within the primary cavity, acoustic perturbations will satisfy the wave equation

$$\frac{1}{C_0^2}\frac{\partial^2 \phi}{\partial t^2} = \nabla^2 \phi \ . \tag{6.4.2}$$

The $\vec{v}$ of the air is

$$\vec{v} = \frac{1}{\rho_0}\vec{\nabla}\phi \ . \tag{6.4.3}$$

Assuming adiabadic motion,

$$p = \frac{-1}{P_0}\frac{\partial \phi}{\partial t} \ , \tag{6.4.4}$$

and

$$\rho = -\rho_0 \left(\frac{\partial \phi}{\partial t}\right)^{1/\gamma} P_0^{\frac{1-\gamma}{\gamma}} \quad . \tag{6.4.5}$$

Substituting (6.4.5) into (6.4.2) we have

$$\frac{\partial \rho}{\partial t} = -\rho_0 \frac{1}{\gamma} C_0^2 \nabla^2 \phi \left(\frac{\partial \phi}{\partial t}\right)^{\frac{1-\gamma}{\gamma}} P_o^{\frac{1-\gamma}{\gamma}} \quad , \tag{6.4.6}$$

and since

$$P_0^{\frac{1-\gamma}{\gamma}} \left(\frac{\partial \phi}{\partial t}\right)^{\frac{1-\gamma}{\gamma}} \sim \frac{1}{P_0} \quad , \tag{6.4.7}$$

then

$$\frac{\partial \rho}{\partial t} \sim \frac{\rho_o}{\gamma P_0} C_0^2 \nabla^2 \phi \quad . \tag{6.4.8}$$

Using Green's formula we find

$$\int_{V_1} \frac{C_o^2}{\gamma \rho_0} \nabla^2 \phi dV_1 + \int_{TM} \frac{\partial w_t}{\partial t} dA + u_e A_e + \sum_{i=2}^{n} A_i u_i = 0 \quad , \tag{6.4.9}$$

and

$$\int_{cs} \left\{\frac{C_0^2}{\gamma \rho_0} \vec{\nabla}\phi \cdot \vec{n} + v_s\right\} dS = 0 \quad . \tag{6.4.9}$$

But this expression must be valid for arbitrary control surface selections, so the boundary condition on the control surface is just

$$\frac{1}{\rho_0} \vec{\nabla}\phi \cdot \vec{n} + v_s = 0 \Big|_{\text{Surface}} \tag{6.4.10}$$

The equations presented assume that small perturbation assumptions of acoustics are valid and complete the model.

6.5 Comments on the Lightly Forced or Damped Linear Problem

Suppose behavior of the system can be described by linear operators in time and space such that the following general form is obtained;

$$L[u(x)] + \lambda M[u(x)] = \varepsilon F[x, u^{(n)}] \tag{6.5.1}$$

where x is the independent variable, u is the dependent variable, ε is a small parameter, and L, M and F are linear operators. It is assumed that the boundary conditions are natural, and the general problem is self adjoint. To avoid an order singularity we also require n to be less than the highest order derivative appearing in operators L or M ((n) denotes differentiation n times). The above form is consistent with separated linear plate, shell, or membrane equations subject to small damping or forcing, and hence is expected to be reasonable for the tympanic membrane problem.

Suppose we consider an asymptotic expansion of the form

$$u(x;\varepsilon) = u_0(x) + \varepsilon u_1(x) + \varepsilon^2 u_2(x) + \ldots \quad , \tag{6.5.2}$$

and let

$$\lambda = \lambda_0 + \varepsilon\lambda_1 + \varepsilon^2\lambda_2 + \ldots \quad . \tag{6.5.3}$$

Substitution into the original equation gives the following sequence of problems.

$O(1)$

$$L[u] + \lambda_0 M[u] = 0 \; . \tag{6.5.4}$$

Solution of the first order problem will yield a set of eigenvalues $\lambda_0 \in [\lambda_{on}]$ and associated eigenfunctions $\psi_0 \in [\psi_{on}]$. Suppose there exists an eigenfunction expansion theorem for this problem such that the general solution may be written as an infinite sum of the eigenfunctions.

$$u_0(x) = \sum_{n=1}^{\infty} A_n \psi_n(x;\, \lambda_{on}) \tag{6.5.5}$$

If the original operator were obtained using some sort of separation of variables then the "A" coefficients will be general functions dependent on the other independent variables in the problem. The exact form of the functions can only be determined by inspecting the problem containing all independent variables. An example problem to follow will illustrate this.

The eigenfunction expansion above will automatically meet all boundary conditions of the problem. Associated with the expansion it is assumed that there exists an inner product, such that evaluation of the coefficients is direct.

The next order problem can be written

$O(\varepsilon)$

$$L[u_1] + \lambda_0 M[u_1] = -\lambda_1 M[u_0] + F[x,u_0^{(n)}] \quad . \tag{6.5.6}$$

As before using the eigenfunction expansion theorem, completeness of the set $[\psi_n]$ allows us to write the solution of (6.5.6) as a sum of the eigenfunctions as follows

$$u_1 = \sum_{n=1}^{\infty} B_n \psi_n(x; \lambda_{on}) \quad . \tag{6.5.7}$$

Substituting into the above differential equation

$$\sum_{n=1}^{\infty} \{B_n (L[\psi_n] + \lambda_0 M[\psi_n])\} \tag{6.5.8}$$

$$= -\lambda_1 \sum_{n=1}^{\infty} A_n M[\psi_n] + F[x,u_0^{(n)}] \quad . \tag{6.5.9}$$

For a particular mode of the order one problem we know

$$\sum_{n=1}^{\infty} B_n \left(L[\psi_n] + \lambda_{on} M[\psi_n]\right) = 0$$

Hence we must have

$$\lambda_{1n} \sum_{n=1}^{\infty} A_n M[\psi_n] = F[x,u_0^{(n)}] = F[u_0^{(n)}] \tag{6.5.9}$$

Assuming F is linear, it can be expanded in terms of the eigenfunctions as

$$F[u_0^{(n)}] = \sum_{n=1}^{\infty} A_n F[\psi_n] \tag{6.5.10}$$

Combining the two expressions gives

$$\lambda_{1n} \sum_{n=1}^{\infty} A_n M[\psi_n] = \sum_{n=1}^{\infty} A_n F[\psi_n] \tag{6.5.11}$$

Taking the inner product of each side (using appropriate weight for the operator)

$$\lambda_{1n} = \frac{\langle \psi_m, \sum_{n=1}^{\infty} A_n F[\psi_n] \rangle}{A_m \langle \psi_m, M[\psi_n] \rangle} \quad . \tag{6.5.12}$$

If the problem is self adjoint then the eigenvalue perturbation may be written

$$\lambda_{1m} = \frac{\langle \psi_m, F[\psi_m] \rangle}{\langle \psi_m, M[\psi_m] \rangle} \quad . \tag{6.5.13}$$

Using this, eigenvalues of the full problem to $O(\varepsilon)$ are

$$\lambda_m = \lambda_{0m} + \varepsilon \frac{\langle \psi_m, F[\psi_m] \rangle}{\langle \psi_m, M[\psi_m] \rangle} + O(\varepsilon^2) \quad . \tag{6.5.14}$$

Simple Example Problem

Consider free vibration of a circular, isotropic, flat membrane that is fitted over a closed chamber filled with gas.

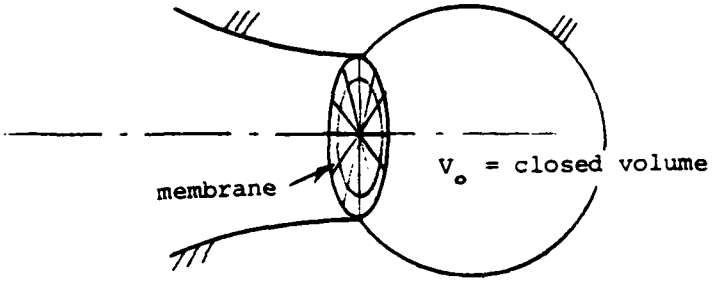

Figure 6.3 Circular membrane over a closed air space.

Assume that we are interested in low frequency vibrations of the membrane such that wave motion in the air space can be neglected. As explained earlier this assumption is valid if the time required for a wave to traverse the air space is much less than the period of vibration of the membrane.

If damping is ignored then vibration of the membrane may be approximated by

$$\nabla^2 u - \frac{B}{C^2 \rho V_0} \iint_D u dA = \frac{1}{C^2} u_{tt} \quad , \quad 0 < r < a \quad , \quad 0 < \theta < 2\pi \tag{6.5.15}$$

where

$$u(a,\theta,t) = 0 \text{ and } u(0,\theta,t) \text{ is bounded} \quad .$$

Parameters in (6.5.15) are B = bulk modulus, ρ = membrane density, V_0 = initial gas volume, and C = membrane sound speed. Separating variables the radial function is of the form

$$u(r,\theta,t) = A_m \sin(m\theta + \psi_m) \sin(\omega_\kappa t + \kappa_\kappa) w(r) \quad ,$$

where

$$\frac{d^2w}{dr^2} + \frac{1}{r}\frac{dw}{dr} + \left(\beta^2 - \frac{m^2}{r^2}\right) w = \frac{B}{TV_0} \int_0^a w 2\pi r dr \quad , \tag{6.5.15}$$

and

$$\epsilon = \frac{B}{TV_0} \quad .$$

If $\epsilon << 1$ then the previous analysis applies. Writing the radial function as a straightforward asymptotic series

$$w = w_0 + \epsilon w_1 + \epsilon^2 w_2 + \ldots \quad . \tag{6.5.16}$$

O(1)

$$\frac{d^2w_0}{dr^2} + \frac{1}{r}\frac{dw_0}{dr} + \left(\beta^2 - \frac{m^2}{r^2}\right) w_0 = 0 \quad ,$$

$$w_0(0) \text{ bounded} \quad , \tag{6.5.17}$$

$$w_0(a) = 0 \quad .$$

The solution to this problem may be written in terms of Bessel functions

$$w_{0nm} = C^*_{nm} J_m(\beta_{0nm} r) + C^{**}_{nm} Y_m(\beta_{0nm} r) \quad , \tag{6.5.18}$$

where the second set of constants must vanish to meet the finite deflection condition at the origin, and the eigenvalues β_{0nm} are determined by imposing the second boundary condition at the outside ring.

$$w_{0nm} = C^*_{nm} J_m(\beta_{0nm} r)$$

$$w_0 = \sum_{n=1}^{\infty} C^*_{nm} J_m(\beta_{0nm} r) \tag{6.5.19}$$

The next order problem is

$O(\epsilon)$

$$L[w_1] + \beta_0^2 M[w_1] = -\beta_1^2 M[w_0] + F[w_0]$$

$$L = r^2 \frac{d^2}{dr^2} + r \frac{d}{dr} - m^2 \qquad (6.5.20)$$

$$M = r^2$$

$$F = r^2 \int_0^a w_0 2\pi r dr$$

Noting that the left side is zero for some eigenvalue, perturbation of the eigenvalues is given by

$$\beta_{1nm}^2 = \frac{\int_0^a \{J_m(\beta_{0nm}r)r^2 \int_0^a \{J_m(\beta_{0nm}n)2\pi n dn\}dr}{\int_0^a r^2(J_m(\beta_{0nm}r))^2 dr} \qquad (6.5.21)$$

The eigenvalues of the full problem may be written to order epsilon as

$$\beta_{nm}^2 \simeq \beta_{0nm}^2 + \epsilon \beta_{1nm}^2 + O(\epsilon^2) \qquad (6.5.22)$$

REFERENCES

1. Bally, GV. (1977): Holographic analysis of tympanic membrane vibrations in human temporal bone preparations using a double pulsed ruby laser system. Applications of Holography and Optical Data Processing, E. Marom and A. A. Frusem eds., Pergamon Press, Oxford, 593-602.

2. Bally, GV. (1979): Otological investigations in living man using holographic interferometry. Holography in Medicine and Biology, G. von Bally ed., Springer-Verlag, Berlin, 198-205.

3. Békésy G. von (1941): On the measurement of the amplitude of vibration of the ossicles with a capacitive probe. Akust. Zeitschr. 6, 1-16.

4. Békésy G. von (1949): The structure of the middle ear and the hearing of one's own voice by bone condution. J. Acoust. Soc. Am. 21, 217-232.

5. Burkhard, M. D. and Sachs, R. M. (1977): Sound pressure in insert earphone couplers and real ears. J. Speech Hear. Res. 20, 799-807.

6. Djupesland, G. and Zwislocki, J. J. (1972): Sound pressure distribution in the outer ear, Scand. Audiol 1, 197-203.

7. Esser, M.H.M. (1947): The mechanism of the middle ear: II. The drum. Bull. Math. Biophys. 9, 75-91.

8. Dancer, A. L.; Franke, R. B.; Smigielski, P.; Albe, F. and Fagot, H. (1975): Holographic interferometry applied to the investigation of tympanic membrane displacements in guinea pig ears subjected to acoustic impulses. J. Acoust. Soc. Am. 58, 223-228.

9. Helmholtz, H.L.F. (1869): The mechanism of the middle-ear ossicles and of the eardrum. Pflugers Arch. f. Physiol. (Bonn) 1, 1-60.

10. Feldman, A. S. (1967): Acoustic impedance studies of the normal ear, J. Speech Hearing Res. 10, 165-176.

11. Frank, O. (1923): Sound Conduction in the ear. Sitzungsber. math. - physikal. Klass. Bayerischen Akad. Wiss. Munchen 1923, 11-77.

12. Fritz, W.; Kreitlow, H. and Ringer, K. (1978): Holographic investigation of the mode of vibration of the human eardrum. Arch. O-R-L 221, 225-259.

13. Fritz, W.; Kreitlow, H. and Winter, D. (1979): On holographic-interferometric investigations of the membrana tympani (living man). Holography in Medicine and Biology, G. von Bally ed., Springer-Verlag, Berlin, 206-211.

14. Funnell, W.R.J. (1975): A theoretical study of the eardrum vibrations using the finite-element method. Ph.D. thesis, McGill University, Montreal.

15. Funnell, W.R.J. and Laszlo, C. A. (1978): Modeling of the cat eardrum as a thin shell using the finite element method. J. Acoust. Soc. Am. 63, 1461-1467.

16. Graff, K. F. (1970): Wave motion in elastic solids. Ohio State University Press, Columbus.

18. Graham, M. D.; Reams, C. and Perkins, R. (1978): Human tympanic membrane-malleus attachment. Ann. O.R.L. 87, 426-431.

19. Gran, S. (1968): The analytical basis of middle ear mechanics. A contribution to the application of the acoustical impedance of the ear. Dissertation, University of Oslo.

20. Helms, J. (1974): Mechanics of the middle ear. Acta O-R-L Belg. 28, 581-585.

21. Helms, J. (1977): Experimental and clinical studies on the function of normal, pathological and surgically treated tympanic membranes. Acta Oto-laryngol. Suppl. 350, 151-255.

22. Holmes, M.H. and Cole, J.D. (1983): Cochlear Mechanics: Analysis for a pure tone.

23. Holmes, M.H. (1982): A mathematical model of the dynamics of the inner ear. J. Fluid Mech., G. Britain, 116, 59-75.

24. Hudde, H. (1980): Messung der Trommelfell impedanz des memschlichen Ohres bis 19 KHz. Dissertation, Abteilung fur Electrotechnik, Ruhr-Universitat Bochum.

25. John, F. (1982): Partial Differential Equations, fourth ed. Applied Math. Sci., 1, Springer-Verlag, New York.

26. Johnson, F. R.; McMinn, R.M.H. and Atfield, G.N. (1968): Ultrastructural and biochemical observations on the tympanic membrane. J. Ant. 103, 297-310.

27. Jones, R. M. (1979): Mechanics of Composite Materials, McGraw Hill, N.Y., 31-84.

28. Kevorkian, J. and Cole, J.D. (1981): Perturbation Methods in Applied Mathematics, Applied Math. Sci. 34, Springer-Verlag, New York.

29. Khanna, S. M. and Tonndorf, J. (1969): Middle ear power transfer. Arch. klin. exp. Ohr. Nas. Kehlk. Heilk. 193, 78-88.

30. Khanna, S. M. and Tonndorf, J. (1972): Tympanic membrane vibrations in cats studied by time-averaged holography. J. Acoust. Soc. Am. 51, 1904-1920.

31. Khanna, S. M. and Tonndorf, J. (1975a): Tympanic membrane shape determined by moire topography. J. Acoust. Soc. Am. 57, S72 (abstract).

32. Khanna, S. M. and Tonndorf, J. (1975b): Tympanic membrane: effect of dc pressure changes in the middle ear of cats. J. Acoust. Soc. Am. 58, S88 (abstract).

33. Killion, M. C. (1981): An engineering view of middle ear surgery. J. Acoust. Soc. Amer. 69, Suppl. 1, S44.

34. Kirikae, I. (1960): The structure and function of the middle ear. University of Tokyo Press, Tokyo.

35. Kinsler, L. E.; Frey, A. R.; Coppens, A. B. and Sanders, J. V. (1982): Fundamentals of Acoustics, third edition, John Wiley and Sons, New York.

36. Lim, D. J. (1968a): Tympanic membrane. Electron microscopy observations. Part I. Pars tensa. Acta Otolaryngol. 66, 181-198.

37. Lim, D. J. (1968b): Tympanic membrane. Part II. Pars Flaccida. Acta Otolaryngol. 66, 515-532.

38. Lim, D. J. (1970): Human tympanic membrane. An ultrastructural observation. Acta Otolaryngol. 70, 176-186.

39. Lokberg, O. J.; Hogmoen, K. and Gundersen, J. (1980): Vibration measurement in the human tympanic membrane - in vivo, Acta Otolaryngol. 89, 37-42.

40. Lynch, T.J., III (1981): Signal processing by the cat middle ear: admittance and transmission, measurement and models. Ph.D. thesis, Mass. Inst. Technol., 257 pp.

41. Manley, G. A., and Johnstone, B. M. (1974): Middle-ear function in the guinea pig. J. Acoust. Soc. Am., 56, 571-576.

42. Mehrgardt, S. and Mellert, V. (1977): Transformation characteristics of the external human ear. J. Acoust. Soc. Amer. 61, 1567-1576.

43. Moller, A. R. (1961): Network model of the middle ear. J. Acoust. Soc. Amer. 33, 168-176.

44. Novozhilov, V. V. (1959): The theory of thin shells, P. Noordhoff Ltd., Groningen, Netherlands.

45. Nuttall, A. L. (1974): Tympanic muscle effects on middle ear transfer characteristic, J. Acoust. Soc. Am. 56, 1239-1247.

46. Oaks, E.C.J. (1967): Structure and function of inflated middle ears of rodents. Ph.D. thesis, Yale University, New Haven.

47. Ogura, Y. (1974): A holographic study of eardrum vibrations. Jibi-inkoka (otolaryngol) 46, 83-88.

48. Ogura, Y. and Kimura, Y. (1974): Vibration analysis of the human eardrum by holographic interferometry. Rinsho-Jika (Clin. Otol.) 1, 10-11.

49. Onchi, I. (1961): Mechanism of the middle ear. J. Acoust. Soc. Am. 33, 794-805.

50. Peake, W. T. and Guinan, J.J. Jr. (1967): A circuit model for the cat's middle ear. M.I.T. Lab. Electron. O. Prog. Report 84, 320-326.

51. Politzer, A. (1889): The anatomical and histological dissection of the human ear in the normal and diseased condition. Enke, Stuttgart.

52. Potter, M. C. and Foss, J. F. (1975): Fluid Mechanics, John Wiley and Sons, New York.

53. Pajara, P. and Lardner, J. J. (1978): Deformations of elastic membranes-Effect of different constitutive relations. Kurze Mitteilungen, Brief Reports. 29, 315-327.

54. Shaw, E.A.G. (1975): The external ear: new knowledge. In Earmoulds and associated problems. Proc. Seventh Danavox Symposium, Gl. Avernaes, Denmark. Scandinavian Audiology, Suppl. 5. 24-50.

55. Shaw, E.A.G. (1974a): The external ear. Handbook of Sensory Physiology, Vol. VII, Auditory System, W. D. Keidel and W. D. Neff Eds., Springer Verlag, Berlin-Heidelberg - New York, 455-490.

56. Shaw, E.A.G. (1974b): Transformation of sound pressure level from the free field to the eardrum in the horizontal plane. J. Acoust. Soc. Amer. 56, 1848-1861.

57. Shaw, E.A.G. (1977): Eardrum representation in middle-ear acoustical networks. Acoust. Soc. Am. 94th meeting, paper E5.

58. Shaw, E.A.G. and Stinson, M. R. (1981): Network Concepts and Energy Flow in the Human Ear. Acoust. Soc. of Am. 101st meeting, paper T2.

59. Shaw, E.A.G. and Thiessen, G. J. (1962): Acoustics of circumaural earphones. J. Acoust. Soc. Amer. 34, 1233-1246.

60. Shimada, T., and Lim, D. J. (1971): The fiber arrangement of the human tympanic membrane: A scanning microscopic observation. Ann O.R.L. 80, 210-217.

61. Steele, C. R. and Taber, L. A. (1979): Comparison of WKB calculation and experimental results for three-dimensional cochlear models, J. Acoust. Soc. Am. 65, 1007-1018.

62. Stinson, M. R.; Shaw, E.A.G. and Lawton, B. W. (1980): Standing wave pressure ratio in the human ear canal. J. Acoust. Soc. Amer. 68, Suppl. 1, S4-5.

63. Stinson, M. R.; Shaw, E.A.G. and Lawton, B. W. (1982): Estimation of acoustical energy reflectance at the eardrum from measurements of pressure distribution in the human ear canal. J. Acoust. Soc. Am. 72, 766-773.

65. Theocaris, P.S. and Pazis, D. (1983): The topography of the core-region around cracks under modes I. II and III of fracture. Int. J. Mech. Sci. 25, 121-136.

66. Tiersten, H. F. and Jahanmir, M. (1977): A theory of Composites modeled as interpenetrating Solid Continua. Arch. Rat. Mech. and Anal. 65, #2, 153-192.

67. Tonndorf, J. and Khanna, S. M. (1970): The role of the tympanic membrane in middle ear transmission. Ann. O.R.L. 79, 743-753.

68. Tonndorf, J. and Khanna, S. M. (1971): Validation of holographic observations on the displacement of the tympanic membrane in cats. J. Acoust. Soc. Am. 50, 92 (abstract).

69. Tonndorf, J. and Khanna, S. M. (1972): Tympanic membrane vibrations in human cadaver ears studied by time-averaged holography. J. Acoust. Soc. Am. 52, 1221-1233.

70. Tonndorf, J.; Khanna, S. M. and Greenfield, E. C. (1971): The function of reconstructed tympanic membranes in cats. Ann. Otol. Rhinol. Laryngol. 80, 861-870.

71. Tonndorf, J.; Khanna, S. M. and Greenfield, E. C. (1972): Total myringoplasty: functional aspects. Acta Otolaryngol. 73, 87-93.

72. Uyemura, J.; Yamamoto, Y.; Udagawa, T.; Ogura, Y. and Kimura, Y. (1974): Vibration analysis by holographic interferometry vibration mode of the tympanic membrane). Bull. Japan Soc. Prec. Eng. 8, 25-26.

73. Yang, W. H. and Feng, W. W. (1970): On axisymmetrical deformations of nonlinear membranes. J. Applied Mechanics, ASME, 1002-1011.

74. Zwislocki, J. (1962): Analysis of middle ear function. Part I. Input impedance. J. Acoust. Soc. Am. 34, 1514-1523.

75. Zwislocki, J. (1963): Analysis of the middle ear function. Part II. Guinea pig ear. J. Acoust. Soc. Am. 35, 1034-1040.

UNCLASSIFIED
SECURITY CLASSIFICATION OF THIS PAGE (When Data Entered)

AD-A163 818

REPORT DOCUMENTATION PAGE		READ INSTRUCTIONS BEFORE COMPLETING FORM
1. REPORT NUMBER RPI Math Report No. 151	2. GOVT ACCESSION NO. N/A	3. RECIPIENT'S CATALOG NUMBER N/A
4. TITLE (and Subtitle) A Dynamic Fiber Compposite Continuum Model of the Tympanic Membrane: Part I: Model Formulation		5. TYPE OF REPORT & PERIOD COVERED 6. PERFORMING ORG. REPORT NUMBER
7. AUTHOR(s) Richard D. Rabbitt		8. CONTRACT OR GRANT NUMBER(s) DAA G29-83-K-0092
9. PERFORMING ORGANIZATION NAME AND ADDRESS Rensselaer Polytechnic Institute Troy, NY 12180		10. PROGRAM ELEMENT, PROJECT, TASK AREA & WORK UNIT NUMBERS
11. CONTROLLING OFFICE NAME AND ADDRESS U. S. Army Research Office Post Office Box 12211 Research Triangle Park, NC 27709		12. REPORT DATE July 31, 1985 13. NUMBER OF PAGES 107
14. MONITORING AGENCY NAME & ADDRESS(if different from Controlling Office)		15. SECURITY CLASS. (of this report) Unclassified 15a. DECLASSIFICATION/DOWNGRADING SCHEDULE

16. DISTRIBUTION STATEMENT (of this Report)

Approved for public release; distribution unlimited.

17. DISTRIBUTION STATEMENT (of the abstract entered in Block 20, if different from Report)

NA

18. SUPPLEMENTARY NOTES

The view, opinions, and/or findings contained in this report are those of the author(s) and should not be construed as an official Department of the Army position, policy, or decision, unless so designated by other documentation.

19. KEY WORDS (Continue on reverse side if necessary and identify by block number)

20. ABSTRACT (Continue on reverse side if necessary and identify by block number)

Fibrous layers of the lamina propria influence dynamic behavior of the tympanic membrane by producing strong anisotropic extensional stiffness, while the mucous and epidermal layers are primarily responsible for curvature dependent structural damping and relatively weak isotropic bending stiffness. These mechanical properties are combined with curvilinear shell equilibrium equations to formulate a comprehensive dynamic continuum model of the tympanic

- continued -

DD FORM 1 JAN 73 1473 EDITION OF 1 NOV 65 IS OBSOLETE

UNCLASSIFIED
SECURITY CLASSIFICATION OF THIS PAGE (When Data Entered)

20. membrane. The resulting model contains several small parameters that are exploited to construct closed form asymptotic solutions for the general problem. Using the geometry and ultrastructure of the cat eardrum coupled with the outer ear, ossicular chain and tympanic cavities, the asymptotic solution reproduces the manifold of experimentally observed frequency and excitation dependent vibrational shapes. Demonstration of the model's ability to duplicate experimental results concludes part I. However, since the model is based on the actual geometry and ultrastructure, future investigations may use the model to address questions related to tympanoplasty, tympanosclerosis, tensor tympani cogency, as well as energy transmission and tympanic cavity coupling.

END

FILMED

3-86

DTIC